

THESIS

THE INFLUENCE OF AEOLIAN DUST ON THE BIOGEOCHEMICAL AND PHYSICAL
CHARACTERISTICS OF SOILS ACROSS THREE BIOCLIMATIC DOMAINS OF THE
WESTERN U.S.

Submitted by

Jessica Callen

Department of Soil and Crop Sciences

In partial fulfillment of the requirements

For the Degree of Master of Science

Colorado State University

Fort Collins, Colorado

Summer 2023

Master's Committee:

Advisor: Eugene Kelly
Co-Advisor: Susan Melzer

Gregory Butters
Jerry Magloughlin

Copyright by Jessica Callen, 2023

All Rights Reserved

ABSTRACT

THE INFLUENCE OF AEOLIAN DUST ON THE BIOGEOCHEMICAL AND PHYSICAL CHARACTERISTICS OF SOILS ACROSS THREE BIOCLIMATIC DOMAINS OF THE WESTERN U.S.

This study investigates the impacts of dust generation and deposition on the biogeochemistry of soils in the western U.S., where aeolian processes are increasing due to climate change and human activities. Contemporary techniques for collecting and analyzing erosion and deposition were utilized at three locations (Moab, Niwot, CPER) to determine the amount and properties of dust present in three bioclimatic domains (Colorado Plateau, Rocky Mountains, Great Plains). The processes that contribute to the aggradation and degradation of the soil were assessed and used to determine the role of dust in the soil-forming processes at each site. These results indicate that the high amount of soil eroding at Moab (160 times more erosion than deposition) was causing a decrease in the soil volume and creating a loss of clay and plant essential nutrients within the surface horizon. For both Niwot and CPER, the soils were formerly in an aggradaing phase but the measurments from soil erosion samplers at these sites indicate the contemporary system are now degrading. The chemical characteristics of deposited dust compared to the soil at Niwot suggest that the Southern Rocky Mountains are receiving dust from non-local sources, specifically Moab within the winter season. The results from CPER suggest deposition is from local dust generation. Based on these findings, it can be inferred that the impact of aeolian processes on the soils varies across bioclimatic domains.

ACKNOWLEDGEMENTS

I would like to first thank Dr. Gene Kelly and Dr. Suellen Melzer for taking me on as a student and advising me throughout this project. I have learned and grown so much as a researcher these past two years, which is attributed to my two advisors' advice and support. Funding for this research was provided by the National Science Foundation through the BII: Regional OneHealth Aerobiome Discovery Network (BROADN) and the Colorado Agricultural Experiment Station at Colorado State University. Thank you to my committee members, Dr. Greg Butters and Dr. Jerry Magloughlin, for offering support and equipment and contributing to this thesis's intellectual merit. Thank you to Molly Blakowski for your academic support and guidance as a fellow dust researcher and for your hospitality in Utah. Janice Brahney allowed me to use her grain size analyzer for the particle size results at Utah State University. Thank you to the Critical Zone network, especially Jeff Munroe, for connecting me to the amazing dust researchers who have guided me along this process. Thank you to the NEON staff for the support in collecting information and samples and assisting in the permitting process and the NEON Moab staff for collecting my Moab samples once a month.

Thank you to the support of my family and friends, especially Owen Clark, for following me out to Colorado so I could pursue my dream of getting a master's. Owen has offered tremendous patience, kindness, and support and has helped me throughout the graduate program immensely. My CSU friends, Paige Hansen, Kristen Johnson, and Gina Cerimelle have offered me support, guidance, and help with my field collections. And as always, thank you, Mom and Dad, and all my sisters, for always pushing me to pursue my dreams and supporting me along the way.

TABLE OF CONTENTS

ABSTRACT.....	ii
ACKNOWLEDGEMENTS.....	iii
CHAPTER 1: INTRODUCTION AND METHODS	1
1. INTRODUCTION	1
1.1 Literature Review	2
1.2 Research Objectives	6
1.3 Site Selection	7
2. EXPERIMENTAL DESIGN.....	11
3. METHODS	16
3.1 Field Methods.....	16
3.2 Laboratory Methods.....	23
CHAPTER 2: SOIL MASS BALANCE RESULTS AND DISCUSSION	25
1. INTRODUCTION	25
2. SECTION OBJECTIVES AND METHODOLOGY	26
2.1 Section Objectives	26
2.2 Mass Balance Determinations	26
3. RESULTS	28
3.1 Soil Classification	28
3.2 Soil Morphology.....	29
3.3 Mass Balance Strain.....	30
3.4 Elemental Mass Transport	33
4. DISCUSSION	38
CHAPTER 3: AEOLIAN FLUXES AND CHARACTERISTICS.....	41
1. INTRODUCTION	41
2. SECTION OBJECTIVE AND METHODS	42
2.1 Sample Methodology Based on Research Objectives	42
2.2 Flux Equation.....	44
2.3 Total Elemental Analysis.....	44
2.4 Elemental Ratios	45
2.5 Statistical Analysis	45
2.6 Sedimentology Statistics.....	48
3. RESULTS	50
3.1 Erosional Variability within the Sites	50
3.2 Chemical Characteristics of Aeolian Input: Seasonal and Site Variability.....	53
3.3 Chemical Characteristics of Aeolian Input: Provenance	57
3.4 Sedimentological Results: Grain Size Distribution Among Sites.....	59
3.5 Sedimentological Results: Grain Size Distribution Within Sites	63
3.1 Aeolian Dust Flux.....	68
4. DISCUSSION	73
CHAPTER 4: CONCLUSIONS.....	78

REFERENCES.....	82
APPENDICES	92
<i>Appendix A: Wind Rose Figures</i>	92
<i>Appendix B: Filter Collection Dates</i>	102
<i>Appendix C: Tables Related to Flux and Particle Size</i>	103

CHAPTER 1: INTRODUCTION AND METHODS

1. INTRODUCTION

Soil occupies the region of the critical zone accessible as a fundamental resource for humans and ecosystem functions. Soils are open systems that dynamically interact with adjacent systems (e.g., the atmosphere) via additions and losses. For example, atmospheric dust deposition can be a source of nutrient additions to the soil. Dust is generated as soils are eroded and the dust is then redeposited locally, regionally, and globally, and this may be a mechanism that connects the biogeochemical environments of ecological systems. It is this land surface-atmosphere interaction via the contribution of dust to soil formation that is of particular interest for this research.

Soil loss via wind erosion is a critical problem throughout the world because of the resultant reduction in soil nutrients and decline in agricultural productivity. Vegetative ground cover stabilizes the soil and minimizes the dispersal of silt and clay particles, thereby being a significant factor in controlling soil erosion. The recognition of the key processes of soil erosion and the physical properties of eroded soil materials is essential in determining the fate and mobility of the eroded soil materials and their impact on ecosystem structure and function.

Additions to soils from dust can chemically and physically alter soil ecosystems upon deposition as it has been found to contribute to nutrient pools, enhance buffering capacity, and increase water and nutrient holding capacity (Chadwick et al., 1999; Litaor, 1987; Muhs & Benedict, 2006). Therefore, the chemical characterization and nature of soil materials in dust can

lead to insights about the impact of deposition on soils within and among diverse ecosystems. Understanding the role of dust in soil formation in contemporary ecosystems will allow us to assess how these drivers of ecosystems structure and function have changed and will be changing during the Anthropocene.

1.1 LITERATURE REVIEW

Soil is an open system formed by internal and external processes. The four categories of soil-forming processes are 1) transformations, 2) translocations, 3) additions, and 4) removals (Simonson, 1959). Soil loss and coinciding dust generation occurs in areas of little or no ground cover where creeping and saltating sand particles move smaller soil particles (silt and clay) into suspension (Tatarko & Presley, 2009). In suspension, dust travels locally (0-10 km), regionally (10-1000 km), and globally (>1000 km), and is deposited through precipitation and gravity (Lawrence & Neff, 2009). The deposition of dust is an essential addition to soil, as it enriches the soil with elements such as Ca, K, Mg, Mn, and P that offer vital nutrients necessary for plant growth (Litaor, 1987; Chadwick et al., 1999). For example, in the Rocky Mountains, where soils commonly develop from nutrient-poor granitic parent material, dust brings clay and silt particles that increase water retention and cation exchange capacity (Muhs & Benedict, 2006). The soil forming process of translocation occurs where soil constituents (e.g., nutrients or elements) move through the soil's horizons. Dust additions contribute to translocation processes as dust-associated particles and nutrients leach from the surface horizon to subsurface soil horizons (Lawrence et al., 2013; Bergstrom et al., 2019).

Erosional soil loss and dust generation are multi-faceted processes, increasing worldwide and exacerbated by human disturbances and climate change. Each year, 75 billion tons of soil is eroded from the world's ecosystems (Kendall & Pimentel, 1994). Soil loss through erosion occurs locally where larger soil particles (0.5-1 mm) creep and smaller particles (0.1-0.5 mm) bounce or saltate along the soil surface. Soil particles less than 0.1 mm may be dislodged from the soil to become suspended in the atmosphere as dust. A combination of land surface roughness, soil particle size distribution, soil moisture content, and land cover can impact dust saltation and suspension events. Climatic shifts toward aridity in the western U.S., along with strong wind speeds and low soil moisture, are useful predictors of large dust bowl-type events (Kim & Choi, 2015).

Vegetation, rocks, and biological soil crust make up the soil's ground cover, protecting the soil from erosion. Perennial grasses with fibrous root structures have the greatest influence over soil stability as they trap easily erodible soil particles. Land grazed by cattle, that preferentially eat perennial grasses, may have long-lasting impacts on soil erosion (Okin et al., 2006; Aubault et al., 2015). This selective herbivory of cattle increases woody and exotic annual species cover, with taproot systems, and reduces soil stability (Milchunas et al., 1988; Harris et al., 2003; Duniway et al., 2018). A study within the Colorado Plateau found 38-43% less silt and clay within the soil due to soil erosion in an area historically grazed 30 years prior compared to areas that were never grazed (Neff et al., 2005). Also, sediment within the Porphyry and Senator Beck Lake beds located in the San Juan Mountains revealed a 500% increase in dust emissions from the Colorado Plateau after European settlement introduced cattle grazing into the western drylands in the 1800's (Neff et al., 2008). Overall, perennial grasses are a significant factor in

soil stability and have been significantly reduced due to grazing within the western U.S., leading to increased soil erosion.

The biogeochemistry of soils constrains the structure and function of ecosystems. Soil is derived from weathering of geologic materials, which determines the nutrient content (e.g., calcium, phosphorous, potassium, iron, etc.). Over time nutrients become depleted as the bedrock weathers and nutrients are lost to plant uptake, leaching or physical removal (Brimhall & Dietrich, 1985; Chadwick et al., 1999). Nevertheless, well-developed soils with little to no remaining parent material contain mineral-based nutrients due, in part, to the fertilization from dust deposition. Researchers have determined that dust deposition is the source of this fertilization, and in some ecosystems, dust deposition may contribute significantly to the plant available nutrients derived from the weathering of bedrock (Chadwick et al., 1999; Kurtz et al., 2001; Reynolds et al., 2006; Aciego et al., 2017; Bergstrom et al., 2019; Munroe et al., 2020). For example, contribution of dust to soil nutrients was studied in Hawaii, where researchers determined that older weathered soils (~150,000 years old) were 80% atmospherically derived (Chadwick et al., 1999). Additionally, recent research suggests that young and erodible montane environments receive dust in equal to or greater proportions than from bedrock (Lawrence et al., 2013; Aciego et al., 2017; Munroe et al., 2020).

The physical characteristics of dust particulates may play an important role by increasing the plant available water through the deposition of silt and clay size particles. Research from the southern Rocky Mountains indicated that the source of silt and clay within the surface horizon of mountain soils is not from parent material but from dust deposition (Muhs and Benedict, 2006; Mladenov et al., 2012; Bergstrom et al., 2019; Heindel et al., 2020). Furthermore, studies conducted on the Colorado Plateau indicate the elimination of finer soil particles can result in the

depletion of soil nutrients essential to plant growth (Neff et al., 2005; Muhs and Benedict, 2006; Munroe et al., 2020). Additions and losses of materials from soils can have important impacts on the function and structure of ecosystems.

Challenges associated with dust collection include: 1) providing standardized methods across diverse ecosystems, 2) attempting to capture both spatial and temporal variations within and among sites, 3) selecting physical and chemical characterization methods on limited sample volumes. To meet these challenges, collaborations were made with the U.S. National Ecological Observatory Network (NEON), the National Wind Research Erosion Network (NWREN), and the Critical Zone Network (CZN).

NEON represents a major investment in scientific infrastructure in support of ecological research at a continental scale. NEON collects data from automated sensors and samples organisms and ecological variables in 20 ecoclimatic domains. Relevant to work in my thesis, NEON has physically and chemically characterized soil pedons within each of the domains and actively monitors atmospheric dust particles of less than 10 microns within each NEON site, including the three represented in this study. The atmospheric dust particle filters are monitored in collaboration with the Colorado Department of Health to map particle size distribution and particulate mass to determine air quality for public health.

NWREN collects erosion and deposition from rangelands and croplands in the United States using a standard wind research erosion model (Webb et al., 2015). NWREN provides open access to dust-associated data, including mass values from wind erosion and deposition. NWREN erosion samples were obtained from the 2021 calendar year to measure the yearly erosional flux at Moab and CPER.

CZN and the Dust Alliance of North America are two organizations that promote communication and collaboration among dust researchers (<https://criticalzone.org/dust2>; <https://dust.cira.colostate.edu/>). During this study, we collaborated with members of CZN to access a grain size particle analyzer for analysis.

1.2 RESEARCH OBJECTIVES

This research is a part of the BII Regional One Health Aerobiome Discovery Network (BROADN). The network seeks to advance biologic discovery by assembling transdisciplinary expertise to study the factors that shape the aerobiome and investigate biotic content ranging from viruses (as small as 20 nm) to microscopic nematodes (on the order of 100 μm), from the Earth's surface to the atmosphere. Most research focused on the influence of dust on soil development and soil biogeochemistry is site-specific and not conducted in a manner that allows assessment of regional variability in diverse ecosystems (Aarons et al., 2017; Heindel et al., 2020; Munroe et al., 2020). This study aims to characterize the soil and ecosystems properties that regulate dust losses and inputs within and among key ecosystems in the western U.S.

Specific Research Objectives:

- (1) Identify the key soil-forming processes and environmental conditions that influence soil aggradation and degradation within and among soils of different bioclimatic domains.

- (2) Quantify the contemporary aeolian inputs and outputs by measuring erosion and deposition rates and characterizing the physical and chemical composition of aeolian inputs across the three bioclimatic domains.

1.3 SITE SELECTION

Soils are conditioned by the soil-forming factors of climate, organisms, topographic relief, parent material, and time. Research sites were selected for this study from three bioclimatic domains: the Colorado Plateau, the southern Rocky Mountains, and the western Great Plains (Fig. 1.1). The distinct soil-forming factors of these three sites are shown in Table 1.1.

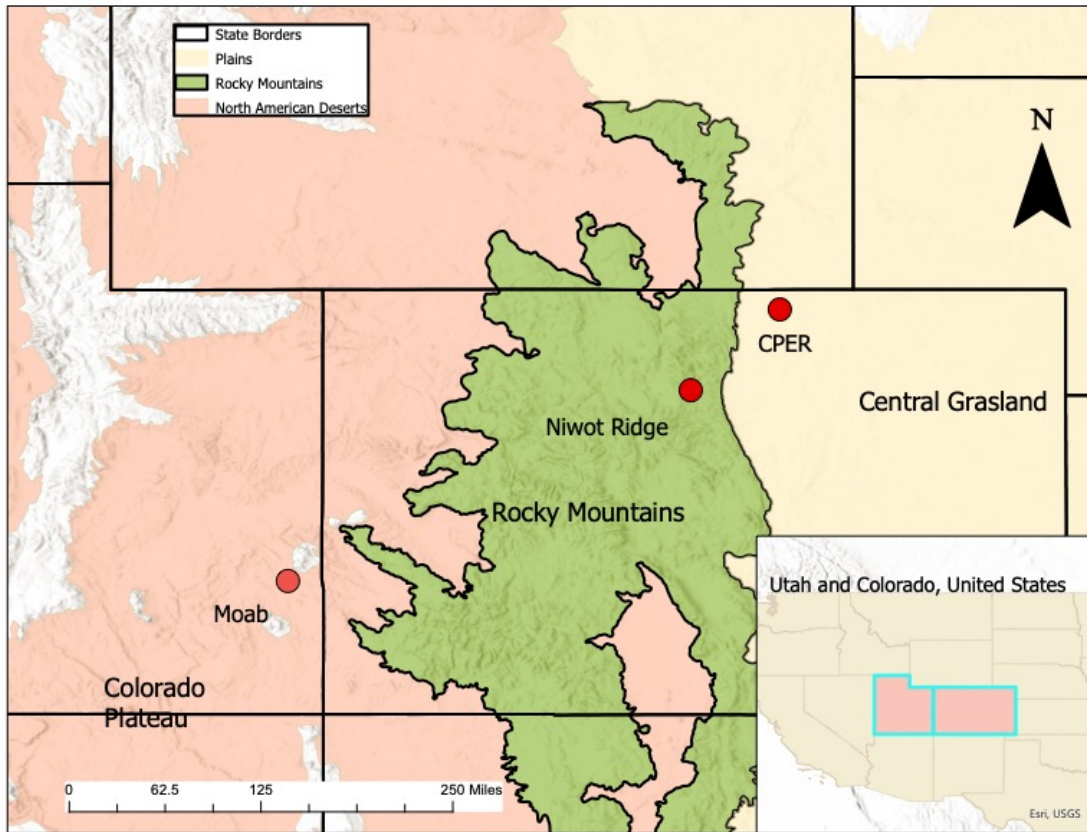


Figure 1.1. Sampling sites and regions: Moab in Grand County, UT; Niwot Ridge in Boulder County, CO; and Central Plains Experimental Region in Weld County, CO. This map indicates the location of the sites and their bioclimatic domains.

Table 1.1. Site descriptions for Moab, Niwot, and CPER. Data from Roehler, 1993; Doesken et al., 2003; Parslow et al., 2016; Steinert et al., 2017; Fabain et al., 2019, and <https://www.neonscience.org/field-sites/moab>.

Site	Soil	Elevation (m)	Parent Material	Geological Formation	Age of Formation	MAT (°C)	MAP (mm)	Dominant Vegetation
Moab	Haplocalcid	1800	Residuum over Sandstone and Aeolian Deposits	Carmel Formation	Middle Jurassic	10.1	320	saltbush, Mormon tea, and Utah Juniper
Niwot	Haplocryoll	3500	Glacial Till of Mixed Gneiss, Granite, and Schist	Pinedale glacial deposits	12-30 Ka	0.3	1005	alpine bluegrass, sagebrush, elk sedge, and Fern Ally
CPER	Argiustoll	1700	Residuum over Sandstone	Fox Hill Formation	69-70 Ma	8.6	344	blue grama, broom snakeweed, and plains prickly pear

The Moab study site is in a high desert ecosystem within the Colorado Plateau, 30 km south of Moab, Utah (Fig. 1.1). The land is managed by the Bureau of Land Management (BLM) and is seasonally grazed. The dominant soil at the Moab site is classified as an ustic haplargid, developing from aeolian deposits over residuum sandstone from the Carmel Formation of Middle Jurassic age (Table 1.1). The dominant vegetation at the site is saltbush, pinyon pine, Mormon tea, and Utah Juniper (Table 1.1). The Moab site has severe temperature fluctuations between day and night with a mean annual temperature (MAT) of 10.1°C, and a lower mean annual precipitation (MAP) of 320 mm than the other sites (Table 1.1) The Colorado Plateau is impacted by overgrazing and other cultural activities, leading to significant soil loss (Neff et al., 2005; Duniway et al., 2018; Nauman et al., 2018). The literature suggests that most of the dust

deposited in the Colorado Plateau is of local origin or regional from surrounding deserts (Reynolds et al., 2006; Neff et al., 2005).

The Niwot Ridge (Niwot) sites are an alpine ecosystem located 24 km west of Boulder, Colorado, in the Southern Rocky Mountain Range (Fig. 1.1). The Niwot is a Long-Term Ecological Research (LTER) site and is maintained and managed by the University of Colorado Mountain Research Station (<https://www.colorado.edu/mrs/>). The dominant soil at the site is classified as a Haplocryol. These soils are developing from a parent material of Rocky Mountain glaciofluvial deposits (12-30 Ka that overlie residuum weathered from granite, gneiss, and schist of Precambrian age (Table 1.1). The vegetation consists of low stature plants such as alpine bluegrass, alpine clover, alpine, sagebrush, elk sedge, Fern Ally, and timber oak grass (Table 1.1). The MAT is the lowest of all sites at 0.3°C, and the MAP is the highest at 1005 mm (Table 1.1).

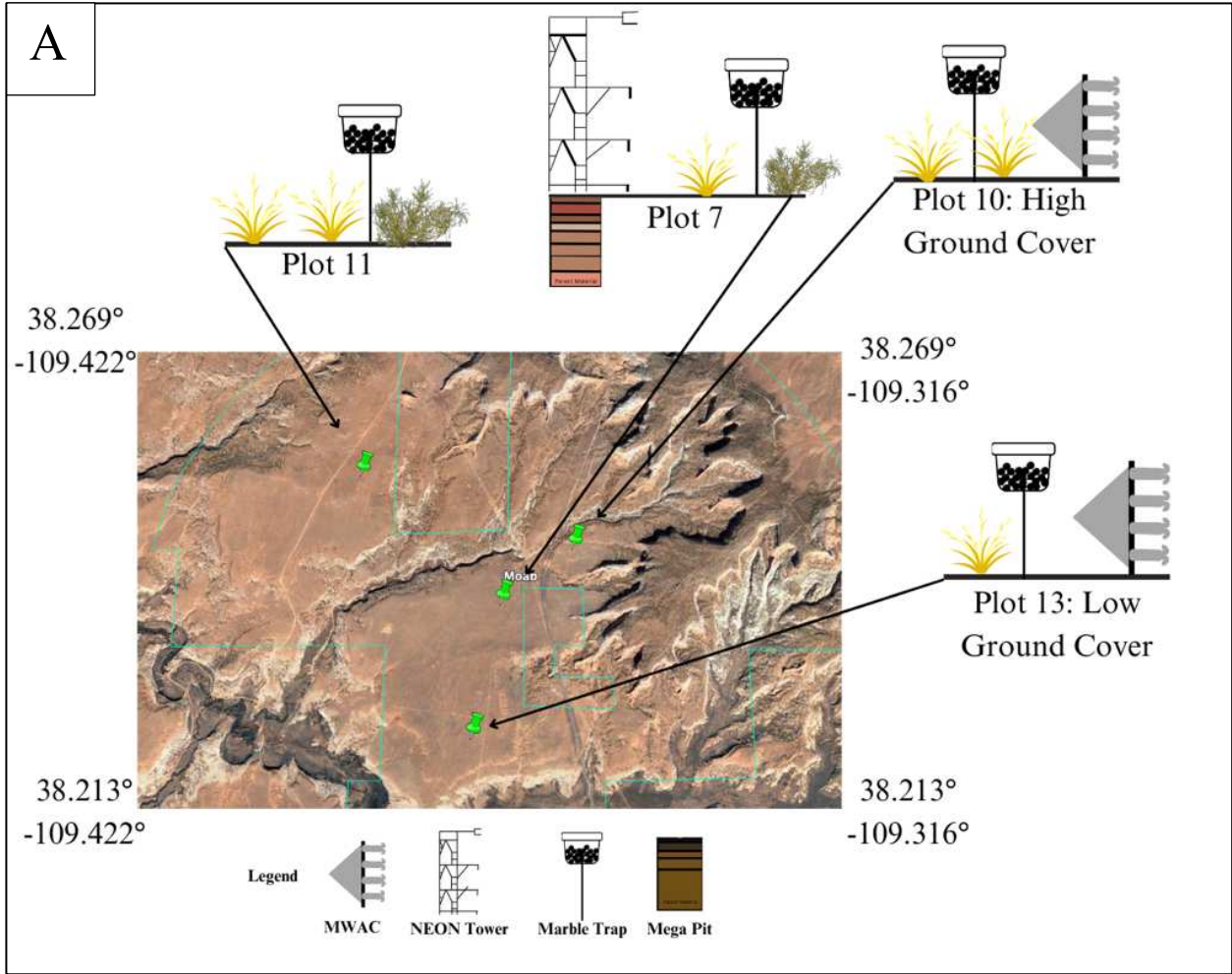
The Central Plains Experimental Range (CPER) study site is within the short-grass steppe ecosystem in the western Great Plains (Fig. 1.1). USDA-ARS manages the land, which is primarily used for research on grazing systems. The dominant soil is classified as an aridic Argiustoll developed from aeolian/alluvial deposits over residuum weathered from the Fox Hills Formation (69-70 Ma) (Table 1.1). The dominant vegetation is blue grama, broom snakeweed, plains prickly pear, sand dropseed, spreading buckwheat, and xanthopormelia lichen. CPER is at an elevation of 1600 m and has a MAT of 8.6 °C and a MAP of 344 mm, and experiences high winds, extreme summer heat, and sub-zero winter temperatures (Table 1.1).

2. EXPERIMENTAL DESIGN

Three sites representative of the bioclimatic domains of the western U.S. were selected for this study. These include Moab, Utah in the Colorado Plateau; Niwot, Colorado in the Rocky Mountain Range; and CPER near Nunn, Colorado in the western Great Plains. At each site, four plots were selected to measure the depositional flux (Fig. 1.2), and two plots were selected to measure erosional flux and particle size respective to differences in percent ground cover (high/low) (Fig. 1.2; Table 1.2). Low and high ground cover plots at Moab and CPER had 43% and 90% ground cover, respectively (Table 1.2). In this study, ground cover was compared within each site, rather than between sites. Therefore, the particle size and flux from the sites were not compared based on their ground cover percentages but were compared based on the relative differences within the domain they represented. Yearly erosional flux at each semi-arid site was determined by obtaining additional erosion samples from the MWACs associated with the National Wind Research Erosion Network (NWREN) at CPER and Moab for the 2021 calendar year. The MWAC samples were analyzed with a grain size analyzer to determine the particle size distribution for the grassland sites (CPER and Moab).

NEON atmospheric filters were collected from Moab for December 30, 2020, to December 12, 2022, from Niwot for December 30, 2020 to December 20, 2022, and from CPER from December 22, 2020 to December 28, 2022, in order to determine how the chemical dust deposition varies at each site and season. Sampling of the NEON filters was carried out every two weeks from the NEON tower at each site. This sampling frequency made them an appropriate method for determining the chemical characteristics of the dust, as it allowed for the accounting of seasonal variations. The collection dates for the filters obtained from NEON are in Appendix B.1.

The data from the NEON Pedons (referred to as megapits) were utilized to determine the chemical and volumetric contribution of dust to the soil at each site. Megapits were considered to reflect the dominant (e.g., common, or abundant) soil within each of the bioclimatic domains. The NEON biomesonet tower was built on top of the selected NEON megapit pedon after it was pedologically characterized and sampled. These data include the morphological and chemical data from the soil horizons of each pedon. The physical and chemical characterization data from the pedons were used to determine the volumetric change as well as the chemical losses and additions within each site. Overall, the contemporary flux, physical, and chemical characteristics of the erosion and deposition samplers were used along with the geochemical mass balance results of the ancient soil to address the main question of how dust generation and deposition impacts the soils within the bioclimatic domains of the western U.S.



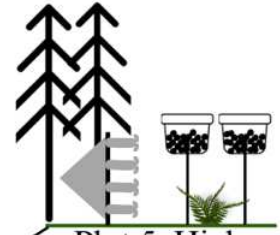
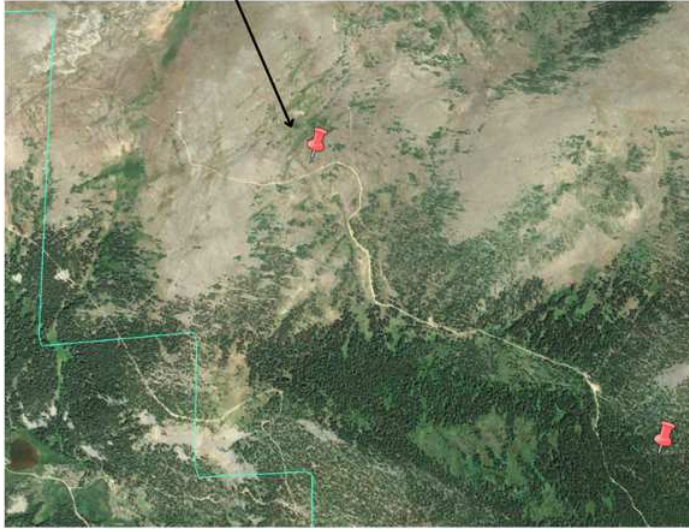
B

40.060°
-105.602°



Plot 18: Low
Ground Cover

40.060°
-105.553°

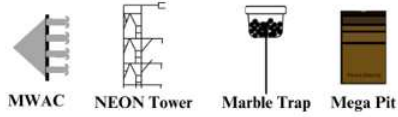


Plot 5: High
Ground Cover

40.038°
-105.602°

40.038°
-105.553°

Legend



MWAC

NEON Tower

Marble Trap

Mega Pit

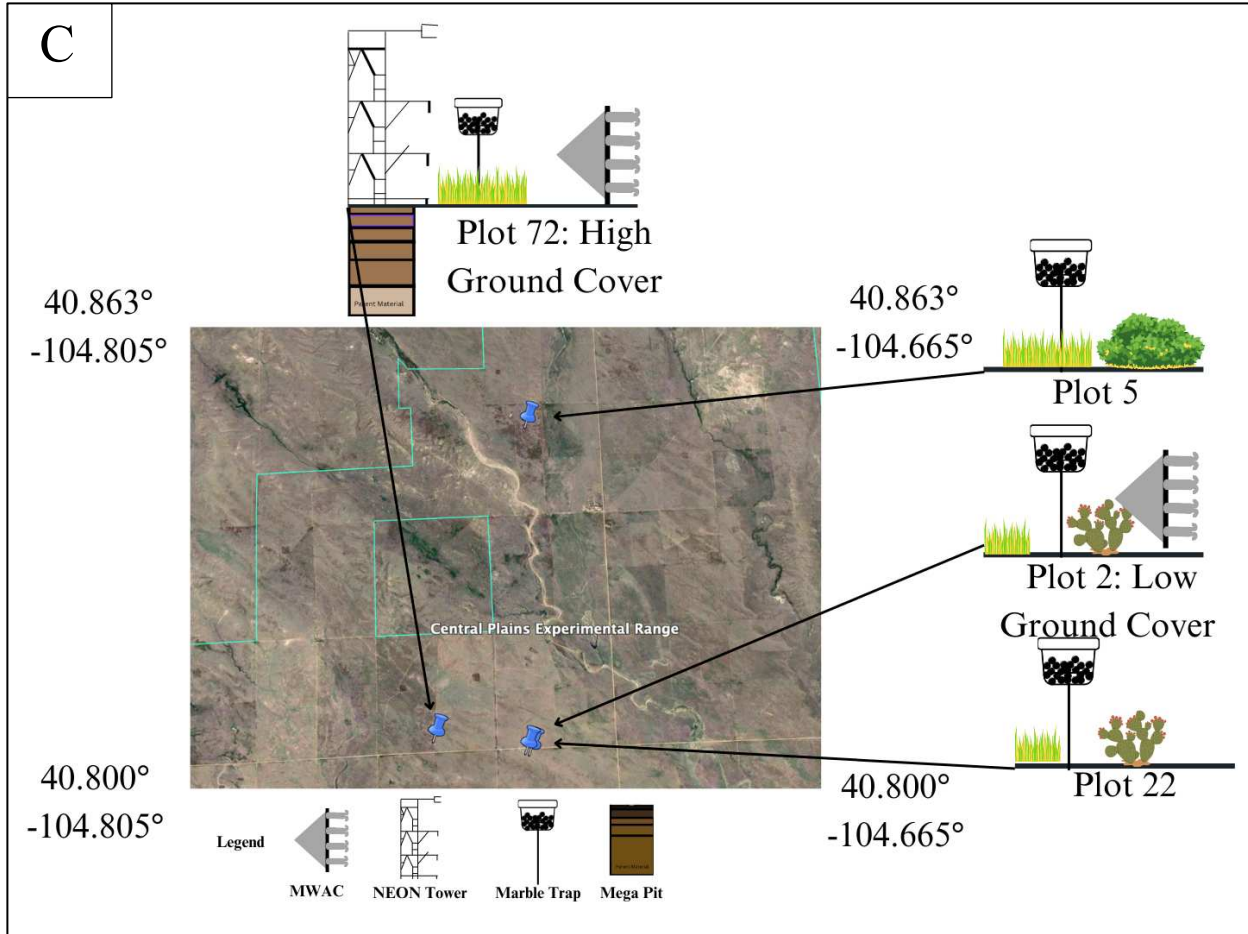


Figure 1.2. Distribution of the samplers at (A) Moab, (B) Niwot, and (C) CPER. The MWACS (1.5 m height) were in of low or high ground cover. The marble traps (2 m height) were in areas that were representative of the variations within site. The Megapit pedons were located underneath each Neon tower to a depth of 200 cm. The atmospheric filters were mounted at the top of each Neon Tower (8 m) at each site. The exact location of each plot is detailed in Table 1.3 and the ground cover percentages are detailed in Table 1.2.

Table 1.2. Site information for the low and high ground cover plots. The percent ground cover was determined by averaging line intercept and transect methods. The signs of erosion were characterized at each site and the soil type data were obtained from the NRCS Web soil survey (websoilsurvey.sc.egov.usda.gov/App/WebSoilSurvey.aspx).

Site	Plot	Ground Cover (%)	Ground Cover Type (Low/High)	Main Vegetation	Signs of Erosion	Soil Type
Moab	10	46	High	Galleta Grass and sagebrush	Pedestaling Class 4	Haplocambid
Moab	13	36	Low	Galleta Grass, sagebrush, and juniper	Pedestaling Class 3	Calciargid
NWREN Moab	N/A	74	N/A	Galleta Grass, sagebrush, and juniper	N/A	Haplocambid
NWREN CPER	N/A	95	N/A	Buffalo Grass, Western Wheat Grass	N/A	Argiustoll
CPER	2	71	Low	Western Wheat Grass and Prickely Pear Cactus	Pedestaling Class 3	Haplargid
CPER	72	90	High	Buffalo Grass, Western Wheat Grass	none	Argiustoll
Niwot	18	95	Alpine	cushion plants, Artemesia, Carex, and low lying alpine wildflowers	none	Dystrocrycept
Niwot	5	95	Sub-Alpine	Lodgepole pines, sub alpine firs, and Grouss Whortleberry	none	Dystrocrycept

3. METHODS

3.1 FIELD METHODS

Within each NEON Domain (terrestrial field sites), soil pits were excavated by NRCS personnel. One soil pedon was characterized and sampled to a depth of ~200 cm (or to a restricted layer) near the biomesonet towers (Table 1.3). Analyses were performed by the NRCS

Kellogg Soil Survey Laboratory. Samples of the pedons were used in this research for mass balance analysis and for soil characterization (Anonymous 2, 2022).

The ground cover at each site was determined using the line-point intercept method (Herrick, 2005), where a flag was dropped every meter for ten meters, and the vegetation that the flag touched or bare soil it landed on was recorded to determine percent bare ground. The line point intercept data were averaged with sampling hoop data where a hoop was randomly thrown in different areas of the plot ten times, and the average area of the ground cover was recorded (Table 1.2).

Traditional marble traps (Reheis & Kihl, 1995) were utilized to capture vertical wet and dry dust deposition at each site. The marble trap consists of marbles suspended on a hardware mesh, filled 2 cm from the top of a collection pan on a 2 m stake (Fig. 1.3). The marble traps were installed at all the sites, one at each of the four plots at CPER and Moab and two at each of the two plots at Niwot (Table 1.3). The sites were chosen as representatives of the variation within each site (different dominant plant species and different soil types) (Fig. 1.2). Samples were collected by suspending the dust within the marble trap in water, collecting the dust water, and vacuum filtering the sample through a 0.2 PES micron filter. The samples from the marble traps were collected seasonally to give time for the dust to accumulate. At Moab, the marble traps were installed May 18, 2022, and sampled September 24, 2022 and November 12, 2022. At Niwot, the marble traps were installed June 24, 2022, and sampled September 15, 2022. At CPER, the marble traps were installed June 9, 2022, and sampled September 7, 2022 and December 6, 2022.

Since dust characteristics have been found to change seasonally (Wells et al., 2007; Aciego et al., 2017; Heindel et al., 2020) based on dust provenance, the seasons for each site were determined based on the dominant wind direction of each month whereas months with similar wind directions at each site were grouped into a season (Table 1.4). The dominant wind direction and wind speed per month was determined based on wind roses from each site (Anonymous 1, 2021; Kittel et al., 2015; Fig.1.5). Notably, the highest wind speeds at Moab were in the spring from the southwest, Niwot in the winter from the west, and CPER in the spring and fall from the north (Appendix A.1-A.3).

NEON atmospheric dust filters were retrieved and analyzed to estimate deposition. The atmospheric filters were mounted on biomesonet towers and collected by NEON and processed by the Colorado Department of Public Health (CDPHE). The 8x10 inch filter paper (Pallflex Tissuquartz manufactured by Pall) was placed within the EcoTech Hivol 3000 collector, which continuously pumped air horizontally through the filter at 68 cubic meters per minute, collecting particulates that were less than 10 micrometers in diameter. The filters accessed and analyzed for this study were collected from December 2020 to December 2022 the exact sampling periods for the filters at each site are in Appendix B.1.

The Modified Wilson and Cook (MWAC) Method (Webb et al., 2015) was utilized to measure soil erosion at different heights. The MWAC consists of four aluminum cans with L-shaped tubes fixed to the lids. The cans were placed horizontally at four heights (10, 25, 50, and 85 cm) and were mounted to a wind vane that moved with the prevailing wind direction (Fig.1.4). One MWAC was installed at the low and high ground cover plots at CPER and Moab and one at each of the subalpine and alpine plots at Niwot according to the experimental design. The MWACs were collected monthly at Moab from May 18, 2022 to March 4, 2023, at Niwot

from June 24 to September 15, 2022, and at CPER from June 9, 2022 to March 3, 2023 (Table 1.3). Erosion samples were also obtained from NWREN from their MWAC samplers at Moab and CPER from January to December 2021.



Figure 1.3. Marble trap at Niwot site.



Figure 1.4. MWAC and marble trap at CPER site.

Table 1.3. Site information, including location, elevation, landscape type, sampling time, and soil type, for the Moab, CPER, and Niwot plots.

Site	Plot Number	Sampler Collection Type	Latitude (Degree)	Longitude (Degree)	Elevation (m)	Landscape Type	Soil Type	Sampling Period
Moab	13	Deposition	38.231889°	-109.393642°	1770	Shrubland	Calciargid	5/18/22 - 11/14/22
Moab	13	Erosion	38.231889°	-109.393642°	1770	Shrubland	Calciargid	5/18/22 - 03/14/23
Moab	7	Deposition	38.247927°	-109.389399°	1800	Shrubland	Calciargid	5/18/22 - 11/14/22
Moab	11	Deposition	38.264449°	-109.412123°	1800	Shrubland	Calciargid	5/18/22 - 11/14/22
Moab	10	Deposition	38.254960°	-109.378116°	1800	Shrubland	Haplocampid	5/18/22 - 11/14/22
Moab	10	Erosion	38.254960°	-109.378116°	1800	Shrubland	Haplocampid	5/18/22 - 03/14/23
Moab	1	Mega Pit soil	38.251360°	-109.388820°	1800	Shrubland	Haplocalcids	4/26/16
Moab	1	PM<10 Filter	38.251360°	-109.388820°	1800	Shrubland	Haplocalcids	12/30/20 - 12/12/22
Niwot	5	Deposition	40.043489°	-105.570411°	3475	Sub-Alpine	Dystocryept	6/24/22 - 9/15/22
Niwot	5	Deposition	40.043489°	-105.570411°	3475	Sub-Alpine	Dystocryept	6/24/22 - 9/15/22
Niwot	5	Erosion	40.043489°	-105.570411°	3475	Sub-Alpine	Dystocryept	6/24/22 - 9/15/22
Niwot	18	Deposition	40.052611°	-105.583639°	3290	Alpine	Dystocryept	6/24/22 - 9/15/22
Niwot	18	Deposition	40.052611°	-105.583639°	3290	Alpine	Dystocryept	6/24/22 - 9/15/22
Niwot	18	Erosion	40.052611°	-105.583639°	3290	Alpine	Dystocryept	6/24/22 - 9/15/22
Niwot	1	Mega Pit soil	40.052360°	-105.583240°	3475	Alpine	Haplocryolls	8/19/18
Niwot	1	PM<10 Filter	40.052360°	-105.583240°	3475	Alpine	Haplocryolls	12/30/20 - 12/20/22
CPER	72	Deposition	40.813444°	-104.744417°	1682	Grassland	Argiustoll	6/9/22 - 12/06/22
CPER	72	Erosion	40.813444°	-104.744417°	1682	Grassland	Argiustoll	6/9/22 - 03/03/23
CPER	2	Deposition	40.811500°	-104.729806°	1650	Grassland	Haplargid	6/9/22 - 12/06/22
CPER	2	Erosion	40.811500°	-104.729806°	1650	Grassland	Haplargid	6/9/22 - 03/03/23
CPER	22	Deposition	40.811333°	-104.729222°	1650	Grassland	Haplargid	6/9/22 - 12/06/22
CPER	5	Deposition	40.852444°	-104.727722°	1673	Grassland	Argiustoll	6/9/22 - 12/06/22
CPER	1	Mega Pit soil	40.812970°	-104.744550°	1682	Grassland	Argiustoll	3/21/16
CPER	1	PM<10 Filter	40.812970°	-104.744550°	1682	Grassland	Argiustoll	12/22/20 - 12/28/22

Table 1.4. The season sampling scheme based on wind roses wind direction per site per month data, which is presented in Appendix A. Wind rose data was taken from Kittel et al., 2015 for Niwot wind roses and Iowa Environmental Mesonet (https://mesonet.agron.iastate.edu/sites/windrose.phtml?station=CNY&network=UT_ASOS)

Sites	Season	Sampling Time Period	Wind Direction
Moab	Winter	Jan - Feb	NW
Moab	Spring	Mar - Jun	SW
Moab	Summer	Jul - Sept	SE/SW
Moab	Fall	Oct-Dec	NW
Niwot	Winter	Jan - Mar	W
Niwot	Spring	Apr - May	E/W
Niwot	Summer	June - Sep	E/W
Niwot	Fall	Oct - Dec	W
CPER	Winter	Jan - Feb	N/NW
CPER	Spring	Mar, April	W
CPER	Summer	May - Sept	S
CPER	Fall	Oct-Dec	N/NW



Windrose Plot for [CNY] MOAB/CANYONLANDS
Obs Between: 01 Mar 1973 03:00 PM - 26 Nov 2022 12:53 AM America/Denver

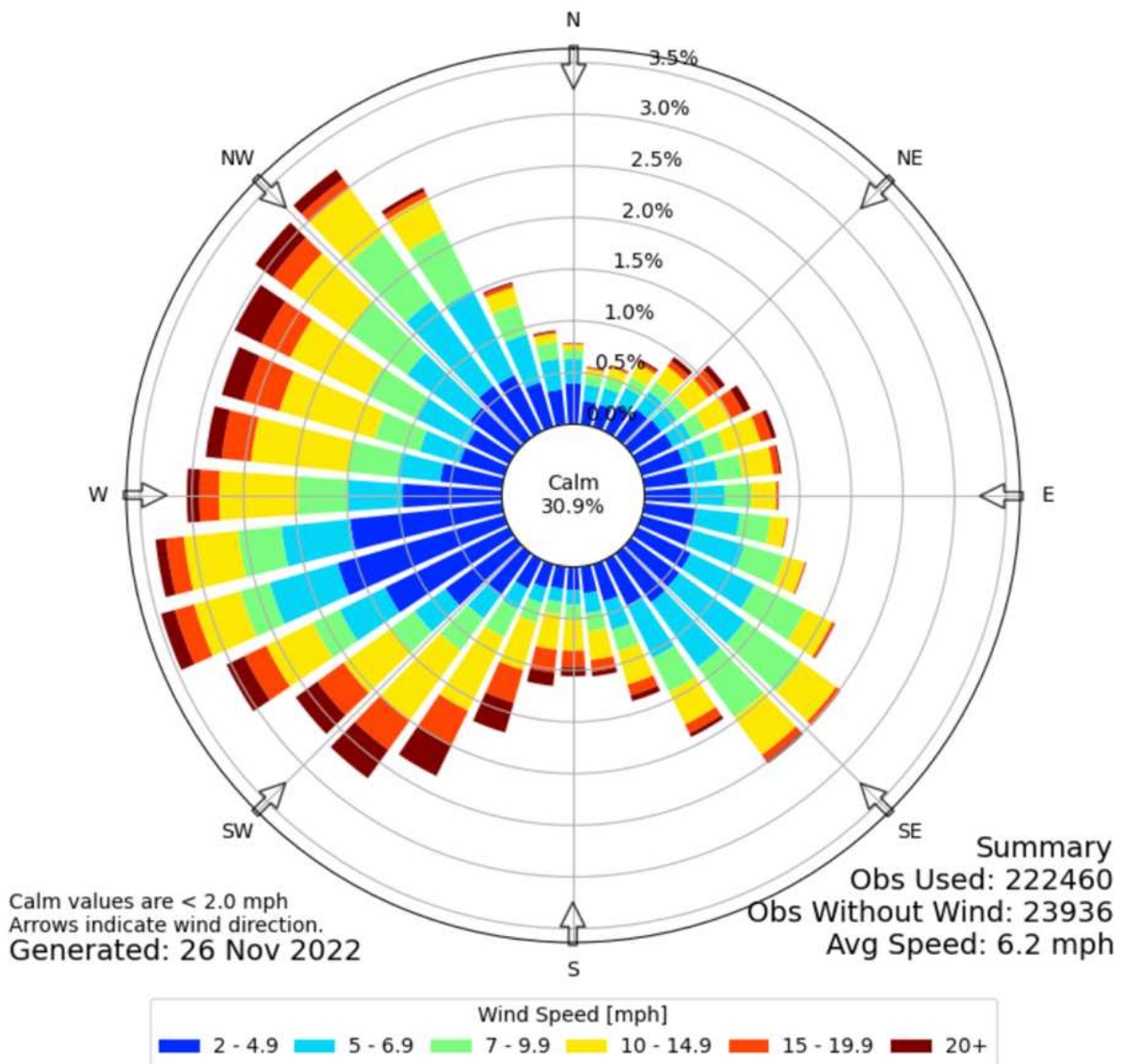


Figure 1.5. Wind rose of wind direction and wind speed averaged over March 1973 (15:00) to November 2022 (1:00), Canyonlands, UT. Wind roses for all months and sites are in Appendix A. Observations from Data taken from Iowa Environmental Mesonet (https://mesonet.agron.iastate.edu/sites/windrose.phtml?station=CNY&network=UT_ASOS)

3.2 LABORATORY METHODS

The NEON pedon soil samples were previously analyzed for total elemental data using an Inductively Coupled Mass Spectrometer (ICP-MS) at the NRCS Laboratory in Lincoln, Nebraska and used the Kellogg Soil Survey Laboratory Methods for acid digestion (Soil Survey Staff, 2014).

Soil, marble trap, and NEON filter samples were analyzed with a benchtop X-ray Fluorescence Spectrometer (XRF) for total elemental data at the Colorado State University Powerhouse Energy Campus Air Quality Research Laboratory. Samples for XRF analysis were prepared with a 50 mg subsample from each soil horizon, eight Moab marble traps, six CPER marble traps, and one Niwot marble trap. Each sample was aerosolized onto a 37 mm MTE PTFE filter and analyzed using an ARL QUANT'X EDXRF Spectrometer, drawing air at 6 L/min for five minutes. The NEON filters did not have to be aerosolized but were analyzed using the same ARL QUANT'X EDXRF Spectrometer. The elements measured were Na, Mg, Al, Si, P, S, K, Ca, Ti, Mn, Fe, Sr, Pb, and Zn. Soil standards of each element were obtained and used for the XRF analysis, and blank filters for the NEON and soil/dust filters.

The ICP-MS results for the soil pedons were used to determine the geochemical mass balance, and the XRF results for the soil, marble trap, and filter samples were used to assess dust contribution to soil and dust chemical characteristics at each site.

Particle size (range of 2.5 to 500 microns) was determined for MWAC samples at the Utah State University Watershed Science Clean Lab using a LISST grain size analyzer after samples were prepared with 20 mL of 3% sodium hexametaphosphate (NaHMP). They were

manually shaken and left overnight and then agitated on a shaker at 200 rpm for 30 minutes and placed in an ultrasonic bath for 10 minutes to disperse particles for analysis.

Since particle size does not change seasonally, we were able to analyze from months that had significant sample mass, or we combined samples to obtain enough mass for analysis.

NWREN samples were obtained from all can heights to measure the overall particle size distribution for Moab from April 7 to June 3, 2021 and for CPER from May 20 to November 15, 2021. To measure the particle size variability within the grassland sites, CPER samples were obtained for 10 and 25 cm can height from June 9 to December 6, 2022. The Moab samples were obtained for all can heights from June 21 to July 12, 2022, and September 24 to November 14, 2022.

CHAPTER 2: SOIL MASS BALANCE RESULTS AND DISCUSSION

1. INTRODUCTION

Soil contains layers of weathered material (soil horizons) that undergo chemical and physical transformations due to the underlying parent material and surface interactions. Soil weathering processes that may include those of aeolian origin such as dust deposition or soil erosion (Eberly et al., 1996; Brimhall et al., 1988) are catalysts in transforming the parent material into the soil to form aggrading or degrading systems (Brimhall & Dietrich, 1985). Aggrading systems are fundamental to supporting ecosystem function and expansion because they are elementally enriched from parent material or exogenous sources. Dust deposits are composed of biological materials, mineral grains, and rock fragments. These materials contain chemical elements that transfer through the soil via water and either accumulate within or are lost from soil horizons.

The aeolian processes that form aggrading and degrading systems can be observed through the mass balance model (Chadwick et al., 1990; Lawrence et al., 2013). The approach can be used to calculate the fate and transport of elements during soil evolution (weathering, neoformation, and leaching). For this research, the mass balance model will be utilized to determine if volumetric change and elemental enrichment and/or depletion are occurring throughout the period of soil formation.

2. SECTION OBJECTIVES AND METHODOLOGY

2.1 SECTION OBJECTIVES

This chapter aims to identify the key soil-forming processes and environmental conditions that influence soil aggradation and degradation within and among soils from the three sites. To achieve this objective, the NEON pedon chemical and morphological characteristics were utilized in the mass balance model to determine the processes driving soil formation.

2.2 MASS BALANCE DETERMINATIONS

The Constituent Mass Balance approach is commonly used to determine the extent of pedogenesis by measuring the soil volumetric changes and elemental movement during pedogenesis (Brimhall & Dietrich, 1985; Chadwick et al., 1990). Soils are determined as aggrading or degrading based on the pedon-scale strain measurements of volumetric collapse or dilation and elemental depletion or enrichment, respectively (Eq. 2.1, from Brimhall and Dietrich, 1985).

$$\varepsilon_{i,w} = \frac{\rho_p C_{i,p}}{\rho_w C_{i,w}} - 1 \quad \text{Equation 2.1}$$

Strain ($\varepsilon_{i,w}$) determines the volumetric change by comparing the difference of the immobile element concentration and bulk density in the parent material to each weathered soil horizon within the soil profile (Eq. 2.1). Where ρ_p is the bulk density of the parent material, ρ_w is the

bulk density of the weathered horizon, $C_{i,p}$ is the concentration of an immobile element in the parent material, and $C_{i,w}$ is the concentration of an immobile element in the weathered horizon. The immobile element may be either zirconium (Zr) or titanium (Ti) and can be determined by independently correlating the strain value of Zr and Ti against the percent clay and sand (Chadwick et al., 1999). For this study, Ti was less correlated to percent clay and sand throughout the soil profile than Zr, so it was used as the ‘immobile’ elemental for all sites. The limitations to the mass balance equations are that the approach is highly dependent on knowing the origin and composition of the parent material at $t=0$ and the model assumes that parent material is homogenous (Chadwick et al., 1999; Lawrence et al., 2013). To address these limitations, a 10% uncertainty factor was incorporated in the bulk density of the parent material at each site.

The chemical mass transport function ($\tau_{j,w}$) is determined for each known element to detect the element that is contributing to the strain within the soil profile (Eq. 2.2, from Brimhall & Dietrich, 1985). The $\tau_{j,w}$ function is the transport function for an element (j) within a weathered horizon (w). $\tau_{j,w}$ values between -1 to 1, indicate elemental mass is from the parent material and $\tau_{j,w}$ values above 1 indicate enrichment from an external source (e.g., dust deposition). Negative $\tau_{j,w}$ values indicate element depletion relative to the parent material. For example, a $\tau_{j,w}$ value of -0.5 suggests that 50% of the mass of element j in the parent material may have been extracted during weathering and transported to lower horizons. A $\tau_{j,w}$ value of 0 indicates that the element is immobile (Chadwick et al., 1999). Conclusions can be drawn about the contribution of dust within the soil profile by mapping the elemental mass transport function with depth in the soil profile. Moreover, elements that are not common within the mineralogy of

the parent material but have a positive mass transport function within the soil profile could be due to dust deposition (Brimhall & Dietrich, 1985; Lawrence et al., 2013). In this experiment, the elements sodium (Na), calcium (Ca), magnesium (Mg), potassium (K), silicon (Si), and phosphorous (P) were chosen as elements to be observed in the elemental mass transport function equation due to their high concentration within dust deposition and relative importance as plant nutrients within the soil.

$$\tau_{j,w} = \frac{\rho_w C_{j,w}}{\rho_p C_{j,p}} (\varepsilon_{i,w} + 1) - 1 \quad \text{Equation 2.2}$$

3. RESULTS

3.1 SOIL CLASSIFICATION

The pedological soil classification at each site indicates the extent of soil weathering and the factors contributing to the soil development. The soil at Moab is a Haplocalids (Aridisol soil order), a typical soil of desert ecosystems with a calcic horizon. Niwot's soil was classified as a Haplocryoll, which indicates the soil has minimal soil horizonation and is in the cryic temperature regime (0-8 °C). Moreover, the soil is of the order mollisol, a well-developed soil characterized by a dark organic matter-rich surface horizon. CPER's soil is classified as an Argiustoll, a mollisol with a clay horizon, and in the ustic moisture regime (dry).

3.2 SOIL MORPHOLOGY

The soil color, horizon differentiation, and other soil properties (e.g., pr) reflect long term soil development. The Moab soil is reddish in color (2.5YR) throughout the soil profile indicating high amounts of iron oxidation (Table 2.1). On the other hand, the Niwot soil has a dark brown (7.5YR 2/1) surface horizon indicating a significant percentage of organic matter. The soil at CPER has similar coloration throughout the soil profile (10YR 5/3). The Bk soil horizons at Moab and CPER indicate accumulation of carbonates, while the Bt horizon at CPER indicates clay accumulation. Niwot is least developed as indicated by the presence of Bw horizons.

Physical properties, such as texture and bulk density, vary among the sites, with CPER and Moab being the most similar in physical composition than Niwot. Niwot has a higher percent of silt (38%) and clay (13%) fractions within the surface horizon than any other site, whereas CPER and Moab are composed of greater than two-thirds sand (Table 2.1). The texture is like the composition of the parent material from which the soils are developing. CPER and Moab are developing from sandstone, and Niwot's soil is forming from glacial till containing a mixture of metamorphic rocks (schist and gneiss). The bulk density of the soil is related to the texture, where a higher component of silt and clay particles decreases the bulk density. Therefore, the lowest bulk density within the surface horizon was at Niwot (1.0 g/cm^3), whereas CPER and Moab have a similar bulk density of about 1.5 g/cm^3 (Table 2.1).

Table 2.1. The physical and chemical characteristics of the soil at each site. The data for this table were obtained by the pedological and chemical characteristics from NEON website (<https://data.neonscience.org/data-products/DP1.00096.001>).

Site	Horizon	Horizon Depth (cm)	Thickness (cm)	Color	Sand %	Silt %	Clay %	Bulk Density (gcm-3)	pH
Moab	A	0-6	6	5YR 5/6	73	20	7	1.5	6.7
Moab	Bw	6-31	25	2.5 YR 4/6	71	17	12	1.5	8.5
Moab	Bk1	31-47	16	5YR 5/6	66	17	17	1.4	8.8
Moab	Bk2	47-62	15	5YR 7/4	70	14	16	1.2	8.8
Moab	Bk3	62-82	20	5YR 6/6	80	10	9	1.6	9.0
Moab	Ck	82-116	34	5YR 6/6	82	10	7	1.5	8.9
Moab	C1	116-160	44	5YR 6/6	87	8	5	1.7	8.9
Moab	C2	160-200	40	5YR 6/6	78	16	6	2.0	8.7
Niwot	A1	0-14	14	7.5YR 2.5/1	49	38	13	1.0	5.2
Niwot	A2	14-30	16	7.5YR3/2	62	25	13	0.9	5.2
Niwot	Bw1	30-49	19	7.5YR 4/3	81	13	7	0.9	5.3
Niwot	Bw2	49-79	30	7.5YR 4/3	72	23	5	1.2	5.5
Niwot	2C	79-100	31	7.5 YR 4/4	70	27	3	1.1	5.7
Niwot	2C/Cr	110-200	90	7.5 YR 4/4	81	16	3	1.2	6.0
CPER	A	0-10	20	10YR 5/3	72	17	12	1.5	7.8
CPER	BA	10-30	20	10YR 5/3	74	14	12	1.5	6.9
CPER	Bt1	30-54	24	10YR 5/3	67	14	20	1.5	7.5
CPER	Bt2	54-81	27	10YR 5/3	49	28	24	1.7	8.1
CPER	Bk1	81-137	56	10YR 5/3	60	17	23	1.7	8.4
CPER	Bk2	137-181	44	10YR 5/3	59	20	21	1.7	8.4
CPER	2C	181-210	29	10YR7/2	53	21	26	1.9	8.3

3.3 MASS BALANCE STRAIN

The strain results (Fig. 2.1) indicate the volumetric changes in the soils relative to the parent material. The C2 horizon (160-200 cm) represents the parent material horizon at Moab utilized for the mass balance determinations. The strain results at Moab indicate a volumetric collapse of 24% within the A and Bw horizons (0-31 cm) (Fig. 2.1). The Bk, Bk2, Ck, and C1 horizons are dilated by 5.7%, 98%, 76%, and 62% respectively (Fig. 2.1).

The 2C/Cr horizon (100-180 cm) represents the parent material horizon at Niwot utilized for the mass balance determinations. The strain results at Niwot indicate a volumetric dilation of

about 25% within the A horizons (0-30 cm) (Fig. 2.1). The Bw1, Bw2, and 2C horizons are dilated by 55%, 13%, and 4.8%, respectively (Fig. 2.1).

The 2C horizon (180-200 cm) represents the parent material horizon at CPER utilized for the mass balance determinations. The strain results at CPER indicate a volumetric dilation of about 35% within the A horizons (0-30 cm) (Fig. 2.1). The Bt1, Bt2, Bk1, and Bk2 horizons are dilated by 37%, 44%, 20%, 12%, and 16% respectively (Fig. 2.1).

The dilation trend of Niwot is similar to CPER, where there is more dilation occurring in the subsurface than in surface horizons. The soil at Moab, Niwot, and CPER dilate in the subsurface, but they occur at different depths. For Moab, the dilation occurs at 62-116 cm, but at Niwot and CPER, the greatest amount of dilation occurs closer to the surface soil, at 30-49 cm. The mass balance equation indicates that only Moab experiences soil collapse, compared to CPER and Niwot, which are dilating in all soil horizons.

To test the mass balance assumption of parent material homogeneity, the strain equation was conducted for the bulk density of the parent material with a 10% change, and the differences between the original strain and tested strain are the error values presented in Table 2.2. The sign of the strain values did not change for any of the horizons at Moab, Niwot and CPER when accounting for uncertainty except for the 2C horizon at Niwot ($4.8 \pm 10\%$) (Table 2.2). This suggests that the collapsing and dilating trends as well as the mass transport functions are accurate for Moab, CPER, and in general, Niwot.

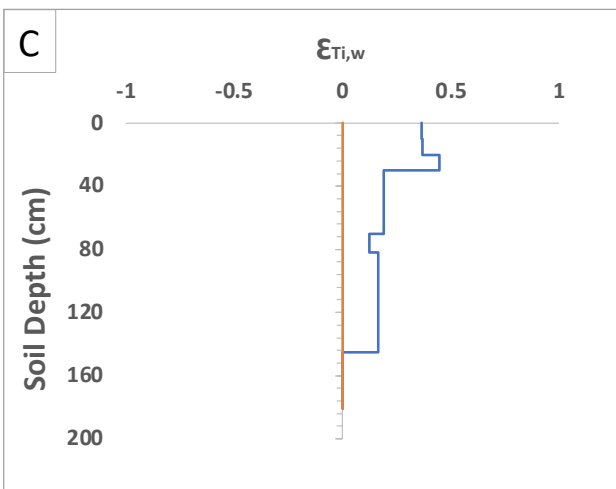
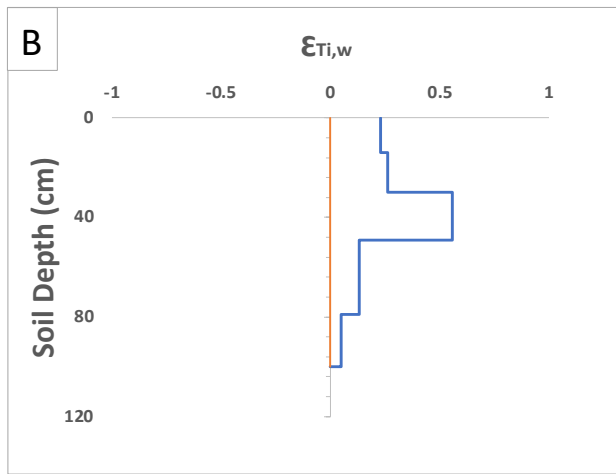
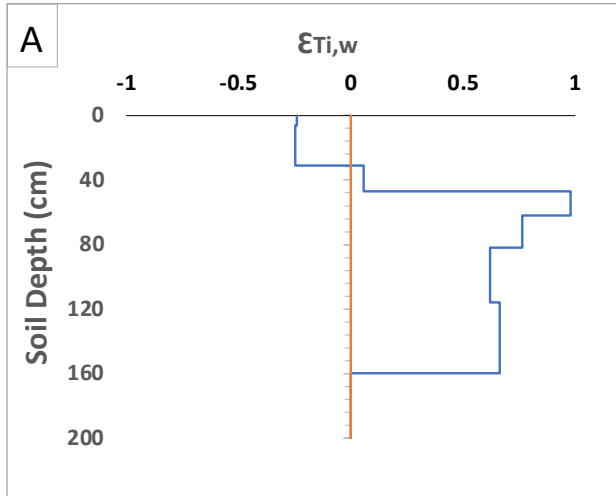


Figure 2.2. The strain (ϵ) ratio as a function of soil depth using Ti as the immobile element for Moab (A), Niwot (B), and CPER (C).

Table 2.2. The strain (ϵ) and mass transport values (τ) in percent values as a function of soil depth (cm) for Ca, K, Mg, Na, P, and Si for each horizon (w) at Moab, Niwot, and CPER. The uncertainty in the strain values is associated with the 10% change in the bulk density of the parent material. Strain and mass transport were calculated using Ti as the immobile element.

Site	Horizon Name	Top Depth	Strain (ϵ) (%)	τ Ca,w (%)	τ K,w (%)	τ Mg,w (%)	τ Na,w (%)	τ P,w (%)	τ Si,w (%)
Moab	A	0-6	-24 \pm 7.6	-97	-45	-22	160	-5	-36
Moab	Bw	6-31	-24 \pm 7.5	-92	-47	-13	120	-34	-42
Moab	Bk1	31-47	5.7 \pm 11	19	-41	27	101	31	-30
Moab	Bk2	47-62	98 \pm 20	300	-30	210	74	110	-12
Moab	Bk3	62-82	76 \pm 18	240	-21	380	27	64	17
Moab	Ck	82-116	62 \pm 16	150	-28	410	14	-15	-8
Moab	C1	116-160	66 \pm 17	160	-16	500	59	70	30
Moab	C2	160-200	0	0	0	0	0	0	0
Niwot	A1	0-14	23 \pm 12	32	87	-4	39	170	-13
Niwot	A2	14-30	26 \pm 12	-1.6	82	-9	30	150	-13
Niwot	Bw1	30-49	55 \pm 16	-21	150	-17	41	90	14
Niwot	Bw2	49-79	13 \pm 11	-26	120	-11	29	55	5
Niwot	2C	79-110	4.8 \pm 10	-16	90	18	19	-46	-11
Niwot	2C/Cr	110-200	0	0	0	0	0	0	0
CPER	A	0-10	36 \pm 14	-61	34	-45	52	36	18
CPER	BA	10-30	37 \pm 14	-70	38	-50	54	36	18
CPER	Bt1	30-54	44 \pm 14	-64	32	-17	37	-2	21
CPER	Bt2	54-81	20 \pm 12	-60	12	-1.3	19	-26	7
CPER	Bk1	81-137	12 \pm 11	42	2.1	20	18	39	-2
CPER	Bk2	137-181	16 \pm 12	37	16	8.5	32	18	5
CPER	2C	181-200	0	0	0	0	0	0	0

3.4 ELEMENTAL MASS TRANSPORT

The mass transport for Si, Na, P, K, Ca, and Mg were calculated for each soil horizon for all the sites and are depicted in Figure 2.2 to 2.4.

The A and Bw horizons at Moab exhibit a range of 5 to 97% loss of Ca, Si, P, K, and Mg, along with a 160% enrichment of Na relative to the parent material (Fig. 2.2). Among these elements, Ca loss or depletion was 97% in the surface horizon and Ca and Mg are substantially

enriched by 19 to 380% in the subsurface (54-160 cm). Much like Ca and Mg, the soil is depleted of silica in the A-Bk2 horizons by 12 to 36% and enriched in the Bk3 and C1 horizons by 17 to 30% at Moab (Fig. 2.1). The plant essential nutrient, P is depleted by 5 to 34%, within the A and Bw horizons, enriched by 34 to 110% in the Bk horizons, and depleted by 15% within the Ck horizons. Potassium, another plant essential nutrient, is depleted throughout the surface horizon at Moab by 16 to 45% (Fig. 2.1).

The A1 and A2 surface horizons (0-30 cm) at Niwot exhibit an enrichment of most elements such as an 82 to 87% addition of K, 30 to 39% of Na, and 150 to 170% of P (Fig. 2.2). Magnesium and Si are depleted at 4 to 9% and 13%, respectively and enriched by 18% and 5 to 14%, respectively (Fig. 2.2). Calcium exhibits a 32% enrichment at Niwot within the A1 horizon and then a subsequent loss of 1.6 to 26% within the deeper horizons (14-110 cm) (Fig. 2.3). Phosphorous is most enriched at 170% within the surface horizon and is less enriched at greater depths (55 to 150%), eventually showing a 46% loss within the 2C horizon (Fig. 2.3). Potassium is also substantially enriched throughout the soil profile with the greatest enrichment in the subsurface Bw1 horizon at 150% (Fig. 2.2).

Surface horizons at CPER (A and BA) exhibit a 41 to 60% loss of Ca and Mg (Fig. 2.3). The Ca and Mg ions are depleted, ranging from 1.3 to 67%, until reaching the Bk horizons where an enrichment range of 18 to 42% is observed (Fig. 2.3). Like Moab, the Ca and Mg ions within the pedon at CPER are enriched in the Bk horizons due to carbonate formation. Surface horizons are enriched with P, Si, Na, and K by 36%, 18%, 52 to 54 %, and 34 to 38%, respectively (Fig. 2.3). Phosphorus is enriched in the surface horizon, depleted by 2 to 26% at a depth of 30-81cm, and enriched by 18 to 39% at a depth of 81-200cm soil depth (Fig. 2.3).

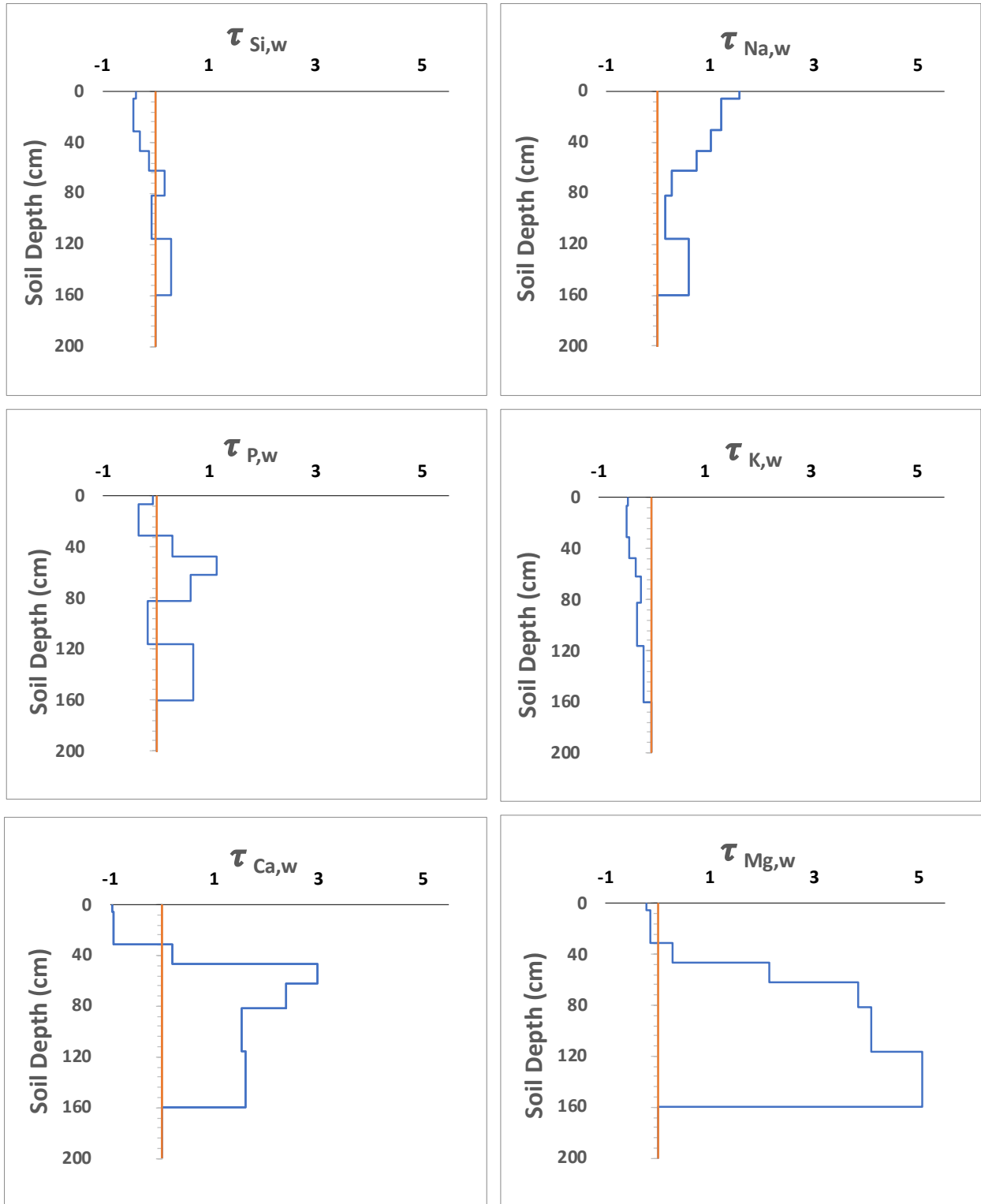


Figure 2.2. The mass transport (τ) ratios for Si, Na, P, K, Ca, and Mg as a function of soil depth for Moab, using Ti as the immobile element.

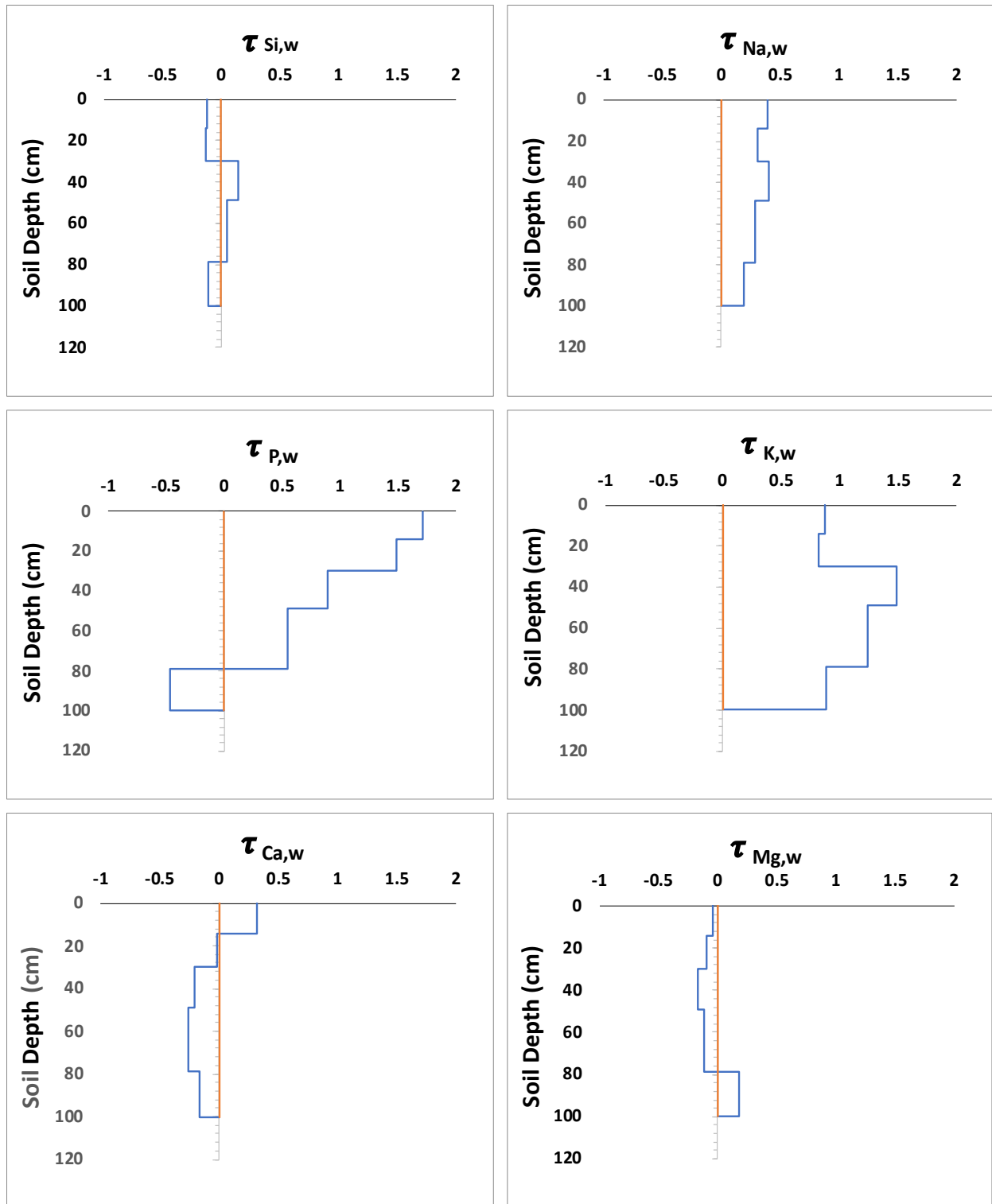


Figure 2.3. The mass transport (τ) ratios for Si, Na, P, K, Ca, and Mg as a function of soil depth for Niwot, using Ti as the immobile element.

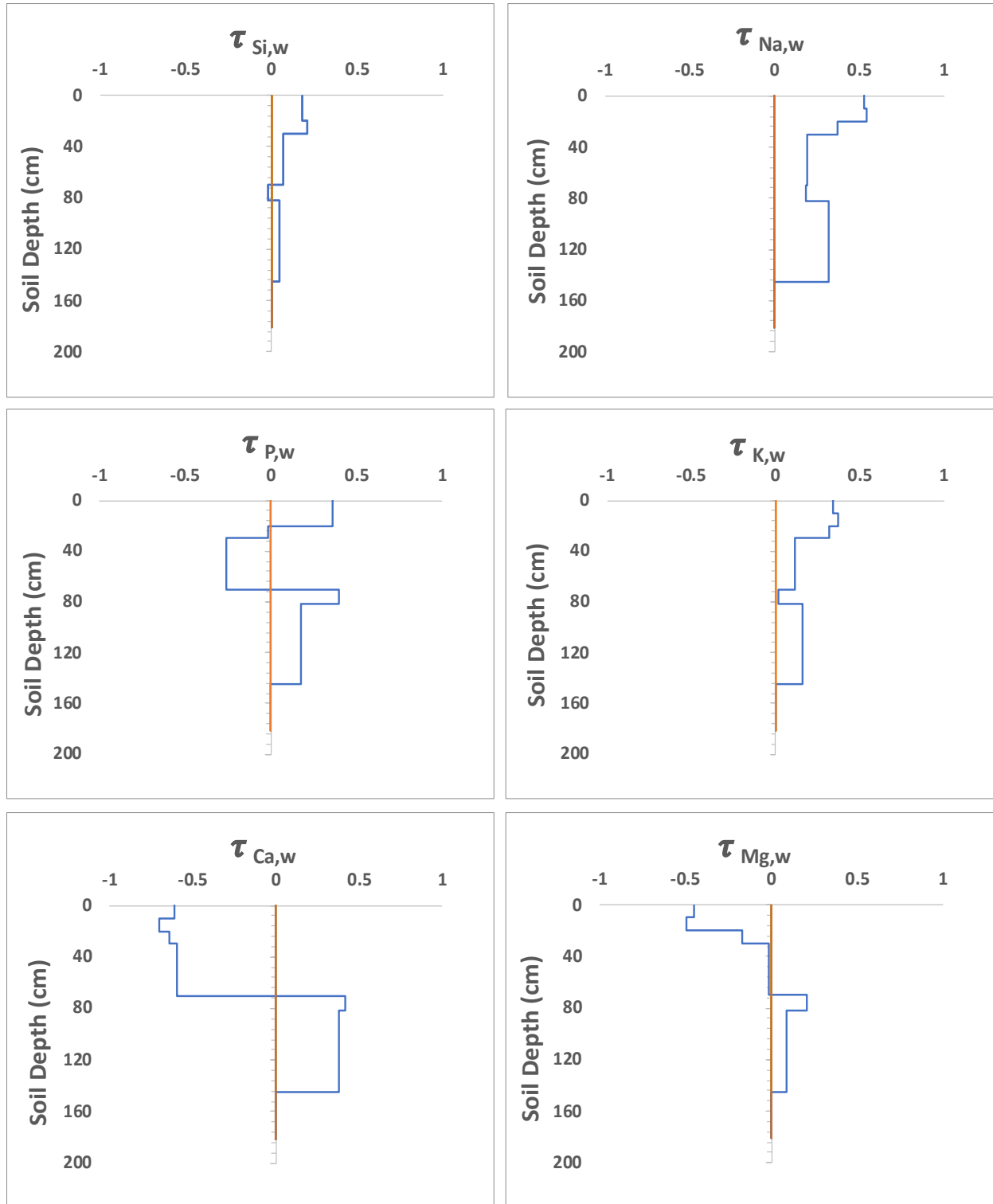


Figure 2.4. The mass transport (τ) ratio for f Si, Na, P, K, Ca, and Mg as a function of soil depth for CPER, using Ti as the immobile element.

4. DISCUSSION

Previous research has revealed that over time the Colorado Plateau ecosystem is both an aeolian source and sink, receiving dust from both local and regional sources and undergoing soil erosion that can result in local and regional deposition (Reynolds et al., 2001; Goldstein et al., 2008; Reynolds et al., 2016). The results from the morphological characteristics of the soil pedon at Moab reflect conditions of low biological activity with high soil color values (light in color), indicating low organic matter content. The physical properties suggest that soils in this system are highly vulnerable to erosion. The physical collapse and depletion of clay-associated elements (Ca, Mg, and K) within the surface horizon could indicate that removal of material is a dominant process (Table 2.1, Figure 2.1).

The Colorado Plateau is an arid grassland with greater evapotranspiration than precipitation, which leads to minimal leaching, limited chemical mineral weathering, and causes certain elements to precipitate out of the soil solution and form carbonates in lower horizons. The enrichment of Na within the surface horizon at Moab is most likely due to Na precipitating out of the soil. The soil pedon at Moab contains carbonate horizons (Bk); therefore, the depletion of Ca and Mg in the surface horizon and accumulation of these elements within the Bk horizon is most likely due to these elements forming carbonate compounds (CaCO_3). Silica is within the matrix of clay particles while Ca and Mg are commonly adsorbed to clay particles. The loss of these elements could be due to the loss of clay seen within the surface horizon of the pedon at Moab (Table 2.1). The loss of K and P throughout the soil profile is most likely due to nutrient uptake by plants. The enrichment of P within the soil could be due to biocycling in which plants remove P from lower horizons to make available at the surface horizon (Read & Campbell,

1981). Overall, the mass balance results indicate that the soil system at Moab is in a degradational phase due to the volumetric and elemental loss within the surface soil. The only element that was not depleted in the surface horizon at Moab was the enrichment of is likely the result of Na (160%) from evapotranspiration resulting in a 2- to 20-fold increase.

The Southern Rocky Mountains is an environment with high precipitation, organic matter, and clay content within the surface horizon, which could lead to chemical mineral weathering, leaching, and elemental accumulation. The accumulation of P, K, and Ca elements within the surface soil could be due to high organic matter and clay content within the surface horizon, retaining ions from leaching to subsurface horizons. The loss of Mg in the soil may result from the displacement of Mg ions due to the enrichment of Ca within the soil, potentially leaching Mg ions to lower depths. Silica loss within the surface soil could be due to chemical weathering, thereby releasing and leaching Si to accumulate within subsurface horizons. Potassium is a major component of minerals such as mica and biotite within metamorphic and igneous rocks such as gneiss, granite, and schist that make up the parent material of the soil at Niwot. The significant presence of K within the soil could be due to the weathering of minerals within the parent material. The accumulation of K in the subsurface horizons can be attributed to the high mobility of K within the soil. The mobile nature of K allows it to readily move throughout the soil profile when leaching occurs. Both P and K had mass transport values greater than 100%, suggesting that along with contributions from mineral weathering these elements are derived from an exogenous source such as dust deposition. Previous alpine research has indicated significant contributions of K, Ca, and P to alpine soil from dust deposition (Lawrence et al., 2010; Brahney et al., 2013, 2014; Aciego et al., 2017; Bergstrom et al., 2019; Munroe, 2022). Research within the Southern Rocky Mountains has also suggested that dust deposition

contributes to the addition of silt and clay within the surface soil (Muhs & Benedict, 2006). Therefore, the retention and significant enrichment of K, Ca, and P could be due to soil contributions from dust deposition at Niwot. Overall, the mass balance results indicate that the soil at Niwot is aggrading due to dilatation values and elemental enrichment in all the soil horizons.

The western Great Plains are a semi-arid environment with relatively low precipitation. The soil at CPER has more overlying vegetation, organic matter, and clay content than Moab. The pedon at CPER contains carbonate horizons (Bk) and clay horizons (Bt), which retain elements leached from the surface horizon. Like Moab, the Ca and Mg ions within the pedon at CPER are enriched in the Bk horizons due to carbonate formation. The enrichment of Si within the surface soil could indicate chemical weathering processes resulting from precipitation. Mineral weathering can lead to the release of Si ions into the soil, contributing to the observed Si enrichment. Similarly, as silicate minerals are weathered, elements such as K and Na may be released leading to an enrichment of these elements within the surface horizon. The additions and losses of P within the soil could be due to biocycling and plant uptake at rooting depth (30-81cm). Unlike Moab and Niwot, at CPER the elemental enrichment is never greater than 100%, suggesting that elemental enrichment is from the weathering of the parent material and not from an exogenous source. Although there is no soil collapse at CPER, the mass balance results at CPER are more like Moab than Niwot, with similar depletion and enrichment patterns for Ca, P, and Na. Similarity between Moab and CPER soil mass balance results suggest that similarity in climatic factors and parent material are proving to be important conditioning variables. These results from the mass balance indicate that the soil at CPER is aggrading due to volumetric dilation and elemental enrichment present throughout the soil profiles.

CHAPTER 3: AEOLIAN FLUXES AND CHARACTERISTICS

1. INTRODUCTION

During the last twenty years, many research projects have attempted to quantify erosion rates in various ecosystems. The results have provided a robust database that allows the specific results to be described at a more conceptual level. Research of this type addresses different aspects of soil erosion processes at different scales (Lavee et al., 1998; Puigdefabregas et al., 1999; Cammeraat, 2002; Calvo-Cases et al., 2003; Brazier, 2004; Cammeraat, 2004; de Vente & Poesen, 2005; Puigdefábregas, 2005; Boix-Fayos et al., 2006), and in extended reviews on collected soil erosion data (Cerdà, 2001; Kosmos et al., 2003). All approaches are important since they permit us to learn from past experiences and help to define future directions and methods of research.

Mineral dust has an important influence on the chemical and physical composition of the atmosphere, whereas dust sedimentation provides external organic and mineral matter to the ground surface and has an important influence on the biological, geological, and chemical processes and environments on Earth. Airborne dust consists of very small particles from soils and/or rocks lifted from the surface of the Earth due to wind abrasion and turbulence under specific weather and soil situations. Therefore, the chemical composition and physical characteristics of dust are significant factors for identifying dust origin areas.

The acquisition of real soil loss data is very complex, involving technical problems that are difficult to solve. Data from experimental measurements must be interpreted in the context of the methods used, which are usually dependent on frequency and spatial scale of measurements. Both methods and scale of measurement must be designed according to the objectives of the research. The validity of the measurements depends on the suitability of the methods for the objectives of the research project. The elements of our monitoring, measurements, and models are discussed further in this section.

2. SECTION OBJECTIVE AND METHODS

2.1 SAMPLE METHODOLOGY BASED ON RESEARCH OBJECTIVES

The objective of this chapter is to quantify the contemporary aeolian inputs and outputs by measuring erosion and deposition rates at the three sites. In addition, we aim to characterize the chemical composition of aeolian inputs and physical characteristics of the aeolian outputs at each site. The primary questions addressed in this chapter include (1) Are there significant differences in contemporary erosional and depositional measurements within and among the sites, and do these measurements suggest soil aggradation or degradation, (2) Do the chemical properties of dust deposition exhibit seasonal variations in provenance when compared to soil and parent material chemical composition at each site, (3) Are there differences in erosion as a function of ground cover?

To measure the yearly aeolian inputs and outputs, dust deposition was collected in marble traps at each site. Soil erosion samples were collected from the National Wind Research Erosion

Network (NWREN) Modified Willison and Cooke (MWAC) samplers from CPER, and MOAB. Each NWREN plot contains 21 MWACs at can heights 10, 25, 50, and 85 cm. The yearly mean flux was calculated from the median flux all each MWAC can height. The median value was obtained for each can height since the data are non-normally distributed. The differences in ground cover were discussed further in the experimental design of this thesis. The MWACs from this research were utilized for all the sites in areas of high and low ground cover to determine if soil erosion flux is dependent on ground cover within the sites.

To address how atmospheric dust chemical composition vary across the western U.S. seasonally, the NEON Particulate Matter less than 10-micron (PM<10) filters were obtained from Moab for December 30, 2020, to December 12, 2022, Niwot for December 30, 2020 to December 20, 2022, and for CPER from December 22, 2020 to December 28, 2022 (exact sampling periods of filters are in located in Appendix B.1). Dust deposition was collected utilizing marble traps; the NEON PM<10 filters, dust from marble traps, and soil samples from each site were chemically analyzed with an ARL QUANT'X EDXRF Spectrometer to determine the chemical composition of each sample.

The NWREN MWAC samples for CPER and Moab sites for all MWAC sampling heights were analyzed with a LISST-Portable grain size analyzer to determine the particle size distribution variation within and among sites. The MWAC CPER and Moab samples were obtained from the several experimental plots to determine particle size in areas of low and high ground cover. The 10 and 25 cm can heights were measured for CPER due to the limited sample size. Grain size analysis was not conducted on Niwot samples due to insufficient mass of samples collected.

2.2 FLUX EQUATION

In dust research, the term “flux” is employed instead of “amount” because it refers to the dust collected in the dust sampler, which represents the dust that has entered and exited the MWAC can sampler tubes or the marble trap pan. Erosion and depositional flux were calculated based on the flux equation (Eq. 3.1), where the area of the MWAC and marble trap opening are 0.00028 m² and 0.043 m², respectively.

$$\text{Flux} \left(\frac{\text{g}}{\text{m}^2 * \text{year}} \right) = \text{mass}(\text{g}) * \text{area}^{-1}(\text{m}^2) * \text{time}^{-1}(\text{year}) \quad \text{Equation 3.1}$$

The flux equation normalizes the mass data to compare the sample amount across sites with different sampling periods. The erosional flux is usually calculated as an integrated horizontal mass flux equation where the can heights are weighted differently (Webb et al., 2015). However, in the present study, the insufficient mass of samples collected required a bulk (combination of samples across can heights) sample analysis (Belnap et al., 2009).

2.3 TOTAL ELEMENTAL ANALYSIS

The NEON filter, soil samples, and dust from the marble traps were analyzed for Al, Ca, Fe, Mg, Mn, Ti, Sr, K, S, Pb, and P utilizing ARL QUANT'X EDXRF Spectrometer. The chemical concentrations were calculated considering the flowrate $\left(\frac{\text{m}^3}{\text{minutes}} \right)$ of the NEON EcoTech Hivol 3000 and surface area (cm²) of NEON PM<10 filter (Eq. 3.2). The concentration is expressed in

micrograms (μg) of element per cubic meter (m^3) of air, following the chemical concentration unit used by the Environmental Protection Agency (EPA).

$$\text{Concentration } \left(\frac{\mu\text{g}}{\text{m}^3} \right) = \frac{\mu\text{g of element}}{\text{flow rate } \left(\frac{\text{m}^3 \text{ air}}{\text{minutes}} \right) * \text{sample duration (minutes)}} \quad \text{Equation 3.2}$$

2.4 ELEMENTAL RATIOS

Elemental ratios of samples can be used as a tool at each site to differentiate if the dust deposition is from local or non-local (global or regional) sources (Muhs & Benedict, 2006; Routson et al., 2019). The selected elements for the elemental ratio consist of Al and trace elements (K, Ca, and Sr) in the numerator, while the immobile element titanium (Ti) is in the denominator. This ratio is employed to evaluate the relative proportions of these elements within dust, soil, and parent material. A greater difference between the surface soil and dust elemental ratios suggests the provenance of the dust is non-local. While similar elemental ratios between parent material and soil surface could suggest local sources of dust contribution to the soil.

2.5 STATISTICAL ANALYSIS

Statistical analyses were conducted using the R software package (version 2023.03). ANOVA (Analysis of Variance) was applied to assess the if there was a significant difference between two or more groups of samples. As a post hoc analysis following ANOVA, Tukey's Honestly Significant Difference (HSD) was applied to identify specific groups that exhibited

significant differences. For these data that did not meet assumptions of normality, the Kruskal Wallis test was applied to determine if there was a significant difference between the median of two or more groups.

Prior to conducting these analyses, the depositional flux data were evaluated for adherence to the assumptions of normality using the Shapiro Wilk test ($\alpha = 0.05$). Since these data met the normality assumption, the ANOVA ($\alpha = 0.05$) and Tukey ($\alpha = 0.05$) tests were utilized to investigate if there is a difference in the average depositional flux among sites and what sites display a significance difference from each other.

The erosional data exhibits a non-normal distribution when analyzed through the Shapiro Wilk test ($\alpha = 0.05$). The Kruskal Wallis ($\alpha = 0.05$) test was utilized to investigate the potential difference in the yearly median depositional flux among sites and to determine if the treatment plots (low and high ground cover) within sites varied significantly.

A multiple linear regression (MLR) model is commonly used in statistics to perform tests on data with multiple independent factors. The independent variables are either multiplied or added in the MLR model depending on the relationship of the variables to one another. When independent variables are multiplied within the MLR model it indicates that the relationship between the dependent and independent variable is dependent on another variable. When the independent variables are added within the MLR model it indicates that each independent variable has its own unique relationship to the dependent variable. A quantile-quantile plot (QQ plot) can be utilized to determine what independent variables should be added or multiplied within the MLR model. The QQ plot determines if the data are normally distributed by graphing the quantiles of the data compared to a theoretically normally distributed dataset. If most of the

theoretical and experimental quantile points align on a 1-1 graphical line it indicates that the experimental model is normally distributed. Unique combinations of MLR models are made by adding or multiplying independent variables, and the MLR model used for the dataset is the one that is the most normally distributed based on the QQ plot. Before performing these statistical tests on MLR models, these data must be normally distributed and show constant variance and linearity. A residual plot is utilized to determine if these data meet these assumptions. To create a residual plot the residuals (difference between observed and predicted values) of the dependent variables for the MLR model are plotted against the independent variables. If the residual points are spaced evenly across the x-axis, then the data show constant variance and linearity. Once the data meets the MLR model requirements, the ANOVA test can be performed to determine if there is a significant difference between the dependent variable and independent variables within the model. The ANOVA test can also be used to determine if these data indicate an interaction between independent factors in the model. The Estimated Marginal Means (EMMs) test can be used as a *post hoc* analysis of these data to determine if there is a significant difference for the dependent variable for each group within and among each independent variable.

For this study, these chemical concentration data were transformed into an MLR model with the dependent variable as the chemical concentration of each element and the independent variables as site, season, and specific element ($\text{lm}(\text{concentration} \sim \text{site} * \text{season} + \text{element})$). This MLR model was based on the QQ plot since the model was most correlated with the experimental data. Although the data showed a relationship in the QQ plot the data were still not normally distributed since the quantile points of the experimental data were not in relation with the theoretical quantile points on the QQ plot. Therefore, the concentration data were first transformed from ($\mu\text{g}/\text{m}^3$) to (ng/m^3) and log transformed to reduce the effect of outliers. When

the data were graphed on a QQ plot and residual plot the transformed data showed normality, constant variance, and linearity.

2.6 SEDIMENTOLOGY STATISTICS

The phi scale was introduced by Krumbein (1934, 1938) as a convenient means of visualizing and statistically analyzing sediment grain size distributions over a wide range of particle sizes (Eq. 3.3). The earlier Udden-Wentworth scale is a millimeter-based scale, with an unchanging ratio between class limits. The phi scale allows more emphasis for the finer grain sizes. Phi size values for the sediment class limits range from -5 phi (for a diameter of 32 mm, or very coarse pebble size) down to $+10$ phi (for a diameter of $1/1,024$ mm, or clay size). The scale was developed specifically as a statistical device to permit the direct application of conventional statistical practices to sedimentary data.

The phi scale has distinct advantages over geometric size scales. Tanner (1969) summarized some of the advantages as follows: geometric basis; equal spacing of size class divisions, with integers representing the limits of the Wentworth size classes; simple nomenclature; potential for fine subdivisions; inclusion of a wide range of grain sizes; wide acceptance; a close match of boundaries between the three important “super classes” (gravel, sand, silt + clay) with the widely recognized deficiencies at about -1 phi (2 mm) and $+4$ phi ($1/16$ mm); ease of plotting on ordinary probability axes; adaptability of phi units to a variety of sophisticated statistical procedures; ease of interpretation of non-Gaussian data; and ready availability of sieve screens in standard phi sizes.

Many calculations can be determined using phi, such as sorting, skewness, and kurtosis. Sorting is the standard deviation of particle size; it measures the spread of size classes around the mean. Within Equation 3.4-3.6 the phi (ϕ) subscripts represents the percentile within the data in which ϕ_{16} indicates the phi value at the 16th percentile. Skewness describes the extent to which the graph is skewed or distorted toward one side or the other (Eq. 3.5). When the phi distribution graph is skewed right (skewness value less than -0.1) there is greater distribution of particles around coarser grains, yet if the graph is skewed left (greater than 0.1) there is greater distribution of particles around finer grains. Kurtosis describes the distribution around the mean (Eq. 3.6). If the data are mesokurtic (kurtosis value between 0.9-1.1), the data are normally distributed around the mean. If the kurtosis is greater than 1.1, the distribution is more narrowly distributed around the mean with a higher peak. If the kurtosis is less than 1.1, this indicates the data show a flatter, more distributed pattern, and thus relatively less centralized around the mean. For particle size, kurtosis can indicate if the phi distribution is centralized around the mean, indicating that the particles are well sorted around one grain size, or if the phi distribution is less centralized, indicating the sample contains a wide distribution of particle sizes.

$$\text{phi } (\phi) = -\log_2 \left(\frac{\text{particle size diameter } \mu\text{m}}{1000} \right) \quad \text{Equation 3.3}$$

$$\text{Sorting} = \frac{\phi_{16} + \phi_{84}}{4} + \frac{\phi_{95} - \phi_5}{6.6} \quad \text{Equation 3.4}$$

$$\text{Skewness} = \frac{\phi_{16} + \phi_{84} + 2\phi_{50}}{2(\phi_{84} - \phi_{16})} + \frac{\phi_5 + \phi_{95} - 2\phi_{50}}{2(\phi_{95} - \phi_5)} \quad \text{Equation 3.5}$$

$$\text{Kurtosis} = \frac{\phi_{95} - \phi_5}{2.44(\phi_{75} - \phi_{25})} \quad \text{Equation 3.6}$$

In the next section, we will determine the mean, sorting, skewness, and kurtosis for the NWREN samples and for the high and low ground cover plot samples for Moab and CPER.

3. RESULTS

3.1 EROSIONAL VARIABILITY WITHIN THE SITES

To assess the variability of erosion across sites with varying degrees of ground cover, the annual erosional flux was computed for both low and high ground cover plots at all the sites. The analysis was based on monthly samples collected from June 12, 2022, to March 14, 2023, for Moab, June 22 to September 29, 2022, for Niwot, and June 19, 2022 to March 24, 2023 for CPER. The mean value was calculated from the can heights flux (10, 25, 50, and 85 cm), which was derived from the median flux across all sampling periods.

The mean erosion flux for the Moab low and high ground cover plot is 7800 ± 8300 g/m²/year and 6300 ± 8900 , respectively (Fig. 3.1). The findings indicate that the high ground cover plot has 20% more erosion compared to the low ground cover plot. The mean erosional flux for CPER at the low and high ground cover plots are 8360 ± 130000 g/m²/year and 980 ± 860 g/m²/year, respectively (Fig. 3.1). The results indicate that at CPER the low ground cover plot experienced approximately eight times the amount of erosion compared to the high ground cover plot. The mean erosional flux for Niwot at the low and high ground cover plots are 75 ± 120 g/m²/year and 980 ± 860 g/m²/year, respectively (Fig. 3.2). The results suggest that at Niwot the high ground cover plot experienced approximately thirteen

times the amount of erosion compared to the low ground cover plot (Fig 3.2). The type of ground cover could be a contributing to the variation within the plots at the grassland sites. Prior research suggests that perennial grasses contribute more to soil stability than shrubs (Okin et al., 2006; Munson et al., 2016; Webb et al., 2021; Rodriguez-Caballero et al., 2022). The dominant vegetation was perennial grass at CPER and shrubs at Moab. The results suggest that a decrease in the percentage of perennial grasses compared to shrubs is associated with a greater increase in erosional flux. Niwot had higher erosional flux in the subalpine site (high ground cover plot) compared to the alpine plot (low ground cover) this could be due to limited amount of collection time, the subalpine plot was located on a slope, which could increase erosion, and the subalpine MWAC was near a gravel forest clearing.

A Kruskal Wallis test was employed to assess whether there is a significant difference between erosional flux at the low ground cover plot compared to the high ground cover plot within all the sites. The test indicates that there is no significant difference between the low and high ground cover plots within the sites (p -value >0.05). The statistical results suggest that there may be other factors influencing the soil erosional flux, along with type and percent ground cover, such as soil texture and moisture, and wind speed.

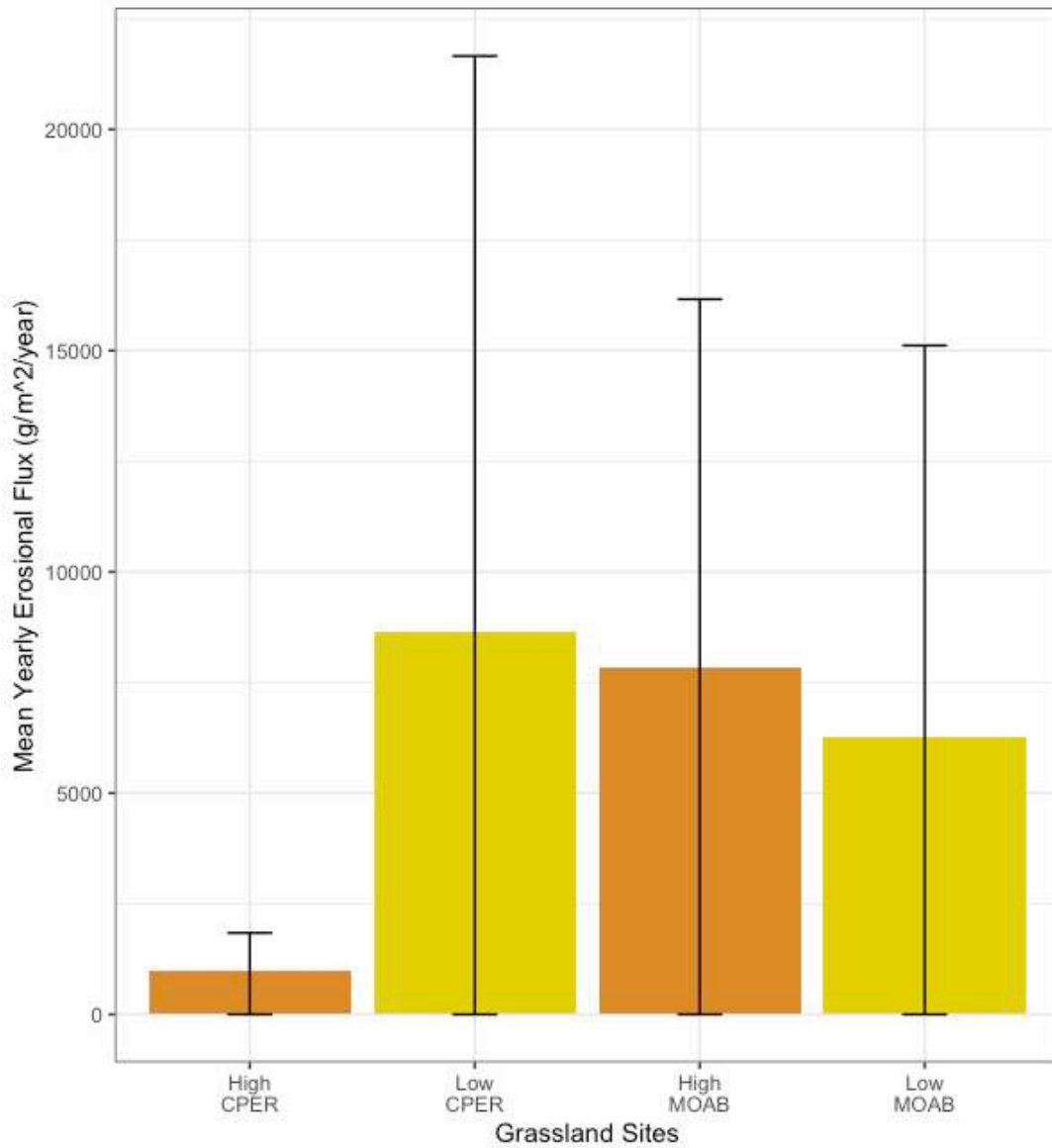


Figure 3.1. Mean erosional flux ($\text{g}/\text{m}^2/\text{year}$) as a function of ground cover for Moab and CPER. Flux was calculated from samples collected June 12, 2022, to March 14, 2023, for Moab and June 19, 2022 to March 24, 2023 for CPER. Values for the figure are presented in Appendix C.1.

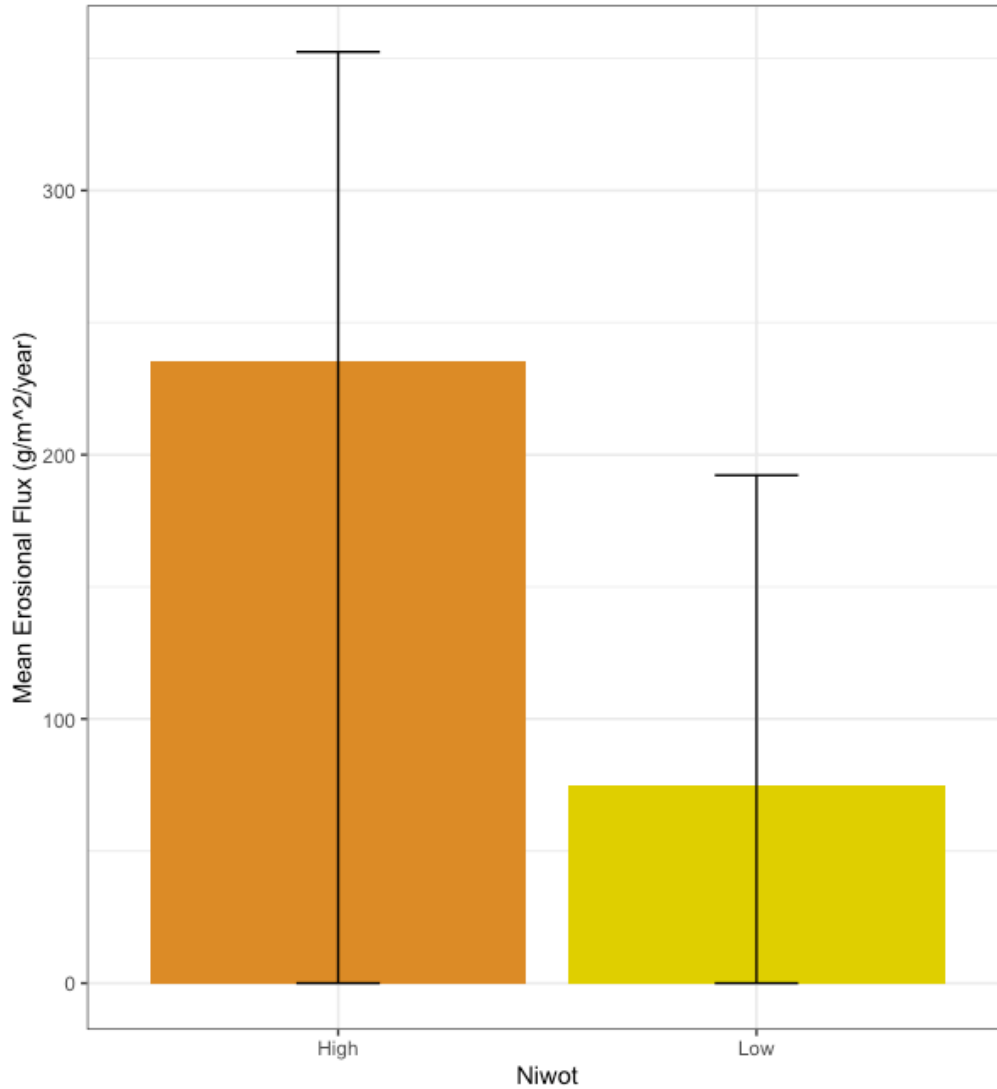


Figure 3.2. Mean erosional flux ($\text{g/m}^2/\text{year}$) as a function of ground cover for Niwot. Flux was calculated from samples collected from June 22 to September 29, 2022. Values for the figure are presented in Appendix C.1.

3.2 CHEMICAL CHARACTERISTICS OF AEOLIAN INPUT: SEASONAL AND SITE VARIABILITY

The chemical concentration of dust deposition varies seasonally, primarily driven by shifts in wind direction and wind speed throughout the year (Aciego et al., 2017; Heindel et al., 2020).

For this study, the wind speed and wind direction were observed for each season to determine if seasonal wind characteristics influenced chemical and physical characteristics of dust erosion and deposition, wind roses for each season are presented in Appendix A.1-A.3. Notably, the highest wind speeds at Moab were in the spring from the southwest, Niwot in the winter from the west, and CPER in the Spring and Fall from the North.

The average chemical concentration ($\mu\text{g}/\text{m}^3$) was measured across months and years (2021-2022) for each site and season from the NEON atmospheric filters (Fig. 3.3). The concentration data were first converted from ($\mu\text{g}/\text{m}^3$) to (ng/m^3) and log transformed to meet MLR model requirements (normally distributed, constant variance, and linearity). The MLR model was statistically tested using ANOVA to determine if there is a significant difference in average log chemical concentrations (ng/m^3) and if there is an interaction between the independent variables (site and season). The ANOVA test revealed that the average log chemical concentrations (ng/m^3) of each element is dependent on the interaction between sites (Moab, Niwot, and CPER) and seasons (winter, fall, spring, and summer) (F-value=7.07, p-value<0.0001). The significant interaction between sites and seasons indicate that seasons must be accounted for when calculating the chemical concentrations of deposition across different domains. Also, the ANOVA findings suggest that there is an overall significant difference in average log chemical concentrations (ng/m^3) per sites and seasons (F-value=15.7, p-value<0.0001). The chemical variation per season is evident for most sites and elements, for instance Moab has a K average log chemical concentration of $4.26 \pm 0.35 \text{ ng}/\text{m}^3$ in the fall, $4.54 \pm 0.58 \text{ ng}/\text{m}^3$ in the spring, $5.01 \pm 0.62 \text{ ng}/\text{m}^3$ in the summer, and $3.48 \pm 1.25 \text{ ng}/\text{m}^3$ in the winter. The highest amount of K at Moab is in the summer, along with many of the other elements for all the sites (Fig. 3.3). Wind

speed and direction could be contributing to the chemical concentration's seasonal variability of concentrations along with other factors such as unusually dry seasons, agriculture, grazing, and changes in ground cover.

The EMMs analysis was conducted after ANOVA analysis to determine which sites were significantly similar to each other for each season. The EMMs results indicate there is no significant difference between the average log concentration of elements at Moab and Niwot in the winter ($p\text{-value} > 0.05$). For instance, the average log concentrations of Ca at Moab and Niwot are $4.69 \pm 0.86 \text{ ng/m}^3$ and $4.82 \pm 0.78 \text{ ng/m}^3$, respectively (Fig. 3.3). During the winter Niwot is covered with snow, resulting in no local generation or deposition of dust. The findings from this study suggest that Niwot is likely receiving dust from the Colorado Plateau in the winter. This is supported by several factors, including the similarity in dust chemical concentration, the absence of local deposition, and the presence of strong westerly winds (Fig. 3.3, Appendix A.2).

Aluminum is a major component of clay and Ca and Fe are commonly adsorbed by clay particles. High amounts of these elements within the filters could indicate that dust deposition within the sites is composed mostly of clay particles. In the summer Al has an average log concentration of $5.77 \pm 0.350 \text{ ng/m}^3$ at Moab, $5.19 \pm 0.298 \text{ ng/m}^3$ at Niwot, and $5.68 \pm 0.307 \text{ ng/m}^3$ at CPER. Calcium has an average log concentration at Moab, Niwot and CPER of $5.81 \pm 4.09 \text{ ng/m}^3$, $5.33 \pm 0.22 \text{ ng/m}^3$, and $5.59 \pm 0.36 \text{ ng/m}^3$, respectively while Fe has an average log concentration at Moab, Niwot and CPER of $5.18 \pm 0.41 \text{ ng/m}^3$, $4.46 \pm 0.36 \text{ ng/m}^3$, and $5.11 \pm 0.33 \text{ ng/m}^3$, respectively. The element with the highest concentration is Al followed by Ca and Fe and the season with the highest amount of these elements is the summer. The chemical result

from the atmospheric filters suggests that the deposition is composed of high amounts of clay at each site over all the seasons, especially in the summer.

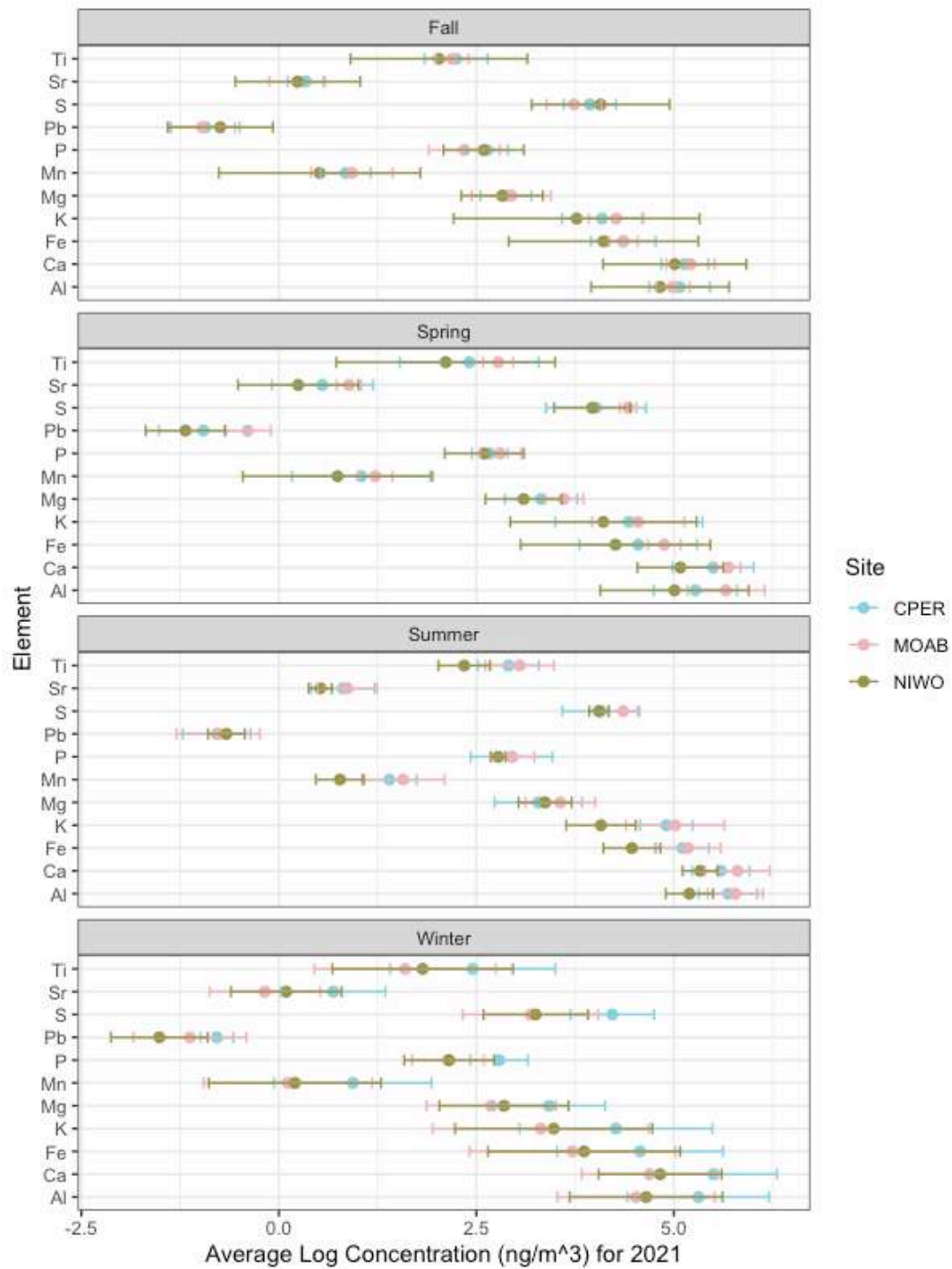


Figure 3.3. The average log chemical concentration (ng/m^3) of the dust from each site for all seasons from filters collected at Moab from December 30, 2020, to December 12, 2022, at Niwot from December 30, 2020 to December 20, 2022, and at CPER from December 22, 2020 to December 28, 2022. Error bars show standard deviation within the data. Data obtained from XRF analysis of the NEON filters.

3.3 CHEMICAL CHARACTERISTICS OF AEOLIAN INPUT: PROVENANCE

The elemental ratio of Al/Ti, Ca/Ti, K/Ti, and Sr/Ti were determined for the surface and parent material horizons from the pedon at each site and the dust samples from the marble traps (Table 3.2). These ratios are commonly used in dust research to determine the relative source of the dust (local or regional) (Muhs & Benedict, 2006; Goodman et al., 2019). Elemental ratios are also utilized to assess the proportionate contribution of dust to the surface soil. These ratios can provide insight into whether the surface soil is more closely aligned with the dust or the parent material, as indicated by the similarity of the ratios. Where the dust and surface soil values are significantly different, it could indicate that the dust is not from the local parent material but coming from a regional source (Muhs & Benedict, 2006; Goodman et al., 2019).

The parent material, surface soil, and dust at Moab have Al/Ti ratio of 30, 14, and 11, respectively. These ratios are similar to the results obtained from the Ca/Ti, K/Ti, and Sr/Ti ratios, indicating a comparable composition among the elemental ratios (Table 3.1). The parent material, surface soil, and dust at CPER have Al/Ti ratio of 18, 15, and 14, respectively, which is similar to the other elemental ratios (Table 3.1). The elemental ratios in the surface soil and dust at CPER were relatively similar, indicating a consistent composition, suggesting that the dust is generated and deposited locally with no influence from non-local sources. In contrast, the

elemental ratios in the dust and surface soil at Moab differed significantly. While the results suggest a greater similarity between the surface soil and dust compared to the parent material at Moab, they also indicate the potential influence of non-local sources of deposition.

At Niwot, the parent material, surface soil and dust elemental ratios of Al/Ti are 22, 18, and 9.5, respectively. The K/Ti ratios are 5.6, 6.3, and 3.5, respectively (Table 3.1). These ratios suggests that the parent material and surface soil are relatively similar. Dust ratios at Niwot are about half the surface soil ratios, indicating that the dust deposited at Niwot is likely from non-local sources. Previous research has also suggested that elemental ratios of dust deposition from Niwot Ridge are more closely related to the soil from non-local sources such as the Colorado Plateau (Muhs & Benedict, 2006; Goodman et al., 2019). Overall, the surface soil and dust element ratios at CPER for the elemental ratios were relatively similar whereas the dust and the surface soil at Moab and Niwot were different for all the elemental ratios, indicating Moab and Niwot are more influenced by non-local sources of dust deposition (Table 3.1).

Table 3.1. Elemental ratios for the parent material, surface soil, and dust from the marble traps. The parent material is the C2 horizon for Moab, 2C/CR for, and 2C for CPER. The surface soil is first A horizon for all sites. The trace elemental ratios were obtained from the XRF analysis of the marble trap dust, and soil from CPER, Moab, and Niwot.

Elemental Ratio	Site	Parent Material	Surface Soil	Dust
Ca/Ti	Moab	42	1.5	3.1
	Niwot	0.40	1.1	1.7
	CPER	8.4	3.0	3.9
Sr/Ti	Moab	0.08	0.03	0.01
	Niwot	0.02	0.03	0.02
	CPER	0.04	0.04	0.02
K/Ti	Moab	12	5.9	5.0
	Niwot	5.6	6.3	3.5
	CPER	5.0	5.9	5.3
Al/Ti	Moab	30	14	11
	Niwot	22	18	9.5
	CPER	18	15	14

3.4 SEDIMENTOLOGICAL RESULTS: GRAIN SIZE DISTRIBUTION AMONG SITES

By analyzing the particle size distribution of the eroding dust, one may be able to ascertain the distance dust will travel and the extent to which erosion will affect the soil. In this study, the NWREN CPER and Moab particle size distribution were compared for all MWAC collection can heights (10, 25, 50, and 85 cm) (Table 3.2, Fig. 3.4).

The range of the average mean phi size across the can heights at Moab is from 2.5 to 3 and the sorting ranges from 1.0 to 1.75. For CPER, the average mean phi size ranges from 2.4 to 2.9 and the sorting ranges from 1.2 to 1.5 (Table 3.2). These results indicate that the mean grain size and sorting ranges are comparable between Moab and CPER. For distribution results, the skewness for Moab and CPER ranges from 0.7 to 2.0 and 0.3 to 1.3, respectively (Table 3.2). While the kurtosis distribution for Moab and CPER ranges from 1.9 to 2.5, 1.0 to 1.1, respectively (Table 3.2). The skewness and kurtosis relate to the distribution around the mean

value. The kurtosis value suggests that the particle distribution at Moab is more tightly clustered around the mean, while the high skewness values indicate a skew towards finer clay-sized particles, as depicted in Figure 3.4. In contrast, the distribution at CPER is less centralized about the mean and exhibits a lower prevalence of clay-sized particles. These findings indicate that although the mean grain size being eroded is similar at both Moab and CPER, there are differences in the grain size distribution patterns between the two sites.

At CPER, as the height increased, skewness decreased but kurtosis and sorting did not vary (skewness: -1.33, sorting: -0.13, kurtosis: 0.01) (Table 3.2). The skewness results indicate that at CPER as the height increases from the ground, the grain size distribution becomes more symmetrically distributed around the mean grain size. The sorting and skewness results at CPER are similar to previous sedimentological research, which suggests, that as particles travel farther from the source, the sorting and skewness will decrease (McLaren & Bowles, 1985; Gao & Collins, 1992).

These findings are the opposite for Moab. Skewness and sorting increased (skewness: 1.62, sorting: 0.24, kurtosis: -0.59), indicating that as the height increases, the average particle size becomes better sorted and less symmetrically centralized around the mean grain size (Table 3.2). Even though the mean particle size at Moab is in the fine sand range, there is an increase of particles within the clay range as height increases. Many factors could contribute to the difference in sorting and skewness trend, such as variations in soil texture, soil moisture, and wind speed.

Table 3.2. Moab and CPER NWREN sites mean (ϕ), sorting, kurtosis and skewness distribution for all MWAC can heights (10, 25, 50, and 85 cm above ground). The mean ϕ value, sorting, kurtosis, and skewness is an average of three replicates for each can height sample from each site.

NWREN Sites	Can Height (cm)	Mean (ϕ)	Sorting (ϕ)	Kurtosis	Skewness
Moab	10	2.4	1.2	2.5	0.3
Moab	25	2.6	1.3	2.5	0.5
Moab	50	2.8	1.4	2.3	1.0
Moab	85	2.9	1.5	1.9	1.3
CPER	10	2.5	1.9	1.1	2.0
CPER	25	2.8	1.9	1.0	1.5
CPER	50	3.0	1.8	1.1	1.2
CPER	85	3.0	1.8	1.1	0.7

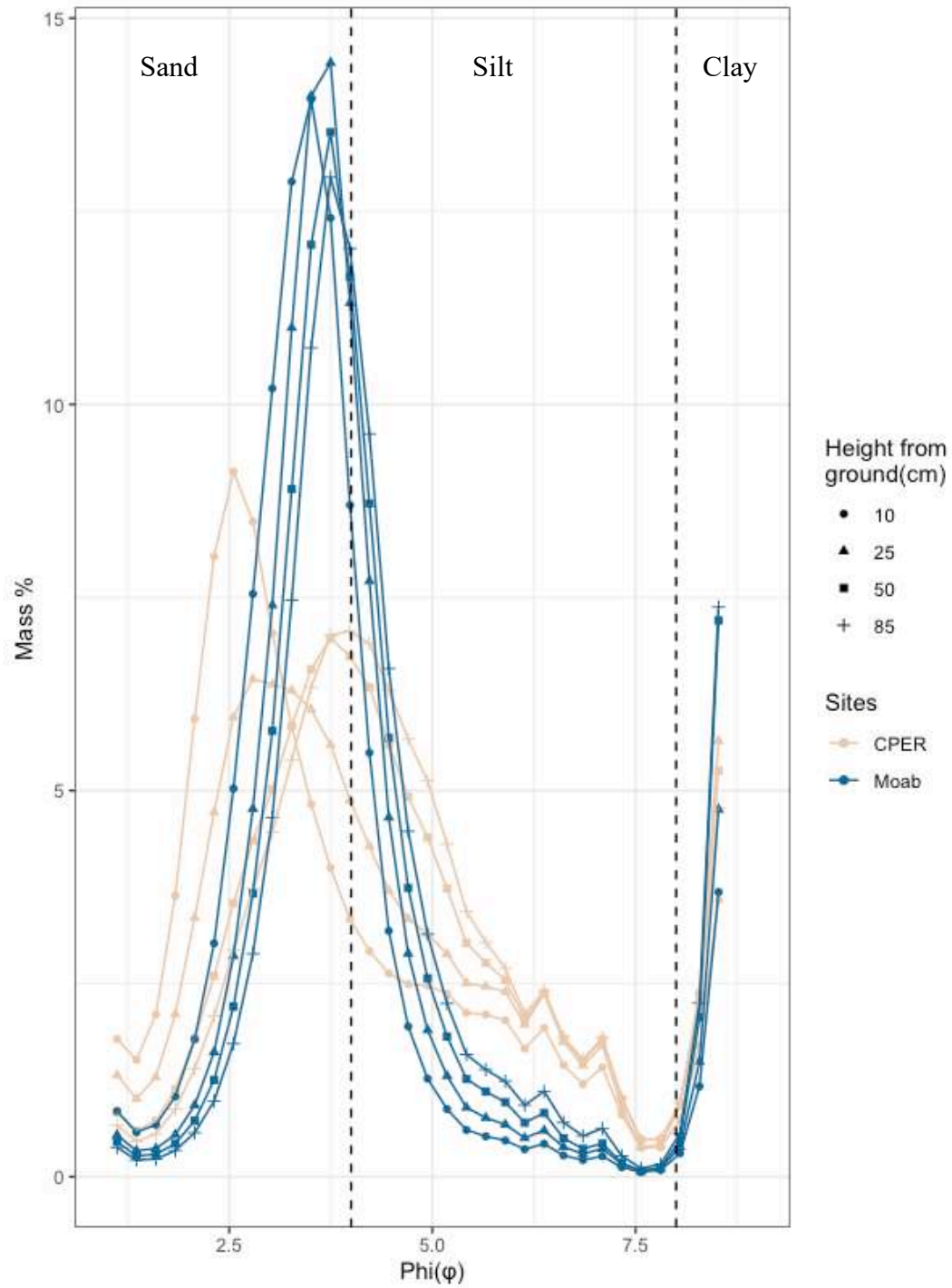


Figure 3.4. Phi distribution of Moab and CPER NWREN sites at can heights (10, 25, 50, and 85 cm from the ground). The distribution from each can height was averaged from three replicates.

3.5 SEDIMENTOLOGICAL RESULTS: GRAIN SIZE DISTRIBUTION WITHIN SITES

Aeolian processes are controlled by the percentage of ground cover, influencing the amount of soil that is eroded in an environment. Although previous research from Belnap et al. (2009) found that the grain size distribution within the Colorado Plateau is not influenced by ground cover percentage, the effect of ground cover on grain size distribution has not been studied in the Central Plains. The grain size distribution was compared for all MWAC collection can heights (10, 25, 50, and 85 cm) at Moab and the lowest can heights (10 and 25 cm) at CPER (Table 3.3, Fig. 3.5, and Fig 3.6).

The mean phi size at Moab ranges from 2.1 to 2.4 for the high ground cover plot and 2.1 to 2.6 for the low ground cover plot. Similar to previous research from Belnap et al. (2009), which found no difference in grain size and ground cover change, these data show no distinct difference between the mean grain size in the low and high ground cover plots within Moab (Fig. 3.6). The mean phi size for CPER ranges from 2.3 to 2.5 for the high ground cover plot and 2.1 to 2.3 for the low ground cover plot (Table 3.3). The mean eroding grain size is distinct between the CPER plots where the high ground cover plot has on average more finer particles eroding the low ground cover plot (Fig. 3.6)

The grain size sorting at Moab ranges from 0.9 to 1.2 at the high ground cover plot and 1.0 to 1.3 for the low ground cover plot (Table 3.3). Skewness at Moab ranges from 0.2 to 0.7 for both low and high ground cover plots while the kurtosis at Moab ranges from 1.2 to 1.7 at the high ground cover plot and 1.4 to 1.9 for the low ground cover plot. The results suggest that the sorting and distribution of grain size for Moab is similar for the low and high ground cover plots. The sorting at CPER ranges from 1.7 to 1.9 at the high ground cover plot and 1.4 to 1.9 for the

low ground cover plot (Table 3.3). The skewness at CPER for the high and low ground cover plot ranges from 2.0 to 2.2 and 1.0 to 2.0, respectively while kurtosis ranges from 1.0 to 1.3 and 1.4 to 2.0, respectively. The sorting values at CPER and Moab are similar within the low and high cover plots, indicating there is no difference in grain size sorting as ground cover percent changes. The graphical distribution values of skewness and kurtosis at CPER differ between ground cover plots while Moab remains the same. The results indicate that a change in ground cover percent at CPER results in a difference in the distribution of particles (Fig. 3.6).

The type of ground cover could be a contributing factor to the changes present in the plots from CPER compared to Moab. Prior research suggests that perennial grasses contribute more to soil stability than shrubs (Okin et al., 2006; Munson et al., 2016; Webb et al., 2021; Rodriguez-Caballero et al., 2022). The dominant vegetation was perennial grass at CPER but shrubs at Moab. The result from this study suggests that the reduction in perennial plants has a significant impact on both the mean grain size and distribution, in contrast to the loss of shrubs.

Table 3.3. Moab and CPER low and ground cover plots mean (ϕ), sorting, kurtosis and skewness distribution for all Moab MWAC can heights (10, 25, 50, and 85 cm above ground) and the lowest CPER MWAC can heights (10 and 25 cm above ground).

Sites	Can Height (cm)	Ground Cover High/Low	Mean (ϕ)	Sorting (ϕ)	Skewness	Kurtosis
Moab	10	High	2.1	0.9	0.4	1.4
Moab	10	Low	2.1	1.0	0.7	1.6
Moab	25	High	2.2	1.1	0.7	1.9
Moab	25	Low	2.3	1.3	0.7	1.7
Moab	50	High	2.4	1.2	0.2	1.2
Moab	50	Low	2.5	1.3	0.3	1.9
Moab	85	High	2.3	1.1	0.5	1.5
Moab	85	Low	2.6	1.3	0.7	1.9
CPER	10	Low	2.3	1.9	2.0	1.4
CPER	10	High	2.3	1.7	2.0	1.3
CPER	25	Low	2.1	1.4	1.0	2.0
CPER	25	High	2.5	1.9	2.2	1.0

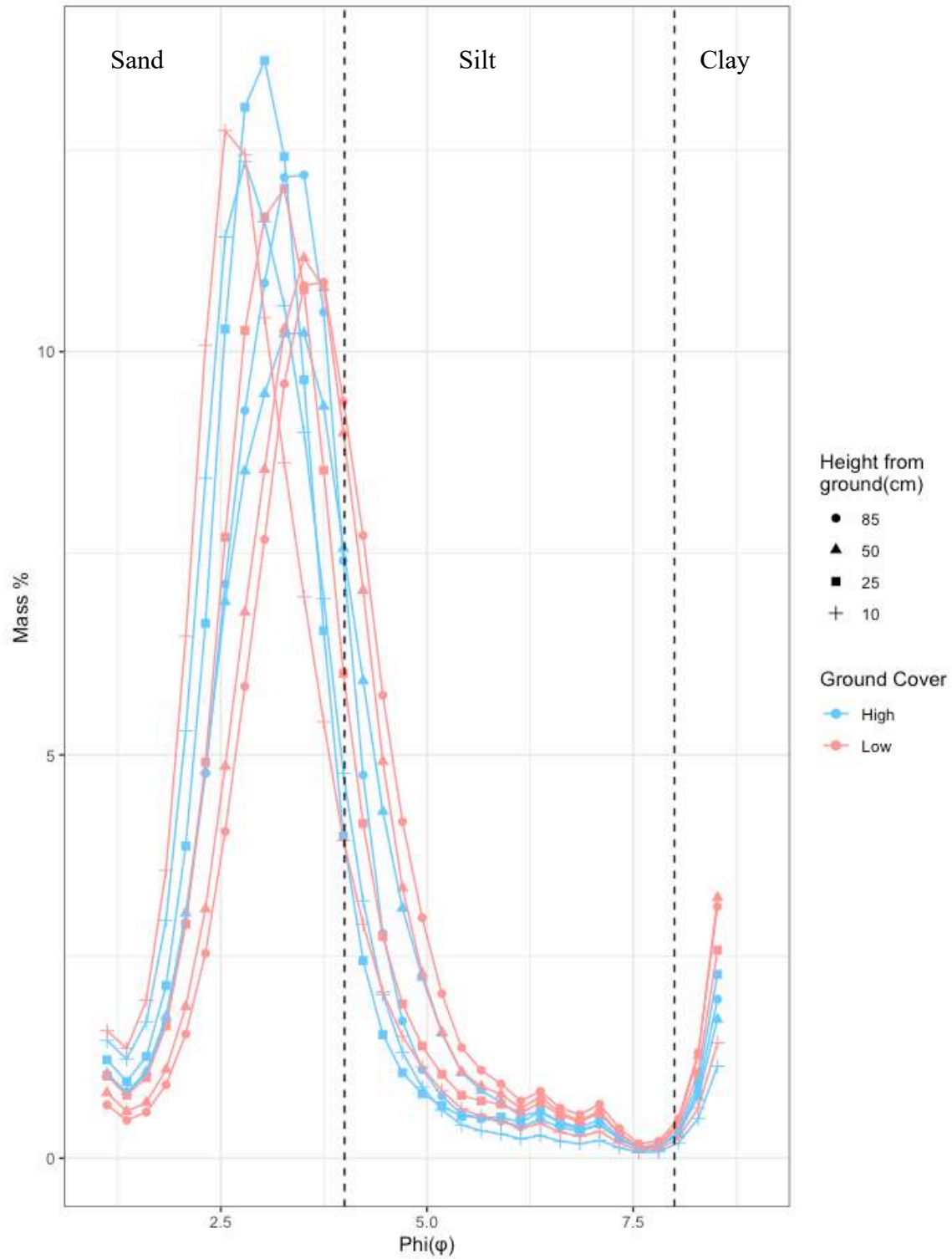


Figure 3.5. Phi distribution for Moab for low and high ground cover plots at all MWAC can heights (10, 25, 50 and 85 cm above ground).

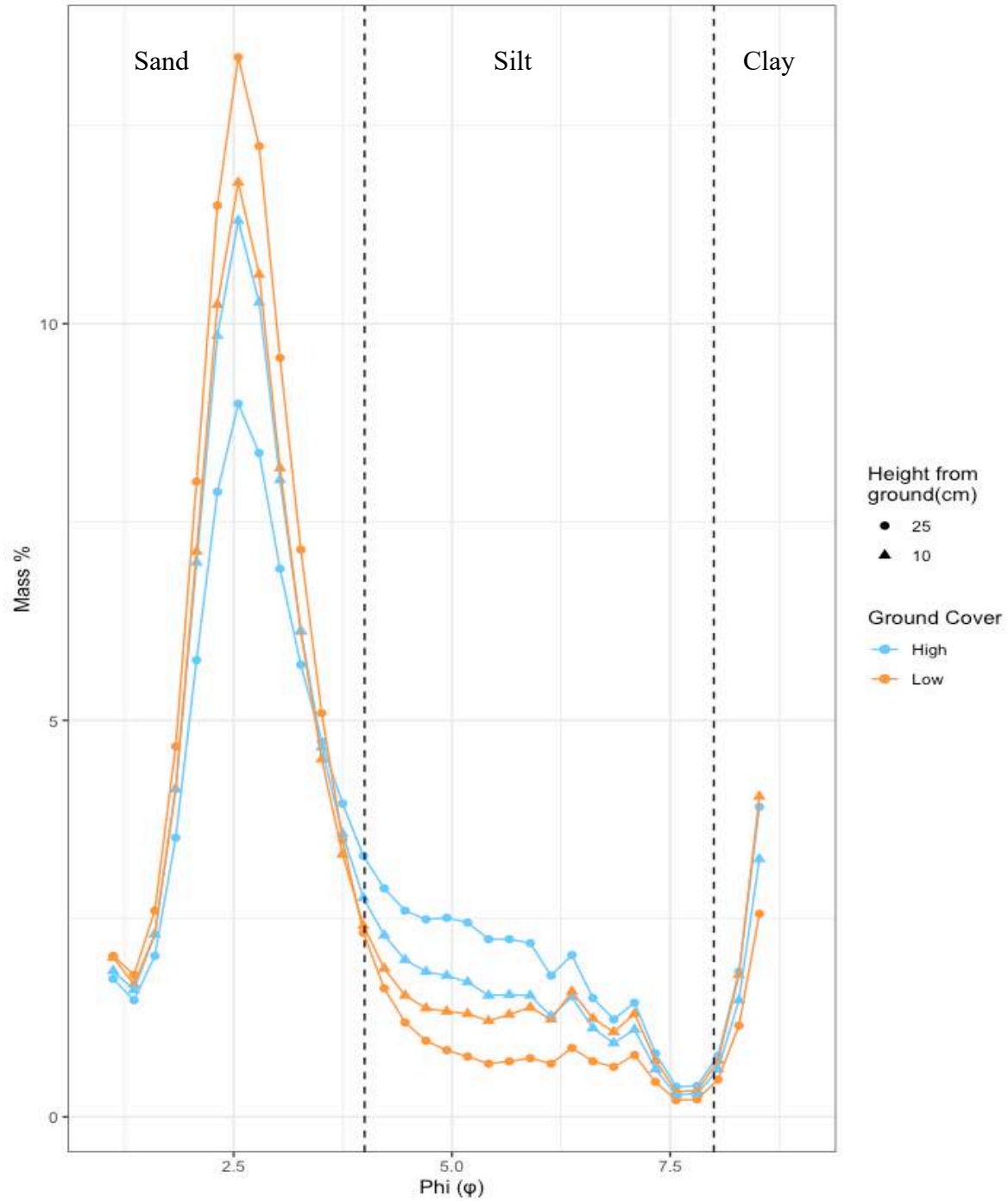


Figure 3.6. Phi distribution for CPER for low and high ground cover plots at lowest MWAC can heights (10 and 25 cm above ground).

3.1 AEOLIAN DUST FLUX

The contemporary dust deposition flux was determined by calculating the mean yearly depositional ($\text{g}/\text{m}^2/\text{year}$) flux at each site (Eq. 3.1). The mean depositional flux was obtained from the average of the sampling periods of the four marble traps at each site. For Moab the marble traps were sampled from May 18 to September 24, 2022, and again on November 12, 2022. For Niwot the marble traps were sampled from June 24 to September 15, 2022. For CPER, the marble traps were sampled from June 9 to September 7, 2022, and again on December 6, 2022. The Shapiro-Wilks test was performed on the depositional flux data to determine if the data were normally distributed. The test indicated the data are normally distributed ($p\text{-value} > 0.05$) meeting the requirements of the ANOVA and Tukey tests. The ANOVA test revealed significant differences among the sites ($F=17.8$, $p\text{-value} < 0.0001$). When the sites were compared using the Tukey HSD test, it was observed that CPER, with a mean depositional flux of $11 \pm 5.8 \text{ g}/\text{m}^2/\text{year}$, and Niwot $4.7 \pm 3.5 \text{ g}/\text{m}^2/\text{year}$ did not exhibit a significant difference ($p\text{-value} > 0.05$) in depositional flux. However, Moab, with a mean depositional flux of $22 \pm 4.4 \text{ g}/\text{m}^2/\text{year}$ demonstrates significantly higher deposition compared to both Niwot ($p\text{-value} = 0.0002$) and CPER ($p\text{-value} = 0.0007$) (Fig. 3.7). Previous research (Belnap et al., 2009) found that within the Colorado Plateau areas with low ground received on average received $32 \text{ g}/\text{m}^2/\text{year}$ of deposition whereas non-disturbed areas with a higher percent of ground cover received on average $14 \text{ g}/\text{m}^2/\text{year}$ from 1999-2007. The evidence from Belnap et al. (2009) suggests that the percent of local ground cover is a significant factor in influencing the amount of dust deposition. The variation in percent ground cover at Moab (36-46% ground cover)

compared to CPER (70-90%) and Niwot (95%) may be contributing to the high depositional rates, in addition to other factors such as wind speed, soil texture, and moisture.

In order to understand the replicability of this study its critical to compare the depositional data from this research collected during part of the year to yearlong depositional studies from similar areas. According to previous research in the Colorado Plateau, a site with similar ground cover percentage as the site from this research received on average 21 g/m²/year of deposition from 1999-2007 (Belnap et al., 2009), which is comparable to the median depositional flux at Moab from this study (22 ± 4.4 g/m²/year). According to Hiendel et al. (2020), the Rocky Mountains received 6.8-11.7 g/m²/year and the Colorado Front Range, 40 miles west of CPER, received 33 g/m²/year in 2019. The findings from this study suggest Niwot receives a median of 4.7 ± 3.5 g/m²/year and CPER at 11 ± 5.8 g/m²/year of deposition (Fig 3.7). Compared to previous research, CPER and Niwot have similar depositional flux to yearlong studies that were within the same area.

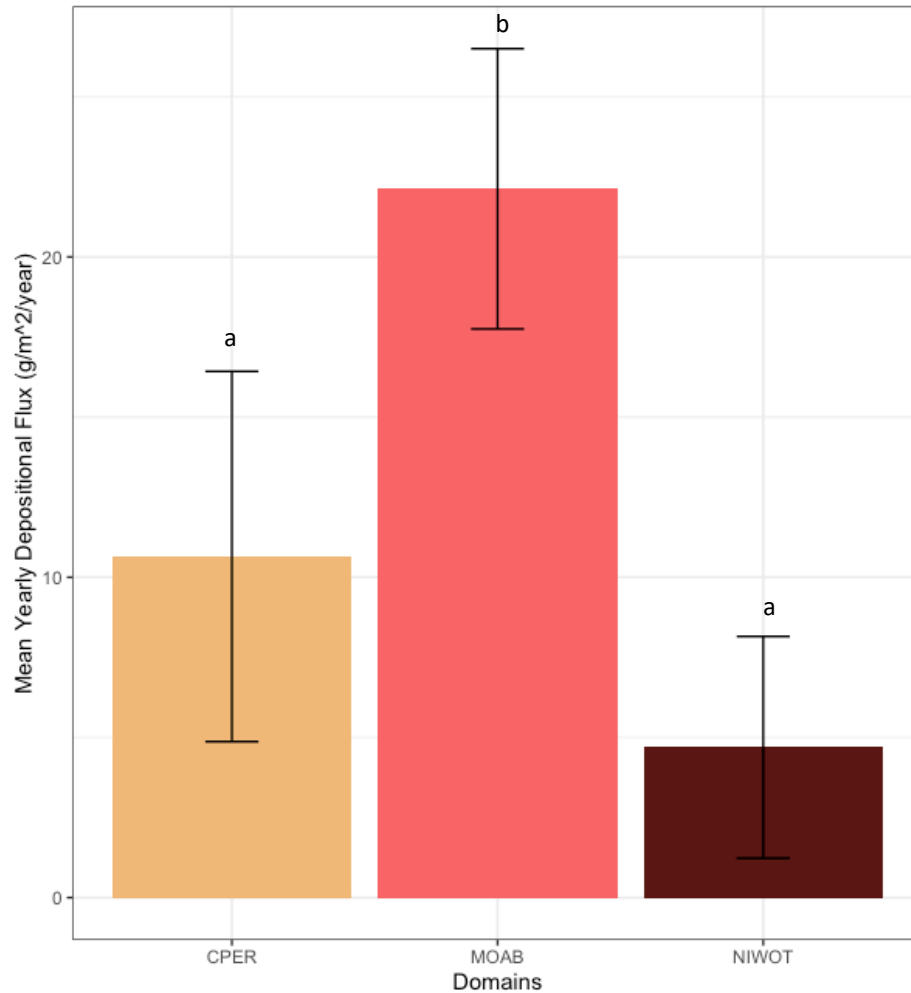


Figure 3.7. The mean depositional flux ($\text{g}/\text{m}^2/\text{year}$) at CPER ($n=8$), Moab ($n=8$), and Niwot ($n=3$) sites, value was averaged over sampling period. Samples were collected for Moab from May 18 - September 24, 2022, and again on November 12, 2022. For Niwot the sampling period was from June 24 - September 15, 2022. For CPER, the sampling periods were from June 9 - September 7, 2022, and again on December 6, 2022. There is a significant difference between the Moab deposition compared to CPER (p -value of 0.0007) and Niwot (p -value of 0.0002), which are denoted with the a and b above the error bar on the graph.

The mean contemporary erosional ($\text{g}/\text{m}^2/\text{year}$) flux and standard deviations were calculated for the NWREN CPER and Moab samples for the 2021 calendar year and for the Niwot samples from this research are from the June 22 to September 29, 2022 (Table 3.4, Figure

3.8). The mean value was calculated from the can heights flux (10, 25, 50, and 85 cm), which was derived from the median flux across all sampling periods. The median value was chosen to determine can height flux due to the non-normality of the data which were tested using the Shapiro-Wilks test, providing a robust representation of the central tendency that is not influenced by extreme values. The mean erosional flux at Moab is 3600 ± 2800 g/m²/year whereas for Niwot and CPER the mean erosional flux is 90 ± 110 g/m²/year and 690 ± 360 g/m²/year respectively (Table 3.4). Overall, Moab, an arid grassland, had almost five times more erosion than CPER, a semi-arid grassland and 40 times more erosion than Niwot, an alpine ecosystem. The Kruskal Wallis test was used to determine if there was a significant difference between the sites. The Kruskal Wallis test showed that there was a significant difference in the mean erosional flux between all the sites ($\chi^2 = 21.5$, p – value < 0.0001).

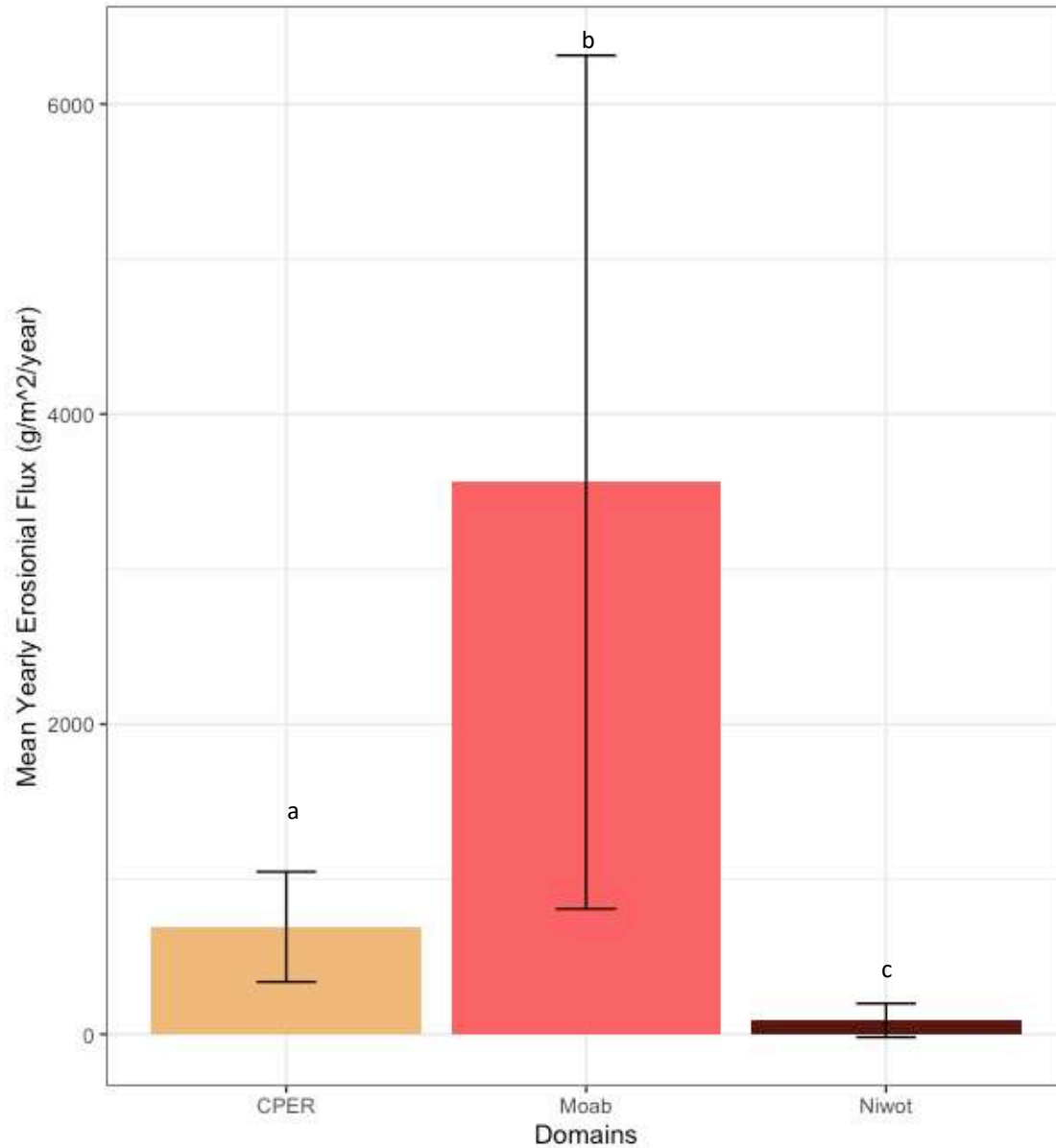


Figure 3.8. Mean yearly erosional flux ($\text{g}/\text{m}^2/\text{year}$) across median can heights flux (10, 25, 50, and 85 cm) at NWREN CPER site ($n=135$ for each can height) and Moab site ($n=243$ for each can height). NWREN CPER and Moab flux calculated from samples collected from January 01, through December 01, 2021. Niwot is not an NWREN site; the data are from this experiment at Niwot Ridge is from June 09 through September 19, 2022 ($n=5$ for each can height). Values presented in Table 3.1.

The mean erosional and depositional fluxes were compared to determine the aeolian input to output ratio at each site (Table 3.4). According to the findings, Moab had 160 ± 640 times

more erosion than deposition, while Niwot and CPER had 20 ± 30 and 60 ± 60 times more erosion than deposition, respectively. The contemporary erosional and depositional outcomes reveal that there are more aeolian outputs than inputs among all the sites.

Table 3.4. Mean erosional flux ($\text{g}/\text{m}^2/\text{year}$) across median can heights (10, 25, 50, and 85 cm) flux. Mean depositional flux ($\text{g}/\text{m}^2/\text{year}$) across sampling periods, and erosion to deposition ratio.

Site	Mean Erosional Flux ($\text{g}/\text{m}^2/\text{year}$)	Mean Depositional Flux ($\text{g}/\text{m}^2/\text{year}$)	Erosion/Deposition
Moab	3600 ± 2800	22 ± 4.4	160 ± 640
Niwot	90 ± 110	4.7 ± 3.5	20 ± 30
CPER	690 ± 360	11 ± 5.8	60 ± 60

4. DISCUSSION

The ecosystems of semi-arid regions are highly susceptible to wind erosion especially with increasing droughts and soil disturbances from tilling, over-grazing, fires and other human disturbances (Klipple & Costello, 1960; Neff et al., 2005; Belnap et al., 2009; Derner et al., 2018; Duniway et al., 2018; Nauman et al., 2018). Moab is an area of increasing regional and local deposition, with regional sources being deserts west of the Colorado Plateau, including the Mojave Desert (Goldstein et al., 2008; Brahney et al., 2013). The results from this research indicate that Moab has significantly more deposition than CPER and Niwot. Yet, the contemporary erosional results indicate that the system is degrading with 160 ± 640 times more erosion occurring at Moab than deposition. Therefore, the Colorado Plateau is an area of significant erosion compared to other ecosystems within the western U.S.

Erosion may continue to increase within the western Great Plains due to the accelerating frequency of droughts and pressures from agricultural activities (Derner et al., 2018). The soil within this region is particularly susceptible to fine particle erosion due to its coarse soil texture (Lyles, 1976). The contemporary erosional data from CPER indicates that the soil is degrading with erosion occurring 60 ± 60 times higher than deposition. Moab and CPER were found to have similar particle size erosion, but a difference in distribution of particles.

The present study conducted a comparative analysis of contemporary erosional and depositional fluxes within the Rocky Mountains. As a result of climate change, the Rocky Mountains are expected to experience more extreme weather patterns, including an increase in the frequency of hot and dry days, which can continue to decrease soil moisture and lead to an increase in soil erosion. In addition, the forest fire season is lengthening and becoming more intense within the Rockies, and the removal of trees and undergrowth can render the soil more vulnerable to wind erosion (Whicker et al., 2006). These contemporary aeolian data revealed that Niwot is degrading with an erosional flux 20 ± 30 times greater than deposition, which could increase in the future because of climate change.

The depositional and erosional samples at Niwot were only collected in the summertime, which could be leading to a skew towards more erosion than deposition since no soil erosion occurs during most of the year at Niwot due to snow cover. Although no erosion occurs within the winter months, the findings from the atmospheric filters suggest a significant amount of dust within the atmosphere in the winter from regional sources. Previous research has also denoted significant amounts of dust on snow occurring within the winter in the southern Rocky Mountain range (Painter et al., 2007; Lawrence et al., 2013).

One of the primary indicators of an increase in soil erosion is loss of ground cover, particularly in arid and semi-arid grasslands (Okin et al., 2006; Munson et al., 2011; Webb et al., 2021; Rodriguez-Caballero et al., 2022). Previous research from arid and semi-arid grasslands indicates variations between areas of heavy grazing or disturbances compared to regions with no disturbance or grazing (Harris et al., 2003; Neff et al., 2005; Belnap et al., 2009; Aubault et al., 2015; Nauman et al., 2018). These differences can be attributed to the fact that grazing reduces perennial grasses that are the main vegetation type of grasslands, having a significant effect on the soil stabilization.

In the present study, the erosional flux was slightly higher in the high ground cover plot at Moab than the low ground cover plot. Moreover, the grain size and distribution of the eroded particles remained the same between the low and high ground cover plots. In this study, the low plot had about 30% ground cover and the high plot had 40%. The results may imply that a 10% difference in ground cover at Moab is not enough of a difference to create significant variability in erosional flux. The erosional flux at Niwot was 13 times higher in the subalpine high ground cover plot than the alpine low ground cover plot. While it was initially predicted that a lack of ground cover would increase soil erosion at all sites due to greater exposure to wind events, this was not the case at Niwot. One potential factor for the increase in erosion at the high ground cover plot was that the MWAC at the subalpine low ground cover plot was located at a bottom of a slope near a small gravel forest clearing, which may have skewed the erosional flux results. The findings at Moab and Niwot suggest that there are other factors besides ground cover percent that are influencing wind erosion. The type of vegetation, the size of the gap between the vegetation, the soil moisture, and the coarseness of the soil may contribute more to particle size change than the percent ground cover.

As the perennial ground cover decreased from 90% to 70%, the erosional flux at CPER increased by a factor of eight. Likewise, the average grain size and distribution varied between the low and high ground cover plot with the high ground cover plot having a greater distribution of finer sized particles than the low ground plot. The variability in erosional flux and eroding grain size distribution within CPER compared to Moab may be contributed to the type of ground cover present. Specifically, the loss of perennial grasses at CPER results causes an increase in erosion and shift in average grain size and distribution. In contrast, at Moab, the loss of shrubs does not significantly decrease erosion or change the grain size distribution of eroding particles.

The chemical characteristics of atmospheric dust changed significantly at each site over the course of the 2021-2022 period, indicating strong seasonal effects. Previous research within the western U.S. has indicated concentrations and chemical characteristics change seasonally with high concentrations in the summer and springtime (Reynolds et al., 2016). For all the sites, summer had the highest concentration of elements, and the elements in the highest concentrations were Al, Ca, and Fe. These elements are either within the chemical makeup of clay or adsorb to clay, indicating that the dust at the sites is composed of mostly clay particles. The mass varied significantly per site and season with CPER having the highest amount of collected dust on the atmospheric filters, which could be due to local grazing and agricultural activities.

Previous research has indicated that the Colorado Plateau and the Front Range are significant contributors to dust within the Rocky Mountains (Mladenov et al., 2012; Brahney et al., 2013; Valerino et al., 2017; Heindel et al., 2020). The chemical characteristics of the dust at Niwot and Moab were similar in the winter, which along with other factors such as high wind speed from the west and lack of local dust emission, the results from this study suggests that the

dust deposited at Niwot in the winter is from the Colorado Plateau. This was also supported by trace elemental ratio results, which indicate that the dust at Niwot is not like the soil, suggesting that the dust is from regional, as opposed to local, sources.

Our findings also suggest that the dust trace element ratio at Moab differs slightly from the soil surface, suggesting that the Colorado Plateau receives deposition from regional sources. Unlike Moab and Niwot, the elemental ratio from CPER indicate that the soil surface, dust, and parent material are similar in composition, suggesting that the chemical concentrations from aeolian inputs at the short grass steppes are due to local deposition.

CHAPTER 4: CONCLUSIONS

This study was designed to explore the impacts of aeolian processes on the soil through contemporary monitoring and soil characterization and modeling across different bioclimatic domains. The main question was, are soils within the domains of the western U.S. aggrading or degrading and is this influenced by contemporary aeolian processes? Furthermore, the effect of ground cover on aeolian processes and soil erosional flux is assessed. My research addressed this question by determining the volumetric and elemental changes of the soils, measuring the aeolian inputs and outputs, chemically characterizing the deposition, and physically characterizing the eroding soil. The results indicate that the soil at Moab was and is undergoing degradation and the soil at both Niwot and CPER were aggrading phase, but the measurements from soil erosion samplers at these sites indicate the contemporary system are now degrading.

The contemporary erosional and depositional results are comparable to the mass balance results of the ancient soil at Moab. The mass balance results at Moab indicate that the system is in a degradational phase. The results from the contemporary dust flux indicate that Moab is more of an erosional than a depositional environment. The particle size results indicate that fine particles are eroding from Moab causing an overall loss of clay within the surface horizon. The ancient soil results indicate there was a loss of soil nutrients while sodium was the only element that was enriched within the surface horizon. High sodium levels within the soil as well as a loss of clay poses several issues, including high soil salinity displaces cations, leading to an overall loss of soil nutrients. Additionally, the reduction in clay content decreases the soil's cation exchange capacity, as well as its ability to retain water and nutrients. As a result, the lack of

nutrients and soil moisture increase plant mortality, leading to an eventual decline in ground cover and further soil erosion. Therefore, the results from this study indicate that not only is Moab in a degradational phase but will continue to be in decline unless soil conservation efforts are put in place to reduce erosion and increase plant essential nutrients within the soil.

The mass balance results from Niwot suggest that the soil system within the Rocky Mountains is overall in an aggrading phase while the contemporary flux measurements indicate the system is degrading. There was greater erosional flux than depositional flux at Niwot, and significantly more in the sub alpine ecosystem than alpine. The contemporary chemical results of deposition compared to the soil suggest that the deposition within the Rocky Mountains is from non-local sources. The chemical characteristics of atmospheric dust at Moab and Niwot are similar in the winter. Additionally, the wind direction at Niwot is westerly, suggesting that the southern Rocky Mountains receive dust deposition from soil eroded from the Colorado Plateau. Unlike Moab, the surface soil at Niwot was enriched in clay and plant essential nutrients such as P and K. The mass balance results indicate that the P and K within the soil at Niwot was from an exogenous source. Along with previous studies of deposition in the Rockies, this research implies that the exogenous source of clay and nutrients at Niwot could be from dust deposition. Therefore, the non-local deposition at Niwot could be contributing to the biological productivity and thus, the high organic content present within the soil. While the ancient soil at Niwot indicates aggradation, there is potential for volumetric and elemental loss if soil erosion continues to persist in the southern Rocky Mountains.

Like Niwot, the ancient soil results at CPER suggest the overall soil system is aggrading while the contemporary results indicate that the soil is in a degrading. The contemporary erosional flux was greater than deposition at CPER and in areas of low ground cover there was

twice as much erosion occurring than in high ground cover. Compared to Moab and Niwot there was more atmospheric dust collected on the filters, most likely from local agricultural activities. According to the current findings, a significant proportion of silt and clay is eroded from the soil, but there is no loss of these particles within the surface horizon compared to the subsurface. Furthermore, the chemical characteristics of the dust were similar to the surface soil, suggesting deposition at CPER is from local erosion. These findings suggest that the soil eroded naturally or from agriculture activities within the western Great Plains remains within the ecosystem and is deposited locally. Overall, the soil at CPER is susceptible to erosion and has high erosional flux but this does not have a direct impact on the ancient soil profile. Although, if soil erosion continues to persist, resulting in the increased loss of clay and nutrients, the soil at CPER will eventually exhibit signs of degradation.

Overall, our research indicates that clay is important to the aeolian processes. The elements in the highest concentrations in the dust at all the sites were Al, which is a main element in clay minerals as well as Ca and Fe, which are typically adsorbed to the surface of clay minerals. Also, clay loss was observed within the soil and eroding dust from Moab, whereas there was twice as much clay within the surface horizons of Niwot than the subsurface due to dust deposition. Clay is fundamental to soil fertility, increases the cation exchange capacity, and retention of water and nutrients within the soil. Microbes are often associated with clay particles since the high surface area provides a suitable habitat for microbial growth (Li et al., 2019). Therefore, the current findings regarding the relationship between clay and dust could be relevant for scientists studying the aerobiome.

Some of the limitations in this research include an insufficient number of erosion and deposition samples for performing analyses and statistical computations, and MWAC

malfunctions. For future studies we recommend installing more MWAC and marble trap samplers at all sampling sites to collect enough samples for analyses and avoid insufficient data due to instrument malfunction. Also, if the dust samplers were installed and collected for more than a year, variations would be observable both seasonally and yearly, to produce accurate flux measurements.

REFERENCES

Aarons, S. M., Blakowski, M. A., Aciego, S. M., Stevenson, E. I., Sims, K. W. W., Scott, S. R., & Aarons, C. (2017). Geochemical characterization of critical dust source regions in the American West. *Geochimica et Cosmochimica Acta*, *215*, 141–161.
<https://doi.org/10.1016/j.gca.2017.07.024>

Aciego, S. M., Riebe, C. S., Hart, S. C., Blakowski, M. A., Carey, C. J., Aarons, S. M., Dove, N. C., Botthoff, J. K., Sims, K. W. W., & Aronson, E. L. (2017). Dust outpaces bedrock in nutrient supply to montane forest ecosystems. *Nature Communications*, *8*(1), 14800.
<https://doi.org/10.1038/ncomms14800>

Anonymous 1. (2021). Wind Roses Yearly Climatology Moab/Canyonlands from 1973 to 2021. *Iowa State University*. accessed 1/5/2022,
https://mesonet.agron.iastate.edu/sites/windrose.phtml?station=CNY&network=UT_ASOS

Anonymous 2. (2022). *Soil physical and chemical properties, Megapit (DP1.00096.001)*. National Ecological Observatory Network (NEON). accessed 11/10/2022,
<https://doi.org/10.48443/10DN-8031>

Aubault, H., Webb, N. P., Strong, C. L., McTainsh, G. H., Leys, J. F., & Scanlan, J. C. (2015). Grazing impacts on the susceptibility of rangelands to wind erosion: The effects of stocking rate, stocking strategy and land condition. *Aeolian Research*, *17*, 89–99.
<https://doi.org/10.1016/j.aeolia.2014.12.005>

Belnap, J., Reynolds, R. L., Reheis, M. C., Phillips, S. L., Urban, F. E., & Goldstein, H. L. (2009). Sediment losses and gains across a gradient of livestock grazing and plant invasion in a cool, semi-arid grassland, Colorado Plateau, USA. *Aeolian Research*, *1*(1–2), 27–43.
<https://doi.org/10.1016/j.aeolia.2009.03.001>

Bergstrom, R. M., Borch, T., Martin, P. H., Melzer, S., Rhoades, C. C., Salley, S. W., & Kelly, E. F. (2019). The generation and redistribution of soil cations in high elevation catenas in the Fraser Experimental Forest, Colorado, U.S. *Geoderma*, *333*, 135–144.
<https://doi.org/10.1016/j.geoderma.2018.07.024>

Boix-Fayos, C., Martínez-Mena, M., Arnau-Rosalén, E., Calvo-Cases, A., Castillo, V., & Albaladejo, J. (2006). Measuring soil erosion by field plots: Understanding the sources of variation. *Earth-Science Reviews*, 78(3), 267–285. <https://doi.org/10.1016/j.earscirev.2006.05.005>

Brahney, J., Ballantyne, A. P., Kociolek, P., Spaulding, S., Otu, M., Porwoll, T., & Neff, J. C. (2014). Dust mediated transfer of phosphorus to alpine lake ecosystems of the Wind River Range, Wyoming, USA. *Biogeochemistry*, 120(1–3), 259–278. <https://doi.org/10.1007/s10533-014-9994-x>

Brahney, J., Ballantyne, A. P., Sievers, C., & Neff, J. C. (2013). Increasing Ca²⁺ deposition in the western US: The role of mineral aerosols. *Aeolian Research*, 10, 77–87. <https://doi.org/10.1016/j.aeolia.2013.04.003>

Brazier, R. E. (2004). Quantifying soil erosion by water in the UK: a review of monitoring and modelling approaches. *Progress in Physical Geography*, 28, 340–365.

Brimhall, G. H., & Dietrich, W. E. (1985). Constitutive mass balance relations between chemical composition, volume, density, porosity, and strain in metasomatic hydrothermal systems: Results on weathering and pedogenesis. *Geochimica et Cosmochimica Acta*, 59, 8–21.

Brimhall, G. H., Lewis, C. J., Ague, J. J., Dietrich, W. E., Hampel, J., Teague, T., & Rix, P. (1988). Metal enrichment in bauxites by deposition of chemically mature aeolian dust. *Nature*, 333(6176), 819–824. <https://doi.org/10.1038/333819a0>

Calvo-Cases, A., Boix-Fayos, C., & Imeson, A. (2003). Runoff generation, sediment movement and soil water behavior on calcareous (limestone) slopes of some Mediterranean environments in southeast Spain. *Emu*, 269–291.

Cammeraat, E. L. H. (2004). Scale dependent thresholds in hydrological and erosion response of a semi-arid catchment in southeast Spain. *Agriculture, Ecosystems & Environment*, 104(2), 317–332.

Cammeraat, L. H. (2002). A review of two strongly contrasting geomorphological systems within the context of scale. *Earth Surface Processes and Landforms*, 27(11), 1201–1222. <https://doi.org/10.1002/esp.421>

Cerdà, A. (2001). Effects of rock fragment cover on soil infiltration, interrill runoff and erosion. *European Journal of Soil Science*, 52(1), 59–68. <https://doi.org/10.1046/j.1365-2389.2001.00354.x>

Chadwick, O. A., Brimhall, G. H., & Hendricks, D. M. (1990). From a Black to Gray Box- a Mass Balance Interpretation of Pedogenesis. *Geomorphology*, 3, 369–390.

Chadwick, O. A., Derry, L. A., Vitousek, P. M., Huebert, B. J., & Hedin, L. O. (1999). Changing sources of nutrients during four million years of ecosystem development. *Nature*, 397(6719), 491–497. <https://doi.org/10.1038/17276>

Cope, F. (1958). *Catchment salting in Victoria*. (Vol. 1). Victoria Soil Conservation Authority.

De Vente, J., & Poesen, J. (2005). Predicting soil erosion and sediment yield at the basin scale: Scale issues and semi-quantitative models. *Earth-Science Reviews*, 71(1), 95–125. <https://doi.org/10.1016/j.earscirev.2005.02.002>

Derner, J., Briske, D., Reeves, M., Brown-Brandl, T., Meehan, M., Blumenthal, D., Travis, W., Augustine, D., Wilmer, H., Scasta, D., Hendrickson, J., Volesky, J., Edwards, L., & Peck, D. (2018). Vulnerability of grazing and confined livestock in the Northern Great Plains to projected mid- and late-twenty-first century climate. *Climatic Change*, 146(1–2), 19–32. <https://doi.org/10.1007/s10584-017-2029-6>

Duniway, M. C., Geiger, E. L., Minnick, T. J., Phillips, S. L., & Belnap, J. (2018). Insights from Long-Term Ungrazed and Grazed Watersheds in a Salt Desert Colorado Plateau Ecosystem. *Rangeland Ecology & Management*, 71(4), 492–505. <https://doi.org/10.1016/j.rama.2018.02.007>

Eberly, P. O., McFadden, L. D., & Watt, P. M. (1996). Eolian dust as a factor in soil development on the Pajarito Plateau, Los Alamos area, northern New Mexico. *The Jemez Mountains Region*, 383–389. <https://doi.org/10.56577/FFC-47.383>

Gao, S., & Collins, M. (1992). Net sediment transport patterns inferred from grain-size trends, based upon definition of “transport vectors.” *Sedimentary Geology*, 81(1–2), 47–60. [https://doi.org/10.1016/0037-0738\(92\)90055-V](https://doi.org/10.1016/0037-0738(92)90055-V)

Goldstein, H. L., Reynolds, R. L., Reheis, M. C., Yount, J. C., & Neff, J. C. (2008). Compositional trends in aeolian dust along a transect across the southwestern United States. *Journal of Geophysical Research*, 113(F2), F02S02. <https://doi.org/10.1029/2007JF000751>

Goodman, M. M., Carling, G. T., Fernandez, D. P., Rey, K. A., Hale, C. A., Bickmore, B. R., Nelson, S. T., & Munroe, J. S. (2019). Trace element chemistry of atmospheric deposition along the Wasatch Front (Utah, USA) reflects regional playa dust and local urban aerosols. *Chemical Geology*, 530, 119317. <https://doi.org/10.1016/j.chemgeo.2019.119317>

Harris, A. T., Asner, G. P., & Miller, M. E. (2003). Changes in Vegetation Structure after Long-term Grazing in Pinyon-Juniper Ecosystems: Integrating Imaging Spectroscopy and Field Studies. *Ecosystems*, 6(4), 368–383. <https://doi.org/10.1007/s10021-003-0168-2>

Heindel, R. C., Putman, A. L., Murphy, S. F., Repert, D. A., & Hinckley, E. -L. S. (2020a). Atmospheric Dust Deposition Varies by Season and Elevation in the Colorado Front Range, USA. *Journal of Geophysical Research: Earth Surface*, 125(5). <https://doi.org/10.1029/2019JF005436>

Hennessy, J. T., Kies, B., Gibbens, R. P., & Tromble, J. M. (1986). Soil Sorting by Forty-five Years of Wind Erosion on a Southern New Mexico Range. *Soil Science Society of America Journal*, 50(2), 391–394. <https://doi.org/10.2136/sssaj1986.03615995005000020027x>

Herrick, J. E. (Ed.). (2005). Core Methods. In *Monitoring manual for grassland, shrubland, and savanna ecosystems* (2nd ed., Vol. 1, pp. 27–37). USDA - ARS Jordana Experimental Range; Distributed by the University of Arizona Press.

Kendall, A. H. W., & Pimentel, D. (1994). Constraints on the Expansion of the Global Food Supply. *Royal Swedish Academy of Science*, 23(3), 198–205.

Kim, H., & Choi, M. (2015). Impact of soil moisture on dust outbreaks in East Asia: Using satellite and assimilation data. *Geophysical Research Letters*, 42(8), 2789–2796. <https://doi.org/10.1002/2015GL063325>

Kittel, T. G. F., Williams, M. W., Chowanski, K., Hartman, M., Ackerman, T., Losleben, M., & Blanken, P. D. (2015). Contrasting long-term alpine and subalpine precipitation trends in a mid-latitude North American mountain system, Colorado Front Range, USA. *Plant Ecology & Diversity*, 8(5–6), 607–624. <https://doi.org/10.1080/17550874.2016.1143536>

Klippel, G. E., & Costello, D. F. (1960). Vegetation and Cattle Responses to Different Intensities of Grazing on Short-Grass Ranges on the Central Great Plains. In *USDA, Washington, D.C.* (pp. 18–20).

Kosmos, C., Danalatos, N. G., Lopez-Berbudez, F., & Romero Diaz, M. A. (2003). The Effect of Land Use on Soil Erosion and Land Degradation under Mediterranean Conditions. In *Mediterranean Desertification: A Mosaic of Processes and Responses* (pp. 57–70). John Wiley & Sons.

Krumbein, W. C. (1934). Size frequency distributions of sediments. *Journal of Sedimentary Research*, 4, 65–77.

Krumbein, W. C. (1938). Size frequency distributions of sediments and the normal phi curve. *Journal of Sedimentary Research*, 8(3), 84–90. <https://doi.org/10.1306/D4269008-2B26-11D7-8648000102C1865D>

Kurtz, A. C., Derry, L. A., & Chadwick, O. A. (2001). Accretion of Asian dust to Hawaiian soils: Isotopic, elemental, and mineral mass balances. *Geochimica et Cosmochimica Acta*, 65(12), 1971–1983. [https://doi.org/10.1016/S0016-7037\(01\)00575-0](https://doi.org/10.1016/S0016-7037(01)00575-0)

Lauchli, A., & Epstein, E. (1990). Plant response to saline and sodic conditions. In *ASCE Manuals Practice* (Vol. 71, pp. 113–137). American Society of Civil Engineering.

Lavee, H., Imeson, A. C., & Sarah, P. (1998). The impact of climate change on geomorphology and desertification along a Mediterranean-arid transect. *Land Degradation & Development*, 9(5), 407–422. [https://doi.org/10.1002/\(SICI\)1099-145X\(199809/10\)9:5<407::AID-LDR302>3.0.CO;2-6](https://doi.org/10.1002/(SICI)1099-145X(199809/10)9:5<407::AID-LDR302>3.0.CO;2-6)

Lawrence, C. R., & Neff, J. C. (2009). The contemporary physical and chemical flux of aeolian dust: A synthesis of direct measurements of dust deposition. *Chemical Geology*, 267(1–2), 46–63. <https://doi.org/10.1016/j.chemgeo.2009.02.005>

Lawrence, C. R., Painter, T. H., Landry, C. C., & Neff, J. C. (2010). Contemporary geochemical composition and flux of aeolian dust to the San Juan Mountains, Colorado, United States. *Journal of Geophysical Research*, 115(G3), G03007. <https://doi.org/10.1029/2009JG001077>

Lawrence, C. R., Reynolds, R. L., Ketterer, M. E., & Neff, J. C. (2013a). Aeolian controls of soil geochemistry and weathering fluxes in high-elevation ecosystems of the Rocky Mountains, Colorado. *Geochimica et Cosmochimica Acta*, 107, 27–46. <https://doi.org/10.1016/j.gca.2012.12.023>

Li, G. L., Zhou, C. H., Fiore, S., & Yu, W. H. (2019). Interactions between microorganisms and clay minerals: New insights and broader applications. *Applied Clay Science*, 177, 91–113. <https://doi.org/10.1016/j.clay.2019.04.025>

Litaor, M. I. (1987). The Influence of Eolian Dust on the Genesis of Alpine Soils in the Front Range, Colorado. *Soil Science Society of America Journal*, 51(1), 142–147. <https://doi.org/10.2136/sssaj1987.03615995005100010031x>

Lyles, L. (1976). Wind Patterns and Soil Erosion on the Great Plains. *USDA, ARS*, 205–214.
McLaren, P., & Bowles, D. (1985). The Effects of Sediment Transport on Grain-Size Distributions. *Journal of Sedimentary Research*, 55(4).

- Milchunas, D. G., Sala, O. E., & Lauenroth, W. K. (1988). A Generalized Model of the Effects of Grazing by Large Herbivores on Grassland Community Structure. *The American Naturalist*, 132(1), 87–106. <https://doi.org/10.1086/284839>
- Mladenov, N., Williams, M. W., Schmidt, S. K., & Cawley, K. (2012). Atmospheric deposition as a source of carbon and nutrients to an alpine catchment of the Colorado Rocky Mountains. *Biogeosciences*, 9(8), 3337–3355. <https://doi.org/10.5194/bg-9-3337-2012>
- Muhs, D. R., & Benedict, J. B. (2006). Eolian Additions to Late Quaternary Alpine Soils, Indian Peaks Wilderness Area, Colorado Front Range. *Arctic, Antarctic, and Alpine Research*, 38(1), 120–130. [https://doi.org/10.1657/1523-0430\(2006\)038\[0120:EATLQA\]2.0.CO;2](https://doi.org/10.1657/1523-0430(2006)038[0120:EATLQA]2.0.CO;2)
- Munroe, J. S. (2022). Relation between regional drought and mountain dust deposition revealed by a 10-year record from an alpine critical zone. *Science of The Total Environment*, 844, 156999. <https://doi.org/10.1016/j.scitotenv.2022.156999>
- Munroe, J. S., Norris, E. D., Olson, P. M., Ryan, P. C., Tappa, M. J., & Beard, B. L. (2020). Quantifying the contribution of dust to alpine soils in the periglacial zone of the Uinta Mountains, Utah, USA. *Geoderma*, 378, 17. <https://doi.org/10.1016/j.geoderma.2020.114631>
- Nauman, T. W., Duniway, M. C., Webb, N. P., & Belnap, J. (2018). Elevated aeolian sediment transport on the Colorado Plateau, USA: The role of grazing, vehicle disturbance, and increasing aridity: Colorado Plateau aeolian transport. *Earth Surface Processes and Landforms*, 43(14), 2897–2914. <https://doi.org/10.1002/esp.4457>
- Neff, J. C., Ballantyne, A. P., Farmer, G. L., Mahowald, N. M., Conroy, J. L., Landry, C. C., Overpeck, J. T., Painter, T. H., Lawrence, C. R., & Reynolds, R. L. (2008). Increasing eolian dust deposition in the western United States linked to human activity. *Nature Geoscience*, 1(3), 189–195. <https://doi.org/10.1038/ngeo133>
- Neff, J. C., Reynolds, R. L., Belnap, J., & Lamothe, P. (2005). Multi-Decadal Impacts of Grazing on Soil Physical and Biogeochemical Properties in Southeast Utah. *Ecological Applications*, 15(1), 87–95. <https://doi.org/10.1890/04-0268>

Okin, G. S., Gillette, D. A., & Herrick, J. E. (2006). Multi-scale controls on and consequences of aeolian processes in landscape change in arid and semi-arid environments. *Journal of Arid Environments*, 65(2), 253–275. <https://doi.org/10.1016/j.jaridenv.2005.06.029>

Painter, T. H., Barrett, A. P., Landry, C. C., Neff, J. C., Cassidy, M. P., Lawrence, C. R., McBride, K. E., & Farmer, G. L. (2007). Impact of disturbed desert soils on duration of mountain snow cover. *Geophysical Research Letters*, 34(12), L12502. <https://doi.org/10.1029/2007GL030284>

Puigdefábregas, J. (2005). The role of vegetation patterns in structuring runoff and sediment fluxes in drylands. *Earth Surface Processes and Landforms*, 30(2), 133–147. <https://doi.org/10.1002/esp.1181>

Puigdefabregas, J., Sole, A., Gutierrez, L., del Barrio, G., & Boer, M. (1999). Scales and processes of water and sediment redistribution in drylands: Results from the Rambla Honda field site in Southeast Spain. *Earth-Science Reviews*, 48(1), 39–70. [https://doi.org/10.1016/S0012-8252\(99\)00046-X](https://doi.org/10.1016/S0012-8252(99)00046-X)

Read, D. W. L., & Campbell, C. A. (1981). Bio-Cycling of Phosphorous in Soil by Plant Roots. *Canadian Journal of Soil Science*, 61(4), 587–589. <https://doi.org/10.4141/cjss81-069>

Reheis, M. C., & Kihl, R. (1995). Dust deposition in southern Nevada and California, 1984–1989: Relations to climate, source area, and source lithology. *Journal of Geophysical Research*, 100(D5), 8893. <https://doi.org/10.1029/94JD03245>

Reynolds, R., Belnap, J., Reheis, M., Lamothe, P., & Luiszer, F. (2001). Aeolian dust in Colorado Plateau soils: Nutrient inputs and recent change in source. *Proceedings of the National Academy of Sciences*, 98(13), 7123–7127. <https://doi.org/10.1073/pnas.121094298>

Reynolds, R. L., Munson, S. M., Fernandez, D., Goldstein, H. L., & Neff, J. C. (2016). Concentrations of mineral aerosol from desert to plains across the central Rocky Mountains, western United States. *Aeolian Research*, 23, 21–35. <https://doi.org/10.1016/j.aeolia.2016.09.001>

Reynolds, R., Neff, J., Reheis, M., & Lamothe, P. (2006). Atmospheric dust in modern soil on aeolian sandstone, Colorado Plateau (USA): Variation with landscape position and contribution to potential plant nutrients. *Geoderma*, *130*(1–2), 108–123. <https://doi.org/10.1016/j.geoderma.2005.01.012>

Routson, C. C., Arcusa, S. H., McKay, N. P., & Overpeck, J. T. (2019). A 4,500-Year-Long Record of Southern Rocky Mountain Dust Deposition. *Geophysical Research Letters*, *46*(14), 8281–8288. <https://doi.org/10.1029/2019GL083255>

Simonson, R. W. (1959). Outline of a Generalized Theory of Soil Genesis. *Soil Science Society of America Proceedings*, 152–156.

Soil Survey Staff. (2014). *Kellogg Soil Survey Laboratory Methods Manual* (No. 42; Soil Surveys Investigation). U.S. Department of Agriculture, Natural Resources Conservation Service.

Sumner, M., Miller, W. P., Kookana, R. S., & Hazelton, P. (1998). Sodic dispersion and environmental quality. In *Sodic Soils: Distribution, Properties, Management, and Environmental Consequences* (pp. 149–172). Oxford University Press.

Tanner, W. F. (1969). The Particle Size Scale. *Journal of Sedimentary Research*, *39*(2), 809–812. <http://archives.datapages.com/data/sepm/journals/v38-41/data/039/039002/0809.htm>

Tatarko, J., & Presley, D. (2009). Principles of Wind Erosion and its Control. *Kansas State University*, 860, 4–5.

Valerino, M. J., Johnson, J. J., Izumi, J., Orozco, D., Hoff, R. M., Delgado, R., & Hennigan, C. J. (2017). Sources and composition of PM_{2.5} in the Colorado Front Range during the DISCOVER-AQ study: PM_{2.5} IN DENVER DURING SUMMER. *Journal of Geophysical Research: Atmospheres*, *122*(1), 566–582. <https://doi.org/10.1002/2016JD025830>

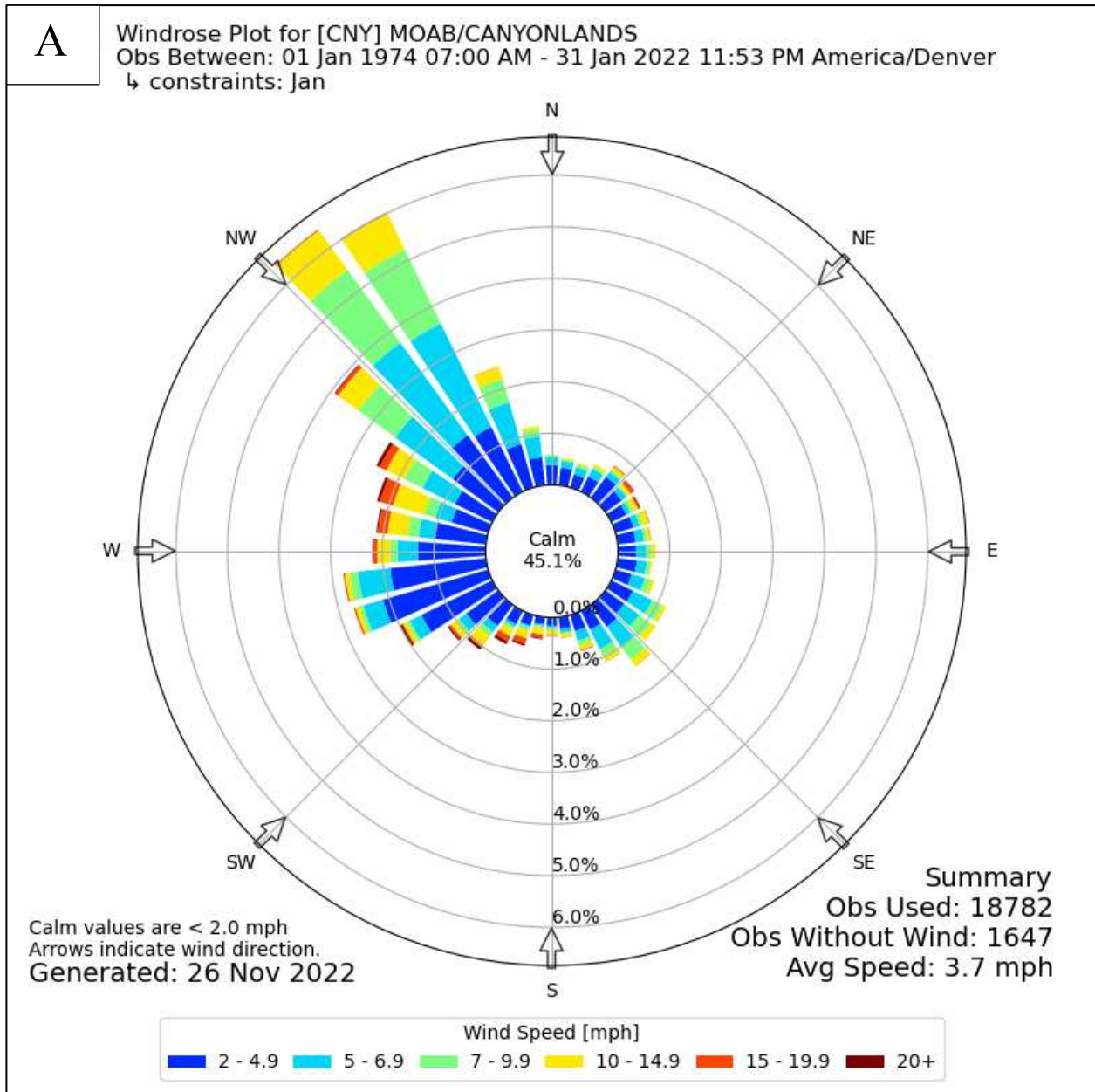
Webb, N. P., Herrick, J. E., Hugenholtz, C. H., Zobeck, T. M., & Okin, G. S. (2015). Standard Methods for Wind Erosion Research and Model Development. *USDA-ARS Jornada Experimental Range*, 10, 65–70.

Wells, K. C., Witek, M., Flatau, P., Kreidenweis, S. M., & Westphal, D. L. (2007). An analysis of seasonal surface dust aerosol concentrations in the western US (2001–2004): Observations and model predictions. *Atmospheric Environment*, 41(31), 6585–6597.
<https://doi.org/10.1016/j.atmosenv.2007.04.034>

Whicker, J. J., Pinder, J. E., & Breshears, D. D. (2006). Increased Wind Erosion from Forest Wildfire: Implications for Contaminant-Related Risks. *Journal of Environmental Quality*, 35(2), 468–478. <https://doi.org/10.2134/jeq2005.0112>

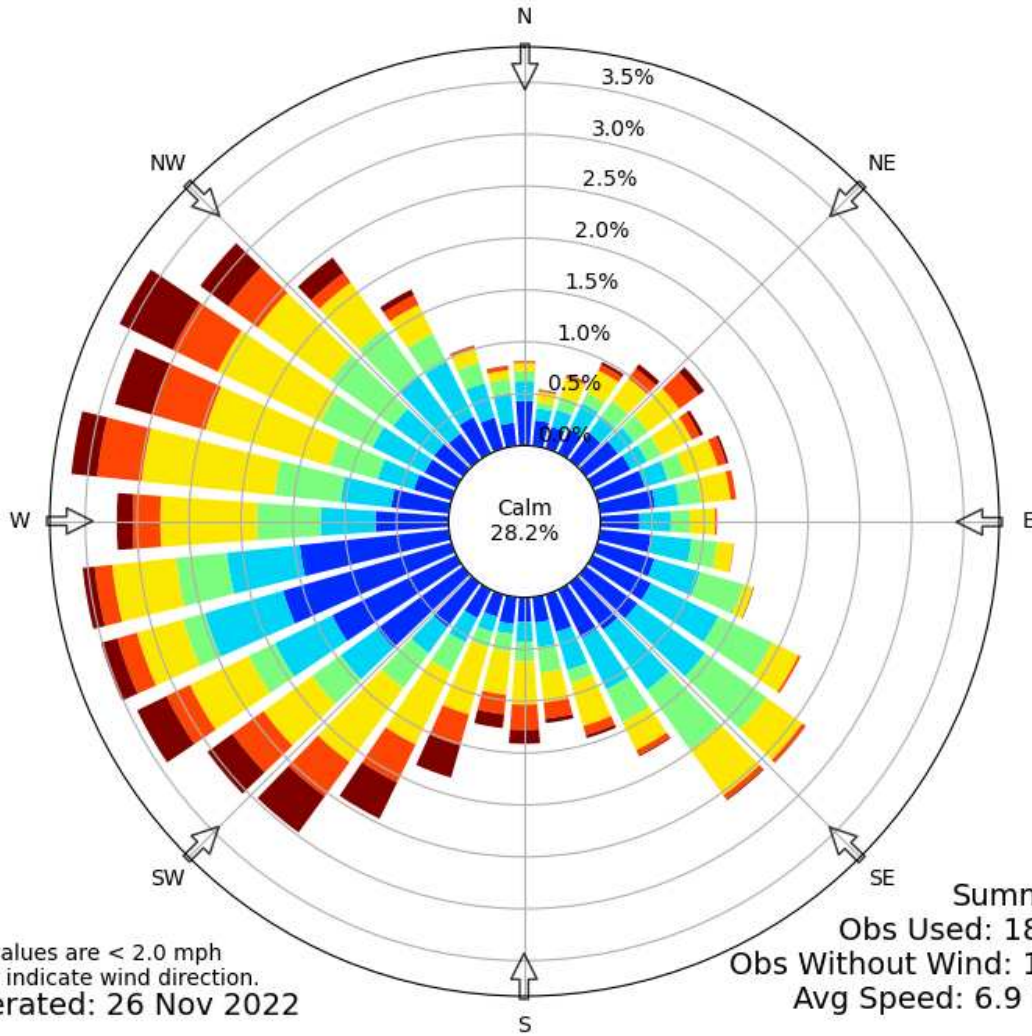
APPENDICES

APPENDIX A: WIND ROSE FIGURES



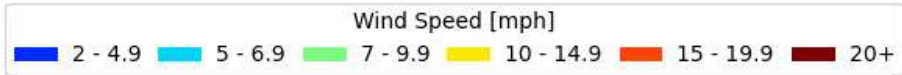
B

Windrose Plot for [CNY] MOAB/CANYONLANDS
Obs Between: 01 Mar 1973 03:00 PM - 31 Mar 2022 11:53 PM America/Denver
↳ constraints: Mar



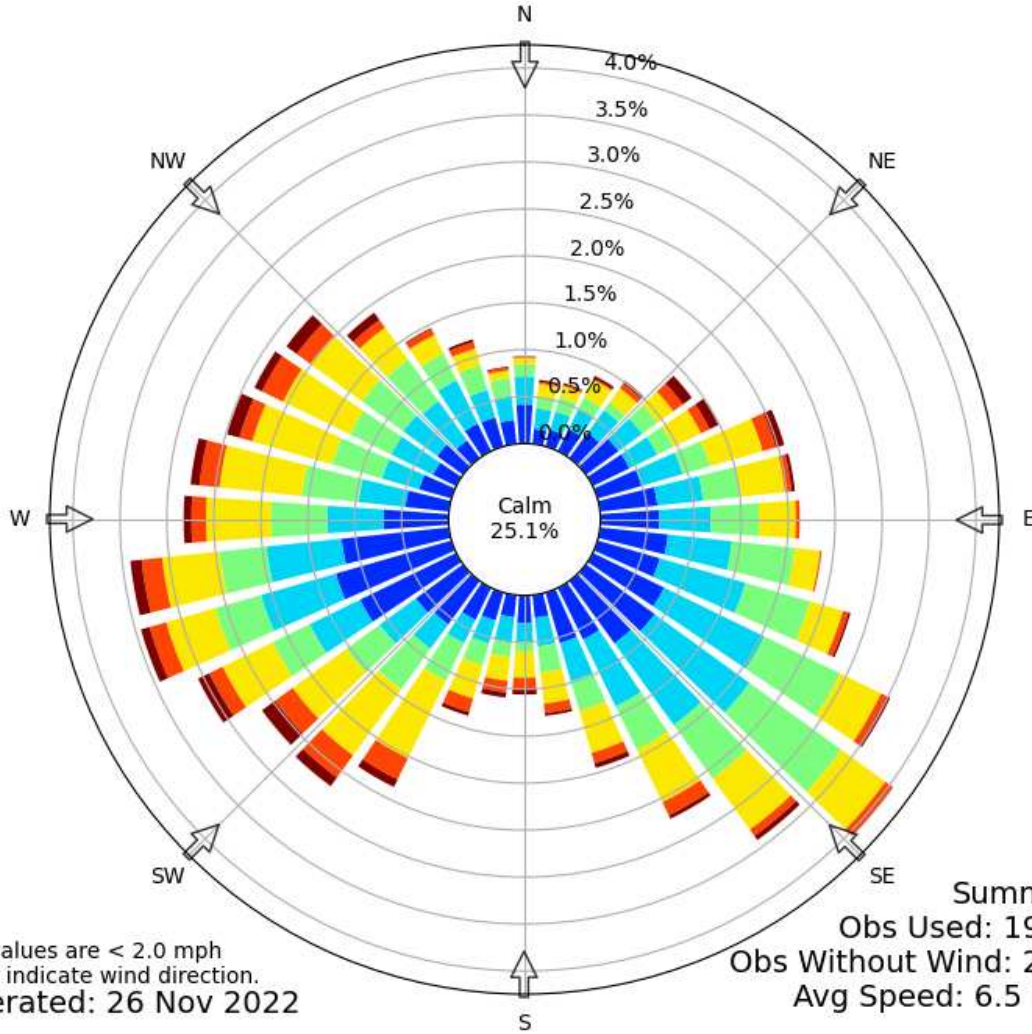
Calm values are < 2.0 mph
Arrows indicate wind direction.
Generated: 26 Nov 2022

Summary
Obs Used: 18433
Obs Without Wind: 1980
Avg Speed: 6.9 mph

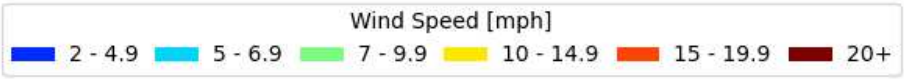


C

Windrose Plot for [CNY] MOAB/CANYONLANDS
Obs Between: 01 Aug 1974 07:00 AM - 31 Aug 2022 11:53 PM America/Denver
↳ constraints: Aug



Calm values are < 2.0 mph
Arrows indicate wind direction.
Generated: 26 Nov 2022



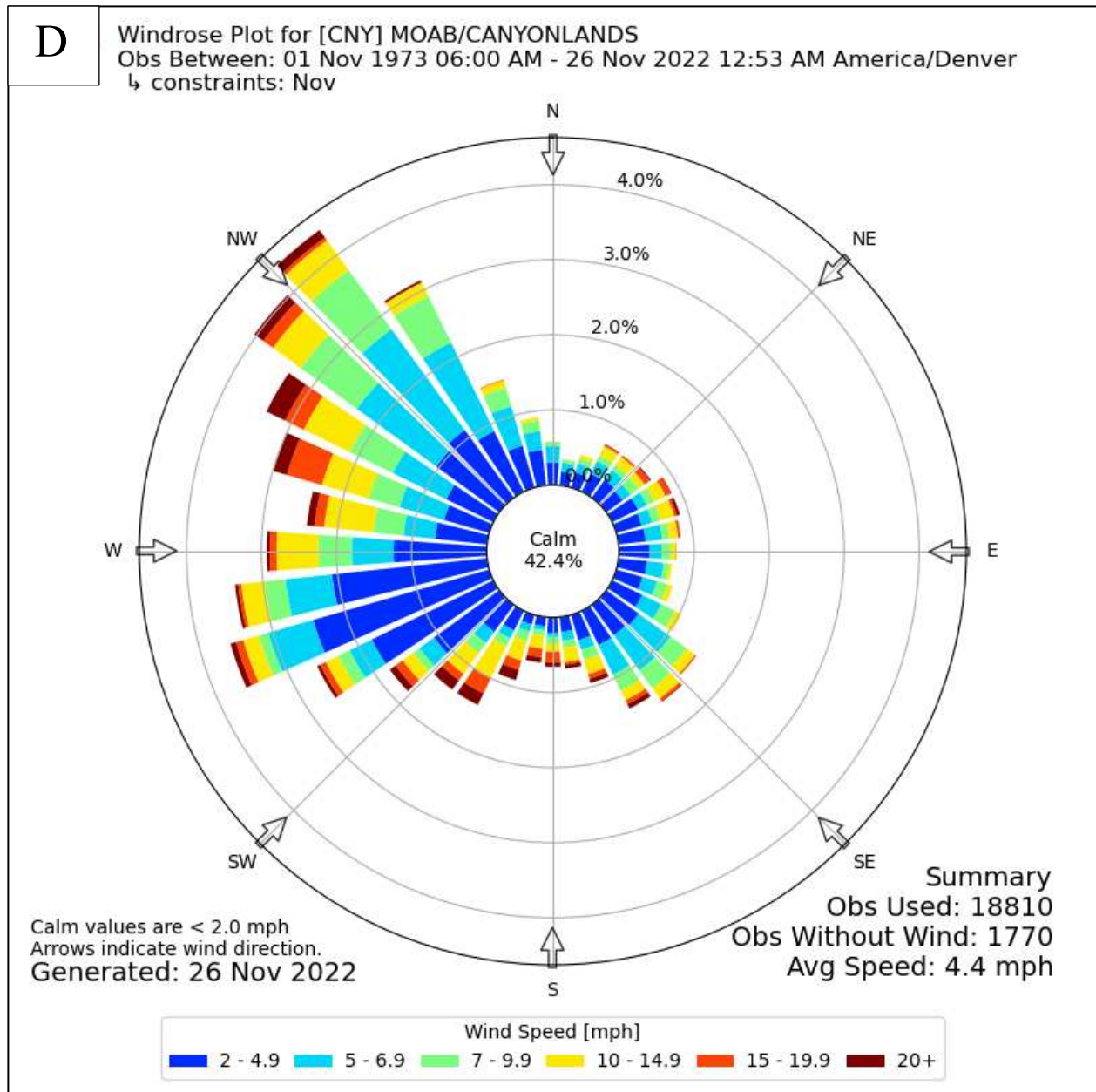
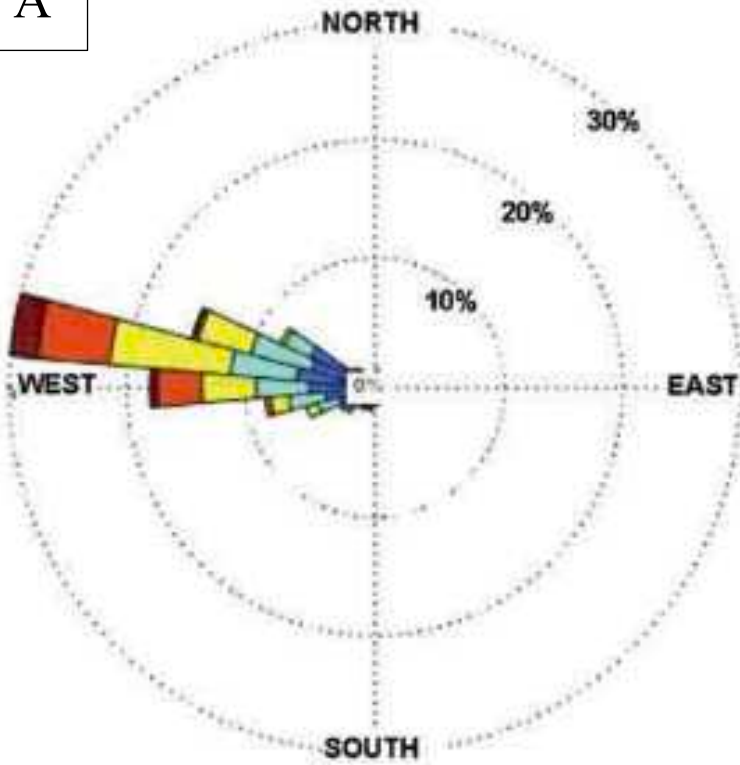
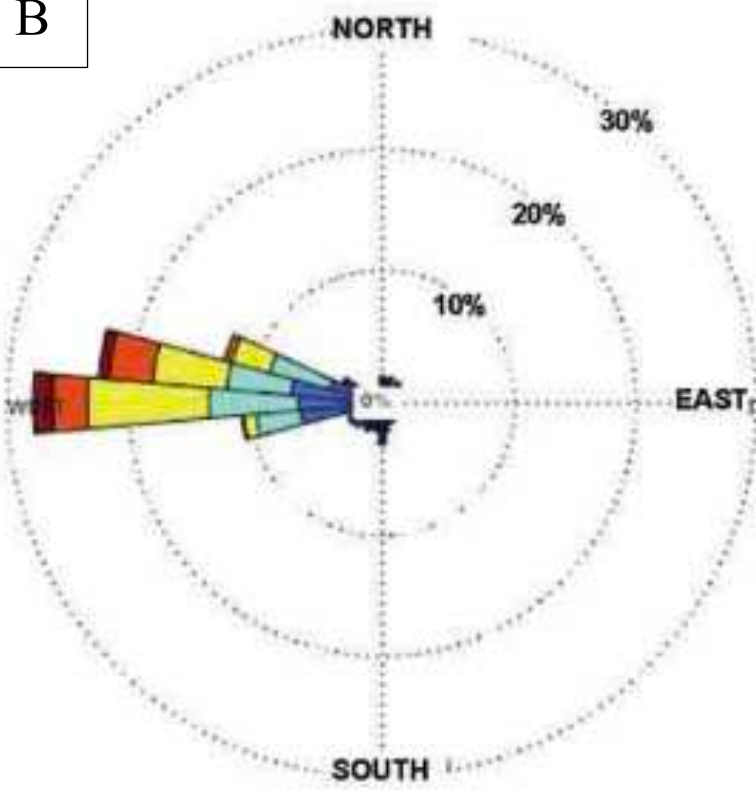


Figure A.1. A monthly wind rose representative of the of wind directions and wind speed for in the Canyonlands, UT for each season (A) January, which is a representative of the winter season (January - February), (B) March, which is a representative of the spring season (March- June), (C) August, which is a representative of the summer season (July - September), (D) November, which is a representative of the fall season (October - December). Seasons were determined by similar wind direction and wind speed patterns per month. Wind speed and wind direction observations between (12:00 – 17:00 local time) averaged over 1974- 2022 for each month. Data from (Anonymous 1, 2021).

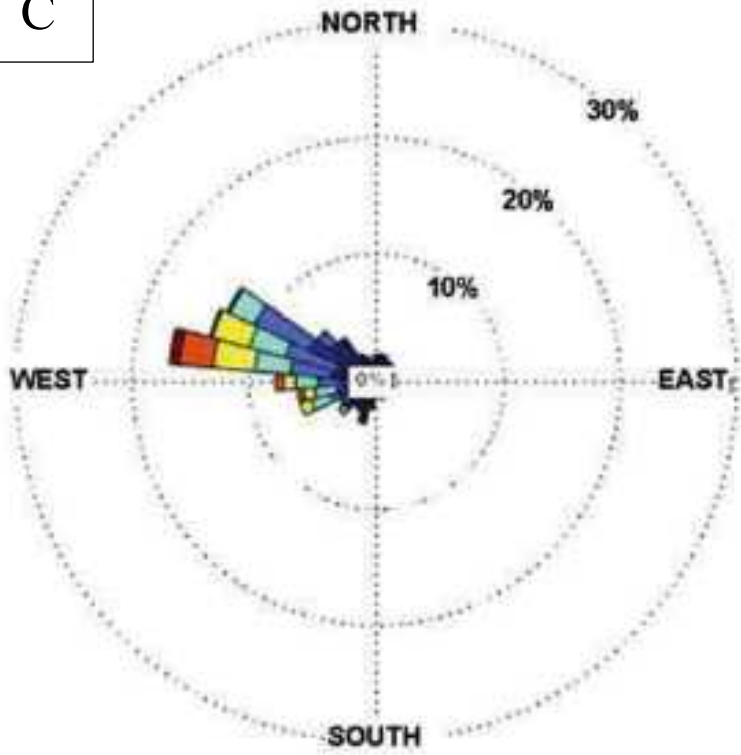
A



B



C



D

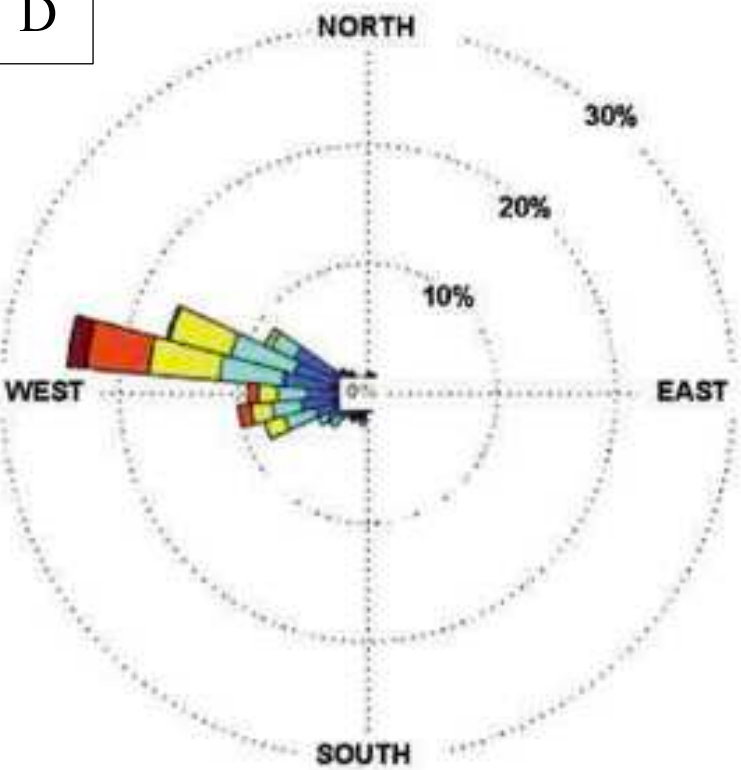
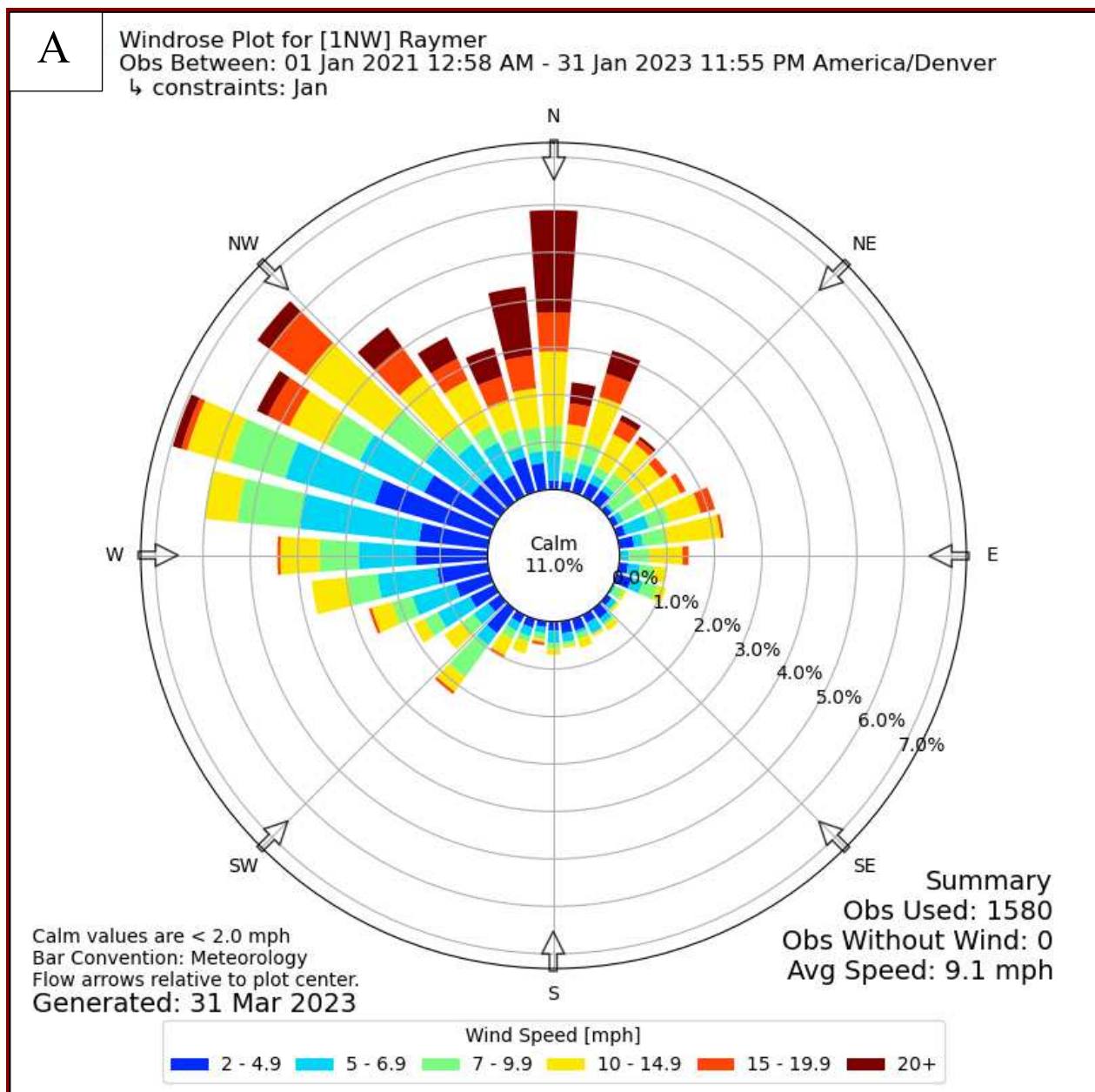
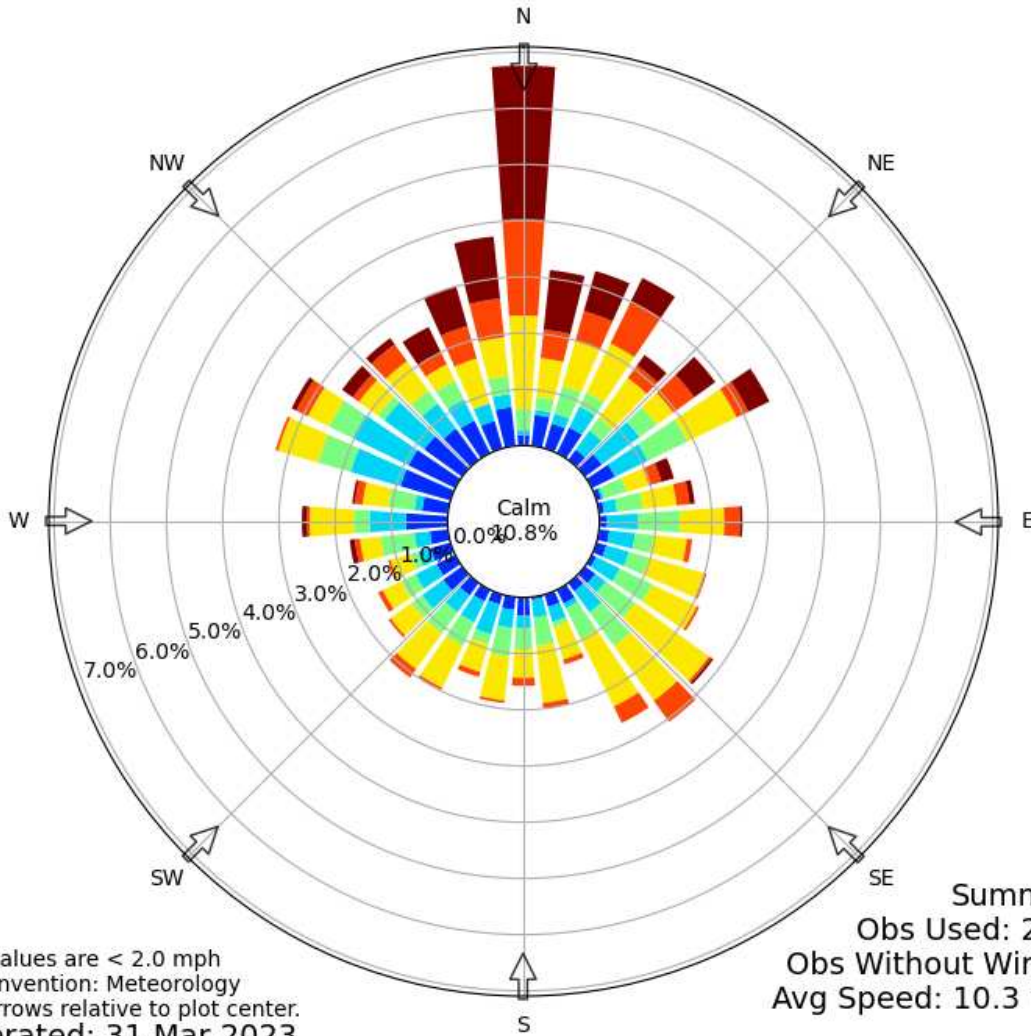


Figure A.2. Wind rose of daytime (8:00AM – 16:00 local time) wind directions and wind speed at Niwot alpine site for (A) winter (December, January, February), (B) spring (March, April, May), (C) summer (June, July, August), (D) fall (September, October, November). The frequency scale (concentric circles) is in 10% steps (0–30%); the wind speed scale is in intervals of 5 m s⁻¹ (dark blue, 0–5ms⁻¹; dark red, 25–30 m s⁻¹). Data taken from (Kittel et al., 2015)



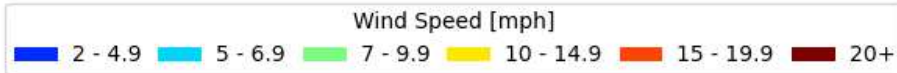
B

Windrose Plot for [1NW] Raymer
Obs Between: 01 Mar 2021 12:58 AM - 30 Mar 2023 04:55 PM America/Denver
↳ constraints: Mar



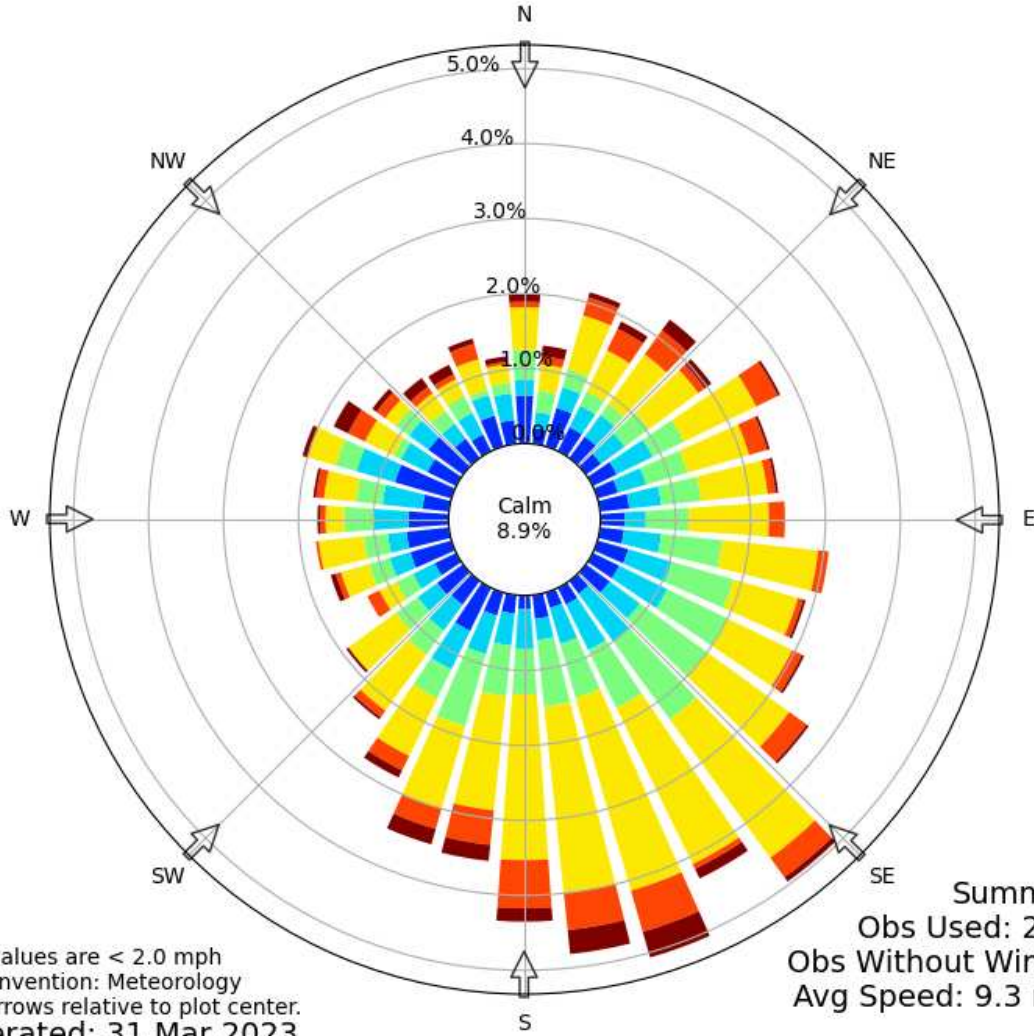
Calm values are < 2.0 mph
Bar Convention: Meteorology
Flow arrows relative to plot center.
Generated: 31 Mar 2023

Summary
Obs Used: 2161
Obs Without Wind: 0
Avg Speed: 10.3 mph

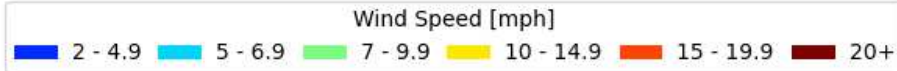


C

Windrose Plot for [1NW] Raymer
Obs Between: 01 Aug 2019 12:58 AM - 31 Aug 2022 11:56 PM America/Denver
↳ constraints: Aug



Calm values are < 2.0 mph
Bar Convention: Meteorology
Flow arrows relative to plot center.
Generated: 31 Mar 2023



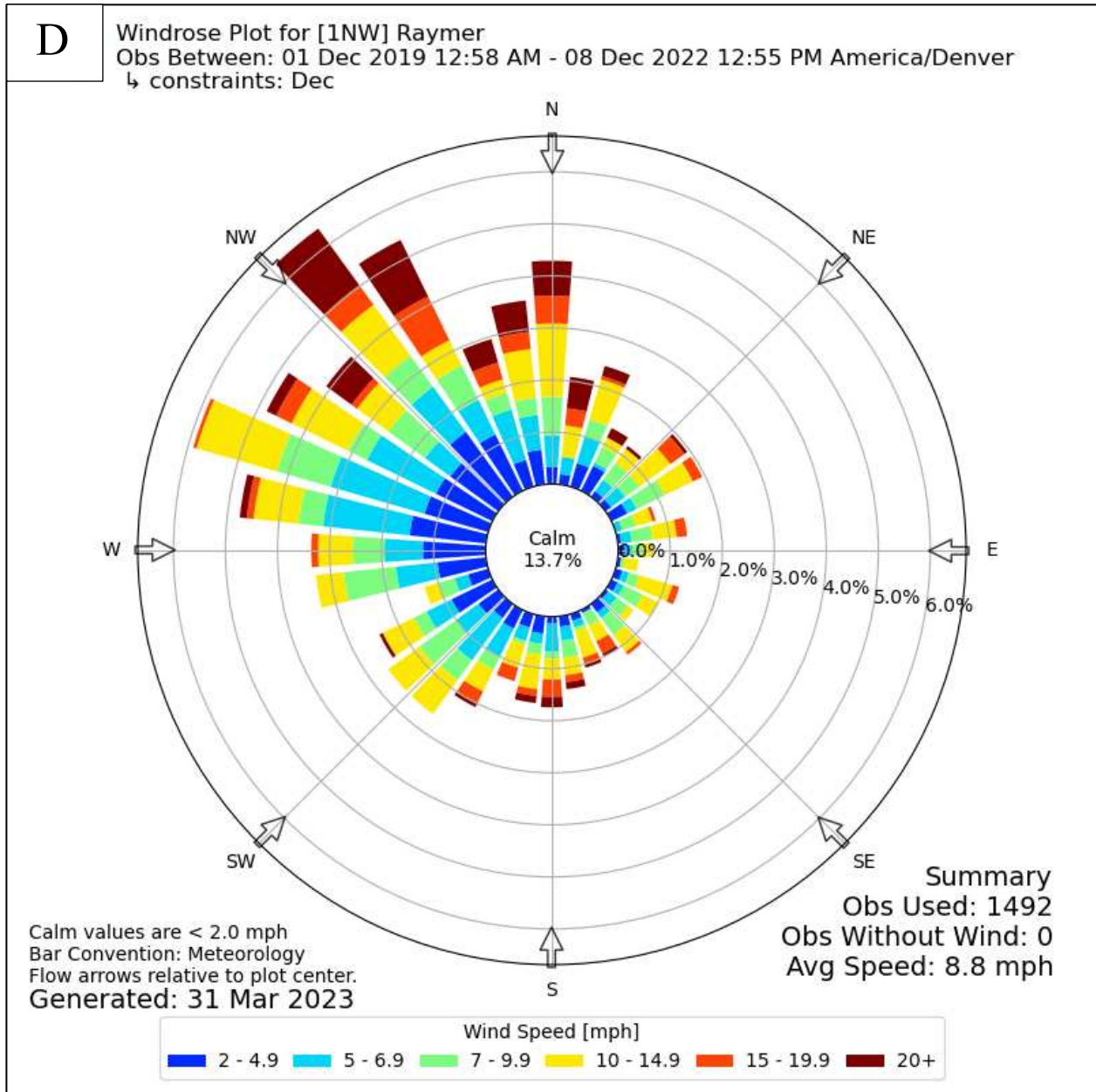


Figure A.3: A monthly wind rose representative of the of wind directions and wind speed for in the Raymer, CO (80 km east of CPER in the western Great Plains) for each season (A) January which is a representative of the winter season (January - February), (B) March which is a representative of the spring season (March- April), (C) August which is a representative of the summer season (June - September), (D) December which is a representative of the fall season (October - December). Seasons were determined by similar wind direction and wind speed patterns per month. Wind speed and wind direction observations between (12:00 – 17:00 local time) averaged over 1974- 2022 for each month. Data from (Anonymous 1, 2021).

APPENDIX B: FILTER COLLECTION DATES

Table B.1. Collected NEON PM<10 filters sampling periods and seasons for Moab, Niwot, and CPER.

Site	ID	Date Start	Date End	Season
CPER	984528	12/14/22	12/28/22	Fall
CPER	984521	11/9/22	11/28/22	Fall
CPER	954592	6/27/22	7/14/22	Summer
CPER	943770	5/4/22	5/18/22	Summer
CPER	943766	4/21/22	5/4/22	Spring
CPER	943749	3/21/22	4/5/22	Spring
CPER	927366	2/15/22	3/8/22	Winter
CPER	927355	1/5/22	1/19/22	Winter
CPER	927347	11/24/21	12/7/21	Fall
CPER	892180	10/19/21	11/10/21	Fall
CPER	892154	9/8/21	9/22/21	Summer
CPER	870829	7/20/21	8/18/21	Summer
CPER	870813	5/25/21	6/14/21	Summer
CPER	870801	4/20/21	5/5/21	Spring
CPER	839625	3/10/21	3/31/21	Spring
CPER	839629	2/16/21	3/10/21	Spring
CPER	839610	1/6/21	1/20/21	Winter
CPER	839609	12/22/20	1/6/21	Winter
Moab	984536	11/1/22	12/12/22	Fall
Moab	984532	10/4/22	10/17/22	Fall
Moab	954607	8/21/22	9/6/22	Summer
Moab	954600	6/27/22	7/10/22	Summer
Moab	943775	4/20/22	5/2/22	Spring
Moab	943755	3/23/22	4/5/22	Spring
Moab	927371	2/22/22	3/8/22	Winter
Moab	927381	1/26/22	2/27/22	Winter
Moab	927377	12/6/21	1/10/22	Winter
Moab	927374	11/10/21	12/6/21	Fall
Moab	892172	10/21/21	11/10/21	Fall
Moab	892170	9/23/21	10/21/21	Fall
Moab	870836	8/12/21	8/24/21	Summer
Moab	870827	7/7/21	7/26/21	Summer
Moab	870806	4/7/21	5/20/21	Spring
Niwot	984525	11/23/22	12/20/22	Fall
Niwot	984517	10/18/22	11/2/22	Fall
Niwot	954594	7/11/22	7/26/22	Summer
Niwot	954589	6/29/22	7/11/22	Summer
Niwot	943771	5/3/22	5/25/22	Spring
Niwot	943750	3/23/22	4/20/22	Spring
Niwot	927364	1/11/22	3/2/22	Winter
Niwot	927352	12/16/21	1/11/22	Winter
Niwot	927348	11/20/21	12/16/21	Fall
Niwot	892166	10/5/21	10/20/21	Fall
Niwot	892155	9/7/21	9/21/21	Fall
Niwot	870831	8/5/21	8/17/21	Summer
Niwot	870816	6/22/21	7/6/21	Summer
Niwot	870810	5/26/21	6/10/21	Summer
Niwot	839633	4/6/21	4/21/21	Spring
Niwot	839617	1/27/21	2/25/21	Winter
Niwot	839608	12/30/20	1/12/21	Winter

APPENDIX C: TABLES RELATED TO FLUX AND PARTICLE SIZE

Table C.1. Mean erosional flux (g/m²/year) across median can heights (10, 25, 50, and 85cm) as function of ground cover percent for Moab, Niwot, and CPER. Flux was calculated from samples collected June 12, 2022, to March 14, 2023, for Moab, June 22 to September 29, 2022 for Niwot, and June 19, 2022 to March 24, 2023 for CPER.

Site	Ground Cover Plots	Mean Erosional Flux (g/m²/ year)
Moab	High	7800 ± 8300
Moab	Low	6300 ± 8900
Niwot	High	240 ± 120
Niwot	Low	75 ± 120
CPER	High	980 ± 860
CPER	Low	8360 ± 13000